

AN ANALYTICAL INVESTIGATION OF
FORCED CONVECTIVE HEAT TRANSFER TO
SUPERCRITICAL CARBON DIOXIDE FLOWING IN A CIRCULAR DUCT

by

Ashok MALHOTRA

B.Tech., M.Tech., Indian Institute of Technology, New Delhi, 1973

A THESIS SUBMITTED IN PARTIAL FULFILLMENT OF
THE REQUIREMENTS FOR THE DEGREE OF
DOCTOR OF PHILOSOPHY

in

THE FACULTY OF GRADUATE STUDIES
Department of Mechanical Engineering

We accept this thesis as conforming
to the required standard

THE UNIVERSITY OF BRITISH COLUMBIA
October, 1977



Ashok Malhotra, 1977

In presenting this thesis in partial fulfilment of the requirements for an advanced degree at the University of British Columbia, I agree that the Library shall make it freely available for reference and study. I further agree that permission for extensive copying of this thesis for scholarly purposes may be granted by the Head of my Department or by his representatives. It is understood that copying or publication of this thesis for financial gain shall not be allowed without my written permission.

ASHOK MALHOTRA

Department of MECHANICAL ENGINEERING

The University of British Columbia
2075 Wesbrook Place
Vancouver, Canada
V6T 1W5

Date NOVEMBER 1977

ABSTRACT

A physical model and a numerical solution procedure has been developed to predict heat transfer behaviour in supercritical fluids. A major area of concentration was the modelling of the turbulent components of shear stress and heat flux. Traditionally, the turbulent fluxes are modelled by algebraic expressions such as the familiar mixing length methods. However, the use of this technique has not been entirely satisfactory. Newer methods for constant-property flows which model turbulent fluxes by considering the transport of quantities such as turbulent kinetic energy and the dissipation rate of turbulence have been extended to supercritical fluids. This involves the solution of two additional partial differential equations that are solved simultaneously with the equations of continuity, energy, and momentum. The numerical scheme has been developed on a completely two-dimensional basis by extending the Pletcher-DuFort-Frankel finite difference method.

Computed results for velocity and temperature profiles as well as wall temperature distributions exhibited reasonable agreement with previous experimental data and therefore indicate the viability of the present method. Computations were carried out for supercritical carbon dioxide flowing through a circular duct in the reduced pressure range 1.0037 to 1.098. A consideration of the influence of buoyancy on the mean momentum balance permitted the calculation of unusual velocity profiles in this investigation. The existence of such velocity profiles had been accepted previously but the nature of their growth along a pipe has probably not been suggested previous to this work. No attempt was made to include buoyancy generated turbulence or additional fluctuating property correlations

in this work, but suggestions are made regarding possible avenues of approach. Some of the incidental outcomes of this work were a new continuous universal velocity profile implicit in cross stream distance and a new mixing length distribution for turbulent pipe flows.

TABLE OF CONTENTS

	Page
ABSTRACT	ii
TABLE OF CONTENTS	iv
LIST OF TABLES	vii
LIST OF FIGURES	viii
LIST OF SYMBOLS	xi
ACKNOWLEDGEMENTS	xiv
 I. INTRODUCTION	 1
1.1 General	1
1.2 Review of Literature	8
1.3 Need for the Present Work	16
 II. THE CONSERVATION EQUATIONS	 18
2.1 General	18
2.2 Statement of Problem	19
2.3 The Governing Equations	21
2.4 Algebraic Formulations for Turbulent Viscosity	24
2.5 Boundary Conditions and Starting Profiles	26
2.6 Concluding Remarks	28
 III. TURBULENCE MODEL	 30
3.1 General	30
3.2 Reynolds Stress Equation	32
3.3 Turbulence Dissipation Equation	37
3.4 Algebraic Stress Modelling and Thin Shear Flow Simplifications	40

	Page
3.5 Boundary Conditions for the Kinetic Energy-dissipation Model of Turbulence	45
3.6 Summary of Mathematical Formulation	53
3.7 Concluding Remarks	54
IV. THE NUMERICAL PROCEDURE	55
4.1 General	55
4.2 Required Capabilities of the Numerical Procedure	55
4.3 Finite Difference Formulation	57
4.4 Method of Solution	62
4.5 Preliminary Results	65
4.5.1 Laminar Flow Along a Flat Plate	65
4.5.2 Turbulent Flow Along a Flat Plate	67
4.5.3 Turbulent Flow in a Pipe	71
V. RESULTS AND DISCUSSION	79
5.1 General	79
5.2 Velocity and Temperature Profiles	80
5.3 Comparison of Wall Temperature Distributions	90
5.4 Scope for Further Results	101
5.5 Concluding Remarks	104
VI. FURTHER DISCUSSION	105
6.1 General	105
6.2 Turbulent Prandtl Number	105
6.3 Enhancement Factors	110
6.4 Free Convective Influences	115
VII. CONCLUSIONS AND RECOMMENDATIONS	121

REFERENCES	123
APPENDIX A. Properties of Supercritical Fluids	130
APPENDIX B. Equations for the Turbulence Model	135
APPENDIX C. Computer Program	144
APPENDIX D. Listing of Computer Program	157

LIST OF TABLES

	Page
TABLE 2.1 Value of F_x	22
TABLE 3.1 Mixing Length Distribution in Turbulent Pipe Flow	49
TABLE 3.2 Summary of Mathematical Formulation	53
TABLE A.1 Properties of Carbon Dioxide (Pressure = 1100.00 PSIA) ...	134
TABLE C.1 Description of Arrays Used in the Main Segment	150
TABLE C.2 Description of Input Variables	152
TABLE C.3 Description of Subroutines	155

LIST OF FIGURES

	Page
FIGURE 1. Locus of Maximum C_p as a Function of Temperature for Supercritical Carbon Dioxide	3
FIGURE 2. Specific Heat (C_p) of Carbon Dioxide as a Function of Temperature	4
FIGURE 3. Thermal Conductivity of Carbon Dioxide as a Function of Temperature	5
FIGURE 4. Density of Carbon Dioxide as a Function of Temperature ..	6
FIGURE 5. Viscosity of Carbon Dioxide as a Function of Temperature	7
FIGURE 6. Schematic Diagram of the Problem	20
FIGURE 7. Properties of Carbon Dioxide Near the Pseudocritical Temperature	41
FIGURE 8. Mixing Length Distribution in Pipe Flow	50
FIGURE 9. Constant $C_{\epsilon 1}$ for the Dissipation Equation	52
FIGURE 10. The Finite Difference Grid	60
FIGURE 11. Blasius Velocity Distribution in the Boundary Layer Along a Flat Plate	68
FIGURE 12. Temperature Distribution on a Heated Flat Plate at Small Eckert Number for $Pr = 2.57$	69

	Page
FIGURE 13. Velocity Distribution in a Turbulent Boundary Layer Along a Flat Plate	72
FIGURE 14. Growth of a Turbulent Boundary Layer and Decline of Shear Stress Along a Plate	73
FIGURE 15. Nusselt Number in Pipe Flow	76
FIGURE 16. Turbulence Kinetic Energy in Pipe Flow	76
FIGURE 17. Velocity Distribution in Turbulent Pipe Flow	77
FIGURE 18. Temperature Profiles for Supercritical Carbon Dioxide ...	82
FIGURE 19. Velocity and Temperature Profiles for Supercritical Carbon Dioxide	83
FIGURE 20. 'Unusual' Velocity Profile in Supercritical Carbon Dioxide	86
FIGURE 21. Development of 'Unusual' Velocity Profiles in Super- critical Carbon Dioxide	87
FIGURE 22. Temperature and Density Profile in Supercritical Carbon Dioxide Corresponding to Data in Figure 20	89
FIGURE 23. Wall Temperatures in Supercritical Carbon Dioxide	93
FIGURE 24. Wall Temperatures in Supercritical Carbon Dioxide	93
FIGURE 25. Wall Temperatures in Supercritical Carbon Dioxide	93
FIGURE 26. Wall Temperatures in Supercritical Carbon Dioxide	95

	Page
FIGURE 27. Wall Temperatures in Supercritical Carbon Dioxide	97
FIGURE 28. Wall Temperatures in Supercritical Carbon Dioxide	99
FIGURE 29. Wall Temperatures in Supercritical Carbon Dioxide	100
FIGURE 30. Development of Unusual Velocity Profiles in Supercritical Carbon Dioxide	102
FIGURE 31. Turbulence Kinetic Energy and Dissipation Profile Corresponding to Computations Illustrated in Figure 19 ..	103
FIGURE 32. Turbulent Prandtl Number Variation Across a Pipe	107
FIGURE 33. Wall Temperature Variations with Different Turbulent Prandtl Numbers	108
FIGURE 34. Enhancement Factors in Supercritical Carbon Dioxide	113
FIGURE 35. Wall Shear Stress Variation	114
FIGURE 36. Wall Temperatures for Upflow and Downflow	117
FIGURE 37. Computed Radial Shear Stress Profiles for Carbon Dioxide at $P/P_c = 1.027$ at a Location $x/D = 30$	119
FIGURE 38. Computed Values of Turbulence Kinetic Energy K for Carbon Dioxide at $P/P_c = 1.027$ at a Location $x/D = 15$. (Data Corresponding to Figure 36.)	119
FIGURE 39. Flow Chart of Computer Program	146
FIGURE 40. Nomenclature for Variables in Subroutines	156

LIST OF SYMBOLS

a	Constant in Van der Waal's equation
A	Area
A^+	Constant in Van Driest's expression
A_1, A_2	Constants in starting profile for turbulence kinetic energy
A_x, A_y	Constants in relationships determining finite difference grid spacing
b	Constant in Van der Waal's equation
C_1, C_2	Constants in pressure strain correlation
$C_{\epsilon 1}, C_{\epsilon 2}$	Constants in the dissipation equation
C'_s	Constant in Reynolds' stress equation
C_μ	Constant in $k - \epsilon$ model
D	Pipe diameter
E	Eckert number for flow over that plate
$f()$	Representing function of quantity in brackets
ϵ'_m, ϵ'_h	Enhanced values of eddy diffusivities due to Hsu and Smith defined by Equation (1.7)
g	Acceleration due to gravity
h	Enthalpy
I, I^y	A constant and a function respectively occurring in radial shear stress expression, defined by equations (1.11) and (1.12)
k	Thermal conductivity
k_t	Turbulence conductivity
K	Turbulence kinetic energy
ℓ	Mixing Length
G	Mass flow rate

Nu_x, Nu_∞	Nusselt number as a function of streamwise location and for fully-developed flow respectively
p	Pressure
p'	Fluctuating component of pressure
P	Production of turbulence kinetic energy
Pr	Prandtl number
Pr_t	Turbulence Prandtl number
q	Heat flux
r	Radial distance from axis of symmetry
R	Radius
Re	Reynolds number
t	Temperature
t^+	Non-dimensionalised temperature
t_b	Bulk temperature
t_e	Outer wall temperature
t_w	Wall temperature in pipe
T	Time
u	Velocity
u'	Fluctuating component of velocity
u^+	Non-dimensionalised velocity = $u / \sqrt{\tau_w / \rho_w}$
\tilde{U}_i	Instantaneous velocity
U_i	Fluctuating Velocity component in i direction
\hat{U}_i	Mean velocity component in i direction
v	Velocity in direction perpendicular to predominant flow direction
v'	Fluctuating component of velocity in direction perpendicular to predominant flow direction

x	Streamwise distance measured from location where heating starts
y	Cross-stream distance measured from the wall
y^+	Non-dimensionalised cross-stream distance = $y \sqrt{\tau_w / \rho_w} / \mu_w / \rho_w$
τ	Shear stress
τ_t	Turbulence shear stress
μ	Viscosity
μ_t	Turbulent viscosity
ρ	Density
ρ'	Fluctuating component of density
ν	Kinematic viscosity
ϵ	Dissipation rate of turbulence kinetic energy
ϵ'	Instantaneous value of ϵ
ϵ_m	Eddy diffusivity of momentum
ϵ_h	Eddy diffusivity of heat
δ	Boundary layer thickness
$\sigma'_k, \sigma'_\epsilon$	Constants occurring in $k - \epsilon$ model
Δ	Used in finite difference formulation as described in Figure 10
Γ	Quantity denoting diffusion of Reynolds stresses
β	Ratio of inner to outer diameter in a pipe
Subscripts	
c	Indicating critical or pseudocritical state
w	Indicating value of quantity at wall
eff	Effective value
ℓ, j, k	Cartesian coordinates direction ℓ , j , and k . ℓ corresponding to x , j to y .
$1, 2$	Horizontal and vertical direction in two-dimensional flows
t	Turbulent

ACKNOWLEDGEMENTS

The author considers himself fortunate to have had an advisor in Dr. E.G. Hauptmann. His guidance and assistance came at every stage of the work, without which this work would not have been possible.

The author also wishes to express his gratitude to Dr. I.S. Gartshore for the interest and advice he rendered towards the present work.

The University of British Columbia provided this wonderful opportunity to study at their institute as well as a much needed fellowship.

Linda Blaine, who is probably one of the best professionals available, did all the typing and much editing. She did this work, not as a professional but as an understanding sister would.

Finally, the author wishes to thank his parents who have continuously provided encouragement from half-way across the world and others who are not recorded here but were nevertheless crucial towards the completion of this work.

I. INTRODUCTION

1.1 General

Forced convection heat transfer to supercritical fluids has attracted the attention of many investigators during the past two decades. This interest has partly stemmed from the challenging nature of the problem and partly as a consequence of several engineering trends. There has been a steady development of power plants towards supercritical conditions in response to increasing demands for cheaper energy. Rocket motors are frequently cooled by fuel at supercritical pressures. Supercritical fluids have been used as coolants for electrical machines and have also been considered as coolants for nuclear reactors.

Very large changes of thermodynamic and physical properties near the critical state are responsible for the unique nature of supercritical heat transfer. Effects which are normally approximated through constant property idealizations become dominant near the critical state. Consequently, several commonly made assumptions and empirical correlations, based on constant property idealizations, become inapplicable in this region. At the present time, there is insufficient knowledge of supercritical heat transfer mechanisms to produce completely satisfactory designs near the critical state. One of the goals of the present work is to improve this situation by an analytical examination of the phenomenon.

The critical point is often defined as the pressure and temperature at which no distinction can be made between the liquid and vapour phase of a fluid. At pressures higher than critical, the fluid is termed supercritical. The term subcritical is used for fluids below their critical pressure. At

supercritical pressures, heating of a fluid brings about a continuous change from a dense liquid-like state to a lighter state resembling a gas (vapour-like). No distinct interface occurs between a liquid and vapour at supercritical pressures. However, the pseudocritical temperature (the temperature at which specific heat attains a local maxima) may be used as an approximate demarcating temperature between the liquid and vapour-like states. An illustration of the preceeding terminology is provided in Figure 1. Property variations become less severe away from critical pressures and correspondingly the heat transfer mechanisms become simpler. The term supercritical heat transfer is normally used only up to pressures where property variations are severe enough to make constant property heat transfer treatment inapplicable. The boundaries of this region are somewhat arbitrary.

Below the critical pressure, boiling does not occur if the fluid state does not encompass the saturation temperature. Therefore, single-phase heat transfer mechanisms apply. In a somewhat similar manner if the state of a supercritical fluid is far removed from the pseudocritical temperature (so that property variations are not significant), conventional single-phase mechanisms apply. Abnormal heat transfer occurs only at or in the vicinity of the pseudocritical temperature.

A brief discussion of the thermodynamic and transport properties of supercritical fluids is provided in Appendix A. Figures 2 to 5 illustrate the variations of viscosity, density, specific heat (C_p) and thermal conductivity of supercritical carbon dioxide at a pressure of 75.84 bars.

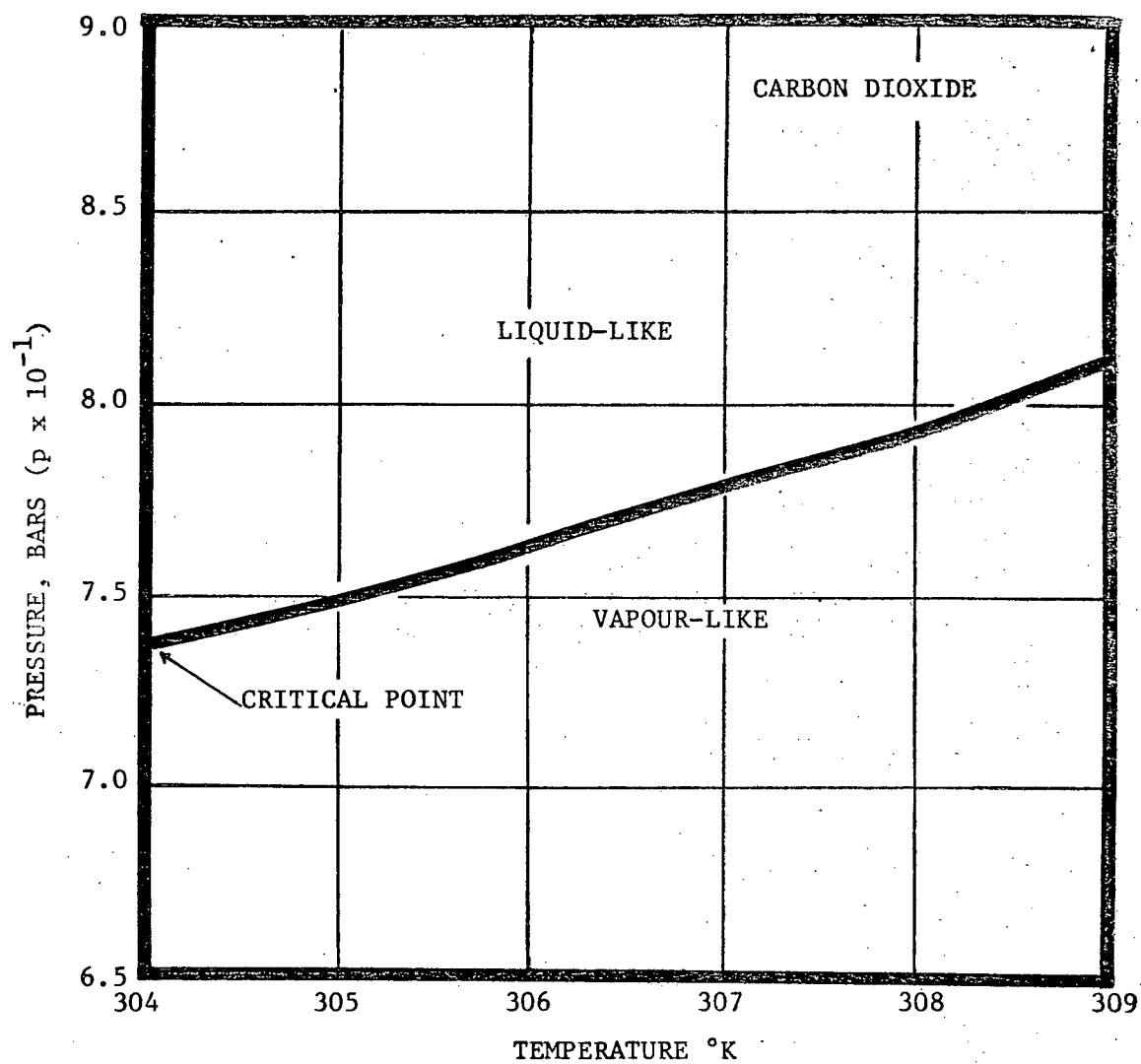


FIGURE 1. Locus of Maximum C_p as a Function of Temperature for Supercritical Carbon Dioxide.

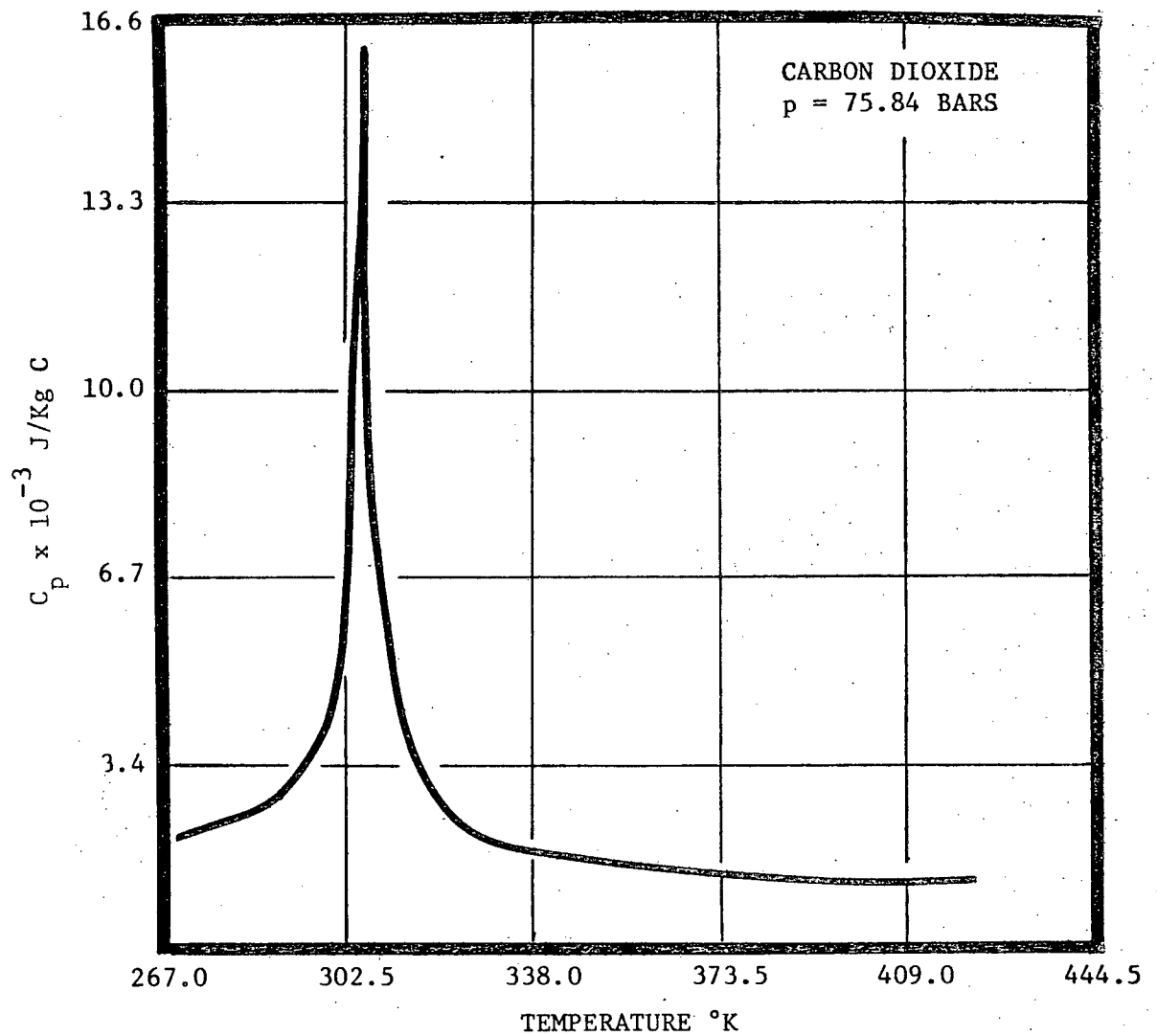


FIGURE 2. Specific Heat (C_p) of Carbon Dioxide as a Function of Temperature.

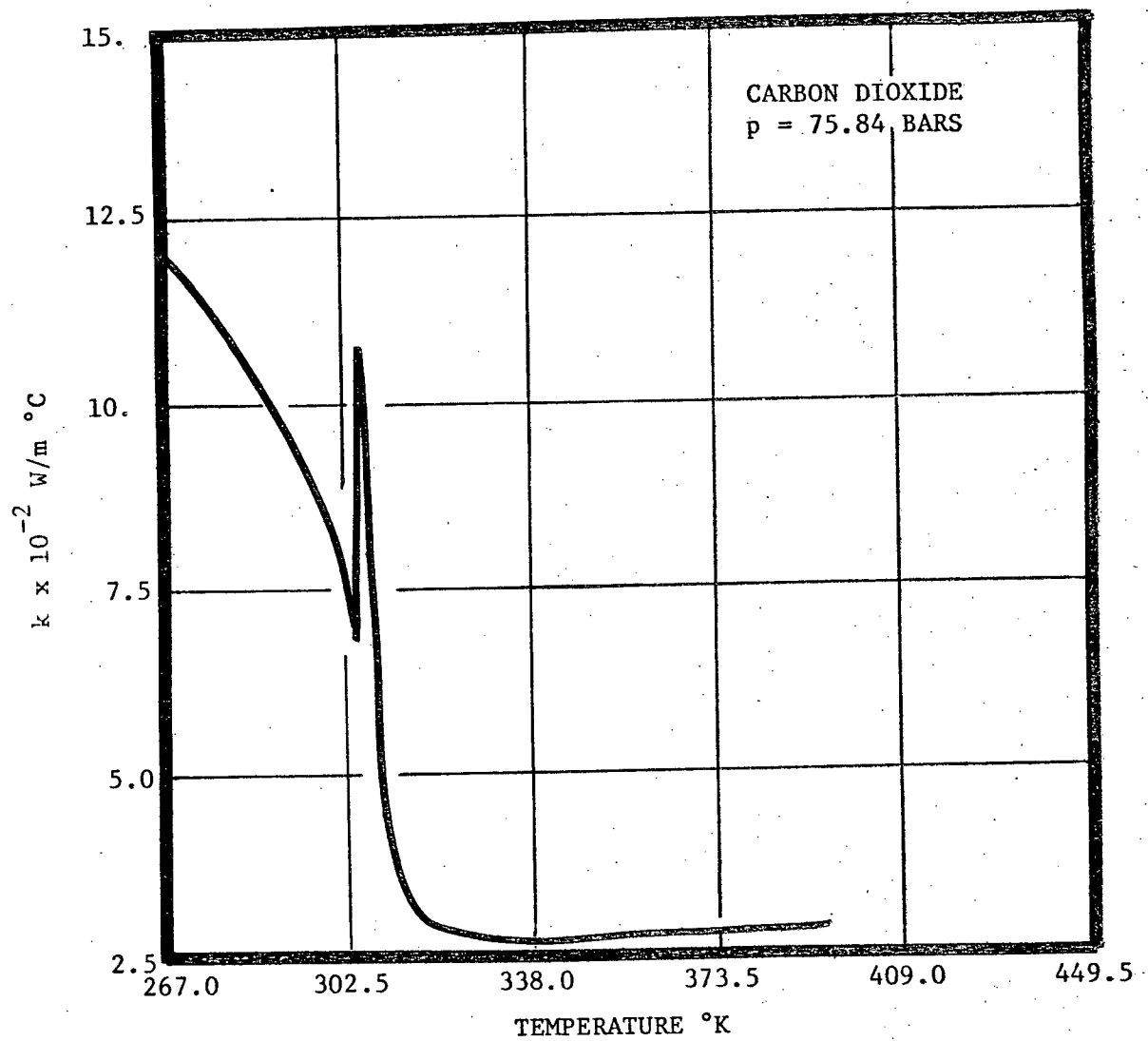


FIGURE 3. Thermal Conductivity of Carbon Dioxide as a Function of Temperature.

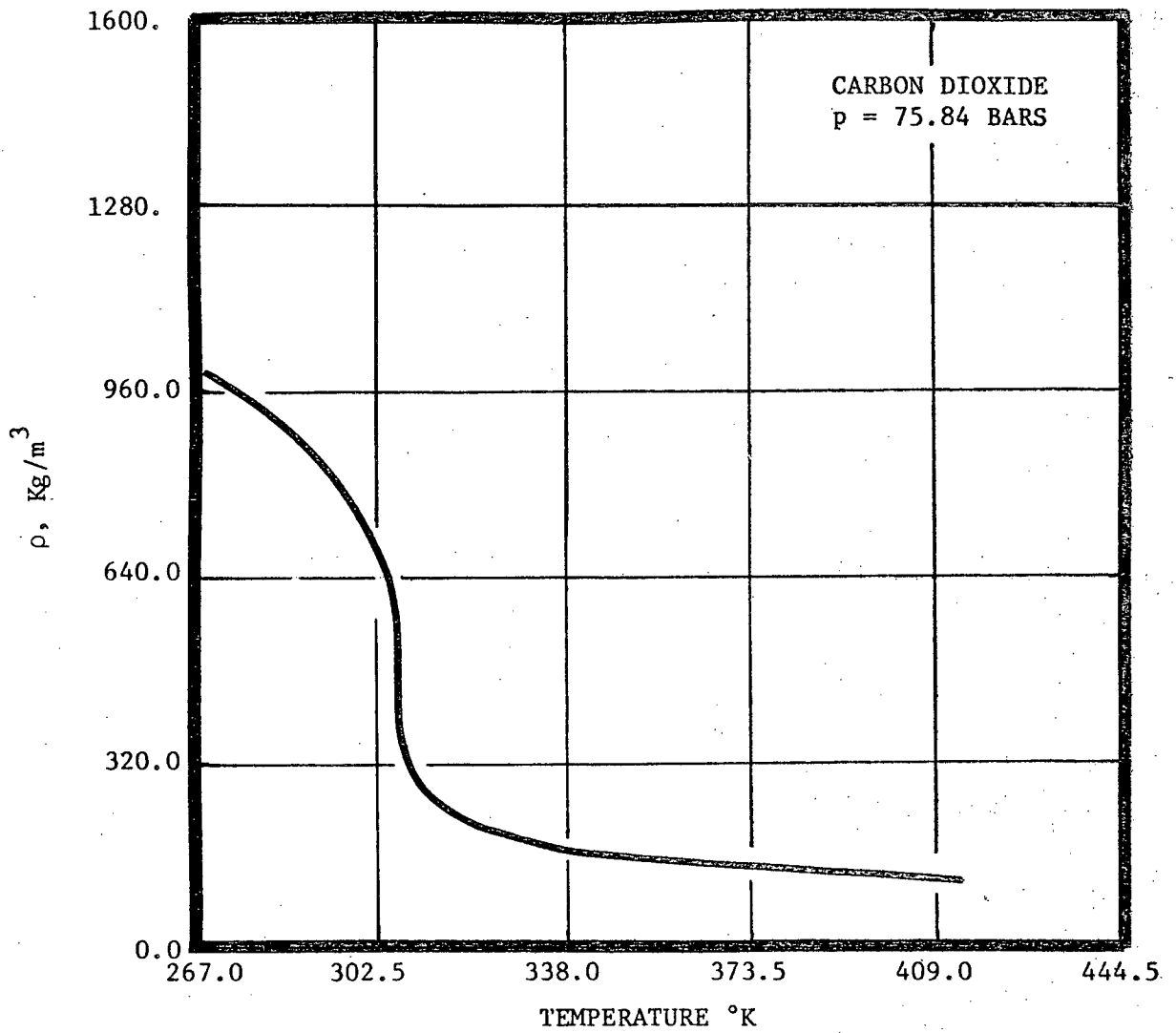


FIGURE 4. Density of Carbon Dioxide as a Function of Temperature.

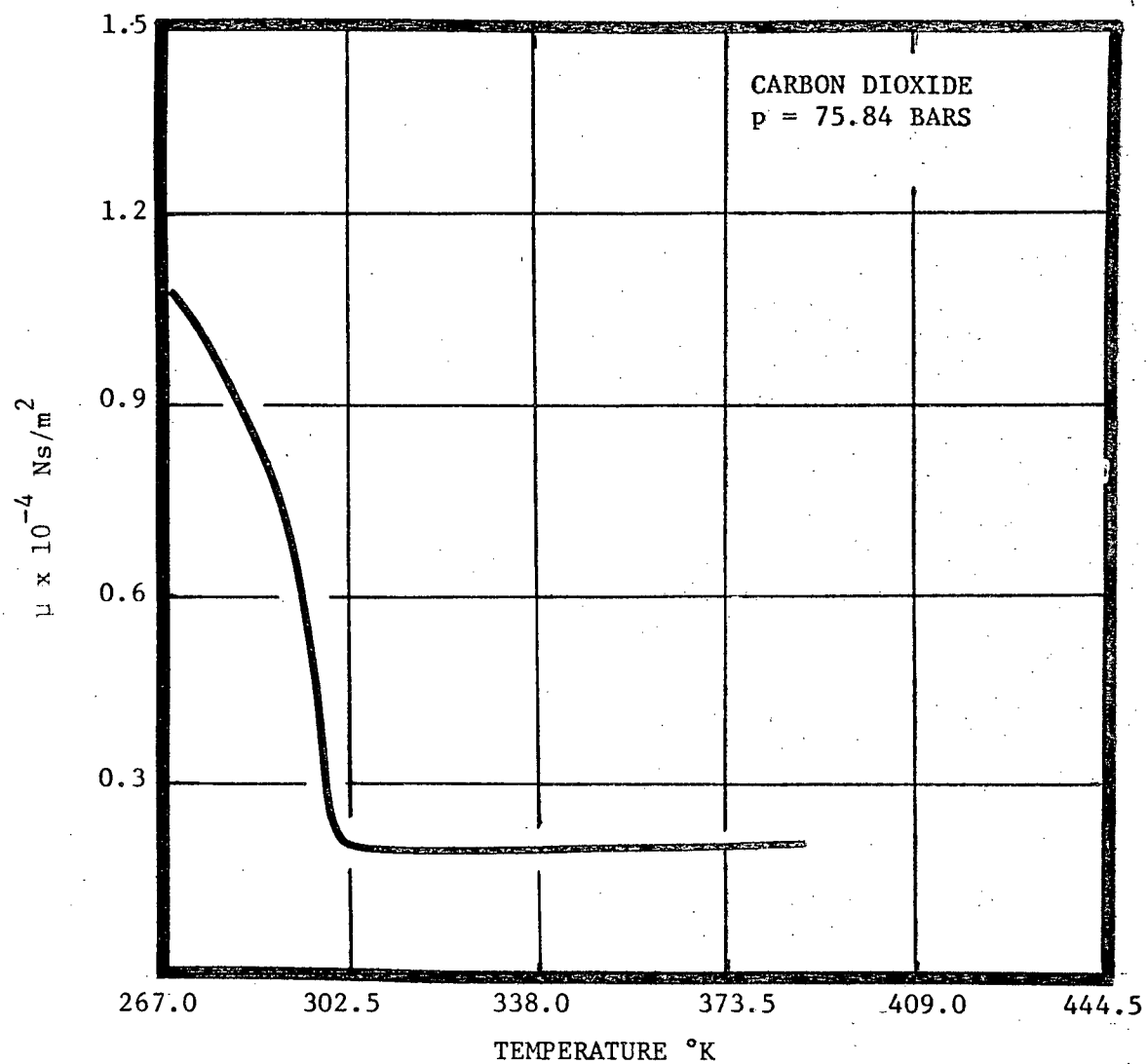


FIGURE 5. Viscosity of Carbon Dioxide as a Function of Temperature.

1.2 Review of Literature

Comprehensive surveys of near critical heat transfer with extensive bibliographies have been made by Hall¹, Hendricks, Simoneau, and Smith², and Hsu and Graham³. The discussion in this section is mainly restricted to forced convection aspects of supercritical heat transfer.

Probably the earliest investigation of heat transfer to supercritical fluids was that of Schmidt, Eckert, and Grigull⁴. They conducted their experiments in a natural convection loop and presented their results in terms of an apparent thermal conductivity, defined as the thermal conductivity required to transfer an equivalent amount of heat at the same temperature difference through a solid material of the same size. They found that apparent thermal conductivity becomes very large near the critical point. A later study by Schmidt⁵ in a closed tube showed that apparent thermal conductivity at supercritical conditions can be as large as 10,000 times that of copper over a narrow range of temperatures. Contrary to this and other studies indicating an improved behaviour at the critical point, several studies⁶ observed a sharp decrease in the heat transfer coefficient near the critical point. This apparent contradiction was resolved when it was demonstrated that maxima and minima in heat transfer can occur depending on the level of heat flux (Hauptmann⁷ and Styrikovich et al.⁸).

Differences between wall temperature and bulk temperature are small in experiments where minima are observed. According to Hsu⁹, the two results can be explained in boiling terms with instances of increased heat transfer coinciding with a mechanism similar to nucleate boiling, whereas a minimum heat transfer coefficient is akin to film boiling. This

postulate was supported by the fact that maximum coefficients generally occurred at low temperature differences as in nucleate boiling. Some of the first direct observations in a supercritical fluid by Griffith and Sabersky¹⁰ indicated the existence of a bubble-like flow around a heating wire. Supercritical heat transfer is sometimes accompanied by boiling-like noise¹¹. Goldmann¹², therefore, was also led to conclude like Hsu⁹ that under certain conditions of non-equilibrium, a boiling-like mechanism will sometimes occur.

Contrary to the preceeding evidence, flow visualisations carried out by Hauptmann^{7,13} and Green¹⁴ have been in favour of single-phase forced convection mechanisms. The strongest argument against the boiling theories is that two distinct phases are not possible under equilibrium at supercritical pressures and sufficient departure from conditions of equilibrium has not yet been proved. Following Deissler¹⁵, it has been shown that conventional forced convection theories that account for large property variations can account for most of the peculiarities including maxima and minima in supercritical fluids. This is the approach adopted in most theoretical investigations and will be pursued further in the present work.

Experimental investigations have mostly made use of smooth pipes of circular cross-section with uniform heat flux boundary conditions. The first detailed study was that of Wood¹⁶, who made very careful measurements of velocity and temperature profiles. He also measured some unusual velocity profiles (which exhibited a maxima away from the center). Similar profiles have also been measured and studied carefully on a flat plate by Simoneau¹⁷. A great deal of effort has been placed on developing

data correlations using either the Dittus Boelter type of equation or its modifications,

$$Nu_X = C Re_X^a Pr_X^b \left(\frac{t_w}{t_b} \right)^d \quad (1.1)$$

Here, 'X' implies that properties are evaluated at a reference temperature t_X . Suggestions for evaluating t_X have been made by Eckert¹⁸ and Bringer and Smith¹⁹ amongst others. Some other notable attempts to develop correlations have been by Hess and Kunz²⁰, Krasnoschchekov et al²¹, Gunson and Kellog²², Swenson et al.²³, and Mirapolsky and Shitsman²⁴.

Although these correlations are useful and one of the few means of predicting supercritical heat transfer, they have not been very successful; to quote Hsu and Graham³: "It would be conceded by most investigators in this field that any of the correlations using the Dittus-Boelter type of equation are not fully acceptable prediction schemes".

Hall¹ also concluded that existing correlations are inadequate as a means of predicting heat transfer in the critical region. As the fluid state moves away from the critical point, property variations become less severe and then these correlations are more nearly applicable.

A rather different approach to correlating and explaining forced convection heat transfer to supercritical fluids has been suggested by Hendricks, Graham, Hsu, and Mediros²⁵, treating the problem as a pseudo-two-phase phenomenon. Another model is the penetration model due to Graham²⁶. The chief value in these latter approaches probably lies in their heuristic description of mechanisms and not in their ability to correlate data.

An alternative approach to predicting near-critical heat transfer is application of turbulent forced convection theories with allowance for property variations. Accordingly, turbulent fluxes are defined as:

$$\tau(y) = (\mu + \rho \epsilon_m) \frac{\partial u}{\partial y}, \quad (1.2)$$

and

$$q(y) = (k + \rho C_p \frac{\epsilon_m}{Pr_t}) \frac{\partial t}{\partial y}. \quad (1.3)$$

The principal unknowns in equation (1.2) and (1.3) are the flux variations $\tau(y)$, $q(y)$, and diffusivity ϵ_m . The turbulent Prandtl number is generally regarded as equal to unity. Deissler^{15,27} pioneered attempts to analyse supercritical fluids and proposed that close to a wall diffusivity is given by:

$$\frac{\epsilon_m}{\nu} = n^2 u^+ y^+ [1 - \exp(-\nu_w n^2 u^+ y^+ / \nu)] . \quad (1.4)$$

Goldmann²⁸ redefined the non-dimensional parameter occurring in the universal velocity profile in order to make them more sensitive to property variations.

According to Tanaka²⁹, Goldman's proposal implies a redefinition of the same parameters occurring in the diffusivity expression which are,

$$y^{++} = \int_0^{y^+} \left(\frac{\rho}{\rho_w}\right)^{1/2} \left(\frac{\mu}{\mu_w}\right) dy^+, \quad (1.5)$$

and

$$u^{++} = \int_0^{y^+} \left(\frac{\rho}{\rho_w} \right)^{1/2} du^+ . \quad (1.6)$$

Hsu and Smith³⁰ modified Deissler's method by considering effect of density derivatives in shear and heat transfer expressions as:

$$\epsilon'_m = (1 + F)\epsilon_m; \quad \epsilon'_h = (1 + F_h)\epsilon_m; \quad (1.7)$$

where,

$$F = \frac{d \ln \rho / d \ln u^+}{d y^+}, \quad (1.8)$$

and,

$$F_h = \frac{d \ln \rho / d y^+}{d \ln C_p / d y^+}. \quad (1.9)$$

The factors inside the parenthesis have been referred to as enhancement factors. Another type of enhancement factor has been suggested by Yoshida³¹.

Tanaka²⁹ used Kato's³² expression for eddy diffusivity and Goldmann's model for calculations. They were able to predict wall temperature peaks typical of deterioration regimes in supercritical heat transfer. Hess and Kunz²⁰, on the other hand, adopted Van Driest's expression for eddy diffusivity for calculations in supercritical hydrogen and went on to develop a widely used correlation that involves an additional parameter v_w/v_b .

Shear stress and heat flux variation have been assumed to be either constant or varying linearly in most investigations. This follows directly from the assumption that streamwise variations are not significant, or equivalently that the flow is one-dimensional. Shiralkar and Griffith³³ found wall shear stress values by an additional mass flow constraint and were able to predict wall temperature trends in the deterioration regimes

for supercritical steam and carbon dioxide. Sastry and Schnurr³⁴, however, did not make the assumption of one-dimensionality except in the near wall region. They adopted the well known Patankar and Spalding scheme and used Van Driest's expression for diffusivity. Their computed results exhibited good agreement for supercritical steam in the enhancement regime.

In another group of studies in which investigators having realized the importance of buoyancy even in predominantly forced convection situations and have allowed the shear stress variations to be influenced by buoyancy. At least three attempts to make such calculations have been made and are due to Hsu and Smith³⁰, Hall³⁵, and Tanaka³⁶.

Before undertaking the main part of investigation, a preliminary one-dimensional^{*} study was carried out in order to gain familiarity with forced convection concepts in supercritical fluids. Calculations were made for pipe flow using a linear shear stress distribution as well as a shear stress distribution that accounts for buoyancy in vertical flows³⁷,

$$\tau(y) = \frac{R-y}{R} \left(\tau_w - \frac{I}{R} \right) + \frac{I}{R-y} - \frac{Iy}{R-y}, \quad (1.10)$$

where,

$$I = \int_0^R \rho g(R-y) dy, \quad (1.11)$$

* The terms one-dimensional and two-dimensional in this investigation make reference to the minimum number of coordinates required to analyse the problem.

and,

$$I^y = \int_0^y \rho g(R-y) dy . \quad (1.12)$$

Equations (1.10) to (1.12) follow directly by integrating the one-dimensional momentum equation. The remaining formulation is essentially similar to that of Shiralkar and Griffith³³. An important innovation in the present investigation was the use of temperature as an independent cross-stream variable in the numerical solution. This was made possible by rearranging equation (1.3) for $\frac{dy}{dt}$ rather than $\frac{dt}{dy}$. Since properties were tabulated as the function of temperature, this eliminated numerous interpolations for the properties which otherwise consume the bulk of computing time. An additional advantage was that inaccuracies associated with interpolation were also reduced. It also becomes possible to divide the grid in equal increments of enthalpy which yields an efficient grid distribution with suitably close points near the wall and in the vicinity of the critical point where properties change rapidly. Although it may appear from the one-dimensional equations that computation time is not a severe limitation, this is not the case due to time-consuming iterations for τ_w and I . As a consequence of this study, a need for an investigation at the two-dimensional level was reinforced.

So far, all analyses discussed have been quantitatively successful only in selected regions. Their main contribution, however, lies in the fact that they have predicted a principal peculiarity of supercritical fluids which is 'enhancement' and 'deterioration' in heat transfer at low and high heat fluxes respectively. A one-dimensional analysis also succeeds in predicting some of the unusual velocity profiles. A more complete range

of velocity profiles has been calculated in this investigation (as discussed in Chapter V).

In conclusion, calculation methods in supercritical fluids fall within two broad categories. The first of these is through the use of empirical correlations and the second through the use of forced convection theories that make use of the mixing length type of algebraic formulations for diffusivity. The latter approach was adopted in this work in order to explore the possibilities that a more rigorous effort in this direction can yield. However, an important change in this investigation was the replacement of the algebraic formulations for diffusivity by some of the more recent methods used for studying constant property turbulence flows. These methods formally referred to as turbulent models, differ according to the level of approximation and may involve one, two, or more additional differential equations for turbulence properties such as the Reynolds stress that are solved simultaneously with the three primary conservation equations (of mass, momentum, and energy). Therefore, this latter form of turbulence modelling is often referred to as multi-equation models of turbulence^{*}. Though still in their early stages of development, these models are regarded as an improvement over algebraic formulations (of the mixing length types) because of their success in application to many engineering situations. By accounting for the transport of turbulence properties, they place the art of turbulence modelling on a physically realistic level.

^{*} See Launder and Spalding³⁸ for multi-equation models of turbulence.

1.3 Need for the Present Work

The designer of heat transfer equipment requires information on wall temperature distribution^{*} (or heat transfer coefficients) and wall shear stresses (or friction factors). It is desirable that the prediction procedure available to him should be versatile enough to cover a wide variety of operating conditions, within which he may explore and optimise a design. Various attempts for supercritical fluids have been outlined in the literature survey but as indicated, they are in need of further development. However, they have pointed to a possible route which needs to be investigated.

The purpose of this dissertation is to develop a numerical procedure which can handle forced convection heat transfer calculation at super-critical conditions. The major areas of improvements in the present work were the inclusion of a multi-equation model of turbulence and the extension of the analysis to a fully two-dimensional level. The procedure is general enough to be used (in most cases with only minor modifications) for any fluid flowing in plane or axisymmetric configurations, but calculations were restricted to flow of supercritical carbon dioxide through circular ducts.

Carbon dioxide has a convenient critical range^{**}. Because of this and also because of its easy handling and availability in a fairly pure form, carbon dioxide has been selected as a working fluid in many experimental

^{*} Heat transfer coefficients in supercritical fluids are heat flux dependent and therefore they do not have the same significance as in constant property fluids.

^{**} $P_c = 73.8$ bars, $t_c = 304^\circ\text{K}$.

investigations. Its properties in the critical region are fairly well known, unlike most other fluids^{*}. Because of this and also because a variety of experimental data is available, carbon dioxide was selected as the fluid for testing the numerical procedure in this investigation.

The problem investigated in this study is also interesting from an academic point of view in that the combination of difficult phenomena such as turbulent flow and large property variations are generalisations of phenomena that occur in most convective heat transfer problems. There is also a need to inquire into the applicability of recent methods in turbulence modelling and numerical analysis under the influence of such conditions.

The contributions of this investigation are twofold. First, the formulation of a physical model and second, the development of a numerical solution procedure. The three primary equations for conservation of mass momentum and energy are discussed in Chapter II. These are fully two-dimensional and include terms for buoyancy and viscous dissipation. The associated turbulence model discussed in Chapter III is a two-equation model of turbulence. Chapter IV describes the main features of the numerical solution procedure along with some preliminary results. The associated computer program is described in Appendix D. The remaining chapters discuss the achievements and shortcoming of the prediction procedure.

^{*}The properties of supercritical steam are also well known.

II. THE CONSERVATION EQUATIONS

2.1 General

The main thrust of this investigation was concerned with flow in circular ducts, but an attempt was made to keep the mathematical formulation sufficiently general so that it would apply to both plane and axisymmetric flow situations.

This investigation was primarily concerned with time-averaged effects. The process of time averaging causes statistical correlations involving fluctuating velocities and temperature to appear in the conservation equations. These unknown correlations are approximated from additional equations which generally take the forms of algebraic formulae (as in the mixing length models); they can also be determined from the solution of differential equations for time-averaged properties of turbulence. The latter approach is relatively recent and has mostly been concerned with constant property fluids. Therefore, it required a review before it was introduced in this investigation.

The complete mathematical model formulated in this work involves differential equations for the fluctuating velocity correlations as well as the three primary conservation equations of mass, momentum, and energy. Only the latter set of equations, along with algebraic formulae for turbulent viscosity, are discussed in this chapter. The remaining equations are taken up in the next chapter. This division has been made for the sake of clarity.

2.2 Statement of Problem

The problem under consideration was forced convective heat transfer to supercritical fluids flowing past rigid surfaces in two-dimensional plane or axisymmetric configurations. Heat addition or removal took place only at the rigid boundaries. The flow was normally turbulent and the mean flow was assumed to be steady (hydrodynamically as well as thermally). The fluid was assumed to be at supercritical pressures and the fluid properties were assumed to be known. Figure 6 shows a schematic diagram of the problem as applicable to pipe flow.

The conservation equations considered in this chapter include a term accounting for buoyancy. The necessity of including this term may be questioned since the primary interest in the present work is forced convection heat transfer. However, it has been indicated by Hauptmann⁷, Hsu and Smith³⁰, and Hall¹ that free convection effects can influence several predominantly forced convection situations. It is difficult to define precisely when these effects are totally absent. Moreover, it is felt that the role of buoyancy in the mean momentum balance for forced convection situations is not fully understood. A consideration of this influence in forced convection heat transfer provides an opportunity to contribute towards a further understanding of this situation. Nevertheless the mathematical model formulated in this work is not generally applicable for both forced and free convection heat transfer since the turbulence model used in this work is primarily meant for forced convection heat transfer. It should be pointed out that in previous analytical investigations (treated as one-dimensional) the free convective influence has been conceived only in terms of a buoyant body force contribution in the mean

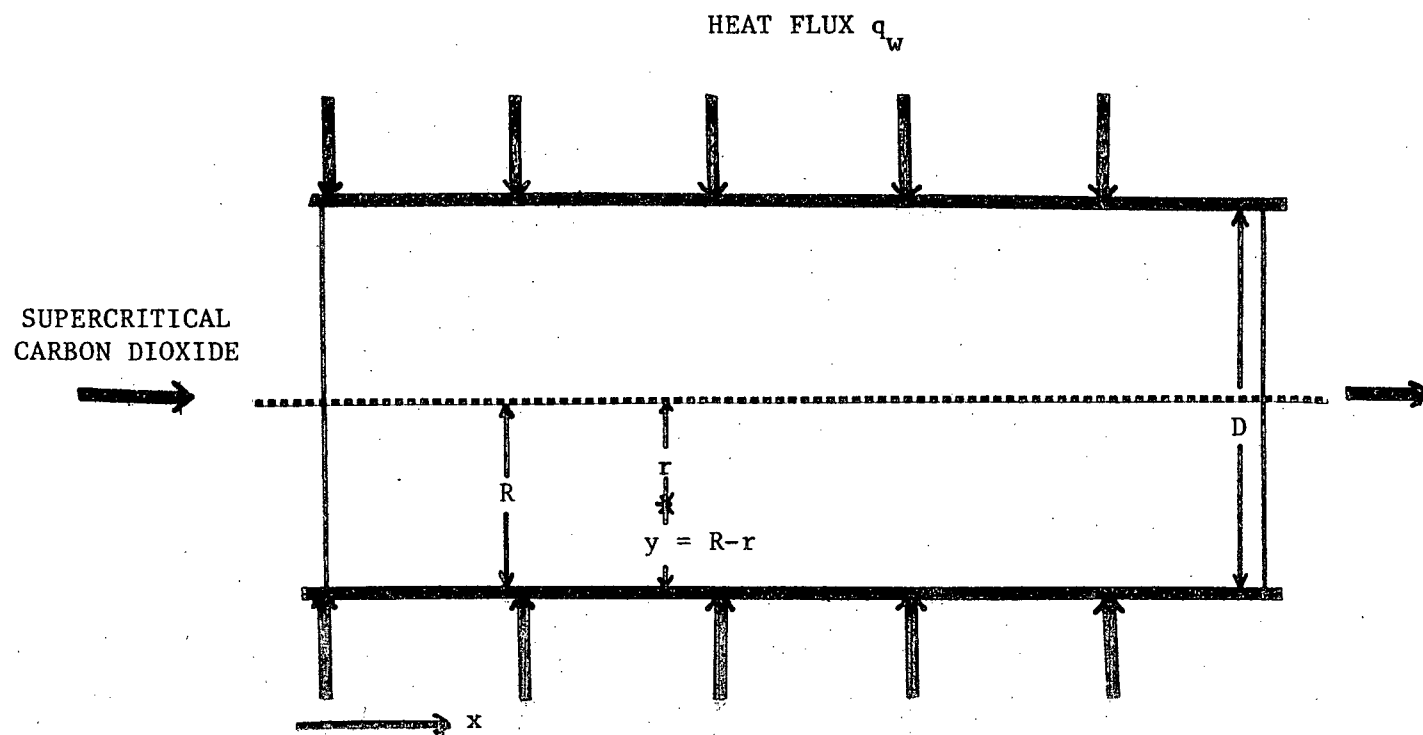


FIGURE 6. Schematic Diagram of the Problem.

momentum balance.

2.3 The Governing Equations

The equations of continuity, energy and momentum governing the flow can be written in such a way that they apply to plane as well as to rotationally symmetric flow. For the problem under consideration, these equations may be written as^{*}:

$$\frac{\partial}{\partial x} (\rho u r^\alpha) + \frac{\partial}{\partial y} (\rho v r^\alpha) = 0 \quad (2.1)$$

$$\rho u \frac{\partial u}{\partial x} + \rho v \frac{\partial u}{\partial y} = - \frac{dp}{dx} + \frac{1}{r^\alpha} \frac{\partial}{\partial y} \left[r^\alpha \left(\mu \frac{\partial u}{\partial y} - \rho \overline{u'v'} \right) \right] + F_x, \quad (2.2)$$

and,

$$\rho u \frac{\partial h}{\partial x} + \rho v \frac{\partial h}{\partial y} = u \frac{dp}{dx} + \frac{1}{r^\alpha} \frac{\partial}{\partial y} \left[r^\alpha \left(k \frac{\partial t}{\partial y} - \rho \overline{h'v'} \right) \right] + \left(\mu - \frac{\rho \overline{u'v'}}{\partial u / \partial y} \right) \left(\frac{\partial u}{\partial y} \right)^2 \quad (2.3)$$

where: $\alpha = 0$ (for plane flows),

$\alpha = 1$ (for axisymmetric flow).

The body force term in the x-momentum equation, F_x , may take the values indicated in Table 1.1.

^{*} See Eckert and Drake³⁹.

TABLE 2.1 Value of F_x

	FLOW CONFIGURATION	F_x
I	Non-buoyant or Horizontal Duct Flow	0
II	Upward Duct Flow	$-\rho g$
III	Downward Duct Flow	$+\rho g$
IV	Upward Facing Flat Plate	$+\frac{\partial}{\partial x} \int_y^\delta \rho g dy$
V	Downward Facing Flat Plate	$-\frac{\partial}{\partial x} \int_y^\delta \rho g dy$

For a horizontal pipe, the indicated body force is zero. This is actually only true for non-buoyant flows. The case of horizontal-pipe buoyant flow cannot be treated here since in that case the axisymmetric condition is violated. The body forces for the flat plate IV and V of Table 1.1 are actually not the body forces; these terms arise due to body forces $\pm \rho g$ in the y-momentum equation. However, since the y-momentum equation is not stated separately, these values can be seen as F_x with dp/dx taking a value equal to zero.

The contribution of fluctuating property correlations has been neglected in previous investigations since it is felt that their overall influence is not significant. As a preliminary step, this practice was continued in the present investigation in the preceding conservation equations. Hall¹ has estimated these correlations and carried out a useful order of magnitude analysis. His conclusion was that these correlations are probably negligible, but further discussion on this issue is provided in Chapter VI.

Since the pressure variations in the cross-stream direction were not significant in this investigation, then:

$$k \frac{\partial t}{\partial y} = \frac{k}{C_p} \frac{\partial h}{\partial y} . \quad (2.4)$$

Whenever indicated by the turbulence model under use that the turbulent fluxes could be expressed as a product of a function (which was either known or could be determined) and the velocity gradient, then this function was called the turbulent viscosity (or conductivity). This is the sense in which the effective viscosity concept has been used in this investigation:

$$- \overline{\rho u'v'} = \mu_t \frac{\partial u}{\partial y} , \quad (2.5)$$

$$- \overline{\rho h'v'} = \frac{k_t}{C_p} \frac{\partial h}{\partial y} , \quad (2.6)$$

and in addition,

$$\mu_{eff} = \mu + \mu_t , \quad (2.7)$$

$$k_{eff} = k + k_t . \quad (2.8)$$

The ratios of the two turbulent coefficients is then the turbulent Prandtl number ($Pr_t = C_p \mu_t / k_t$).

The pressure gradient in the momentum equation for non-confined flows will be known and for the confined flow, it can be found by the additional constraint of known mass flow rate (see section 4.3 for details):

$$G = \int_0^r \rho u dA . \quad (2.9)$$

2.4 Algebraic Formulations for Turbulent Viscosity

No precise way is yet available for completing the preceeding equation set. The conventional means however is through the use of algebraic formulations for the turbulent viscosity. Predominant among these is Prandtl's mixing-length hypothesis. This type of formulation has been used in the past for an analytical treatment of supercritical fluids. However, at the present time it is possible to make use of apparently improved models of turbulence and the intention in this investigation was to explore an alternative model. Nevertheless, the algebraic formulations were still necessary in the laminar and transitional region close to the wall. In addition, they were useful for developing a solution procedure and for deriving certain boundary conditions and starting profiles.

Some of the algebraic expressions that have found use in analytical work dealing with supercritical fluids are due to Deissler, Kato, and Van Driest. These expressions were originally formulated for constant property fluids but are used with the assumption that if the fluid properties appearing in the expressions are allowed to take their local values, they are still applicable. In addition, all the available expressions may be redefined by the use of Goldmann's hypothesis²⁹. However, the general experience in this and other investigations (all one-dimensional analysis) has been that whichever expression is used, the results are not altered significantly. The most widely used formulation is due to Van Driest. It was also selected in the present work,

$$\mu_t = \rho \ell^2 \left| \frac{\partial u}{\partial y} \right|, \quad (2.10)$$

$$\ell = \kappa y [1 - \exp(-y^+/A^+)] , \quad (2.11)$$

where,

$$\kappa = 0.4 \text{ and } A^+ = 26 .$$

For $y^+ > 26$, it is possible to use $\ell = \kappa y$ with comparable accuracy.

However, this was not done in order to ensure a smooth merger of the transitional region with the turbulent region. Beyond $y^+ = 120$, Van Driest's expression reduces to $\ell = \kappa y$ within 1%. At least three different proposals exist for expressing the argument of the exponent in equation (2.11). None of these proposals is advantageous under all circumstances. However, the procedure of using wall properties to evaluate the damping function has been shown to be superior to using local properties for fluids of moderate Prandtl number⁴⁰. Accordingly the expression chosen was:

$$y^+ = y \sqrt{\tau_w / \rho_w} / \mu_w / \rho_w . \quad (2.12)$$

Another expression for the mixing length ℓ , away from the wall, used by Pletcher and Nelson^{40,41}, was used in this investigation for some preliminary testing and is

$$\text{for } \ell > 0.089\delta \text{ replace by } \ell = .089\delta , \quad (2.13)$$

where δ is the thickness of a developing boundary layer. Even for a fully developed boundary layer this mixing length distribution has given good agreement for the velocity profiles and reasonable agreement for the friction factors⁴¹ (about 5% higher).

Once the turbulent viscosity is known, the turbulent conductivity is normally found by the assumption of unity turbulent Prandtl number. This

* See Pletcher and Nelson⁴¹ and McEligot et al⁴².

value has been advocated in previous investigations dealing with supercritical fluids. This assumption is probably a good one when the Prandtl number is close to unity. A value of 0.9 instead of unity has become popular in recent years in numerical studies of convective heat transfer. Accordingly, solutions were made with this value. This quantity is discussed in greater detail in Chapter VI.

2.5 Boundary Conditions and Starting Profiles

The equations of continuity, energy, and momentum require starting profiles and boundary conditions before a solution can be effected. Starting enthalpy profiles were constant in the problems considered. The velocity profiles, however, were not normally constant and these had to be generated by other means. In turbulent flow problems however, it is not necessary to know these precisely since downstream results are not very sensitive to the starting profiles. It was nevertheless necessary to ensure that these profiles were smooth and continuous in order to avoid instabilities in the numerical procedure. In a widely used numerical procedure⁴³, the starting velocity profiles normally follow from the $1/7^{\text{th}}$ power law. This is appropriate in numerical procedures where a one-dimensional analysis is used in the near wall region. In the present solution procedure, a starting profile was also required in the near wall region. In principle it should be possible to use a laminar law profile in the laminar sublayer and part of the transitional region (up to $y^+ = 11$), a log law in the rest of the transitional region and most of the turbulent region with perhaps a $1/7^{\text{th}}$ power law profile near the edge of the boundary layer. Such a procedure will however inevitably introduce discontinuities. A continuous profile due to Spalding⁴⁴ is also available. However, its use

was not convenient for this work because it appears to be implicit in velocity. Continuous profiles explicitly defining u were devised for the present work* but the method of generating the initial profiles by standard solution procedures has been preferred because the latter procedure is more consistent with equation (2.2). In a fully developed constant property pipe flow, the shear stress varies as

$$\tau = \tau_w r/R \quad (2.14)$$

Using these values of shear stresses and noting that the Van Driest hypothesis can be translated to yield

$$\frac{\partial u}{\partial y} = \left[-\mu + (\mu^2 + 4\tau\kappa^2\rho y^2 \{1 - \exp(-y^+/A^+)^2\})^{1/2} \right] / [2\kappa^2\rho y^2 \{1 - \exp(-y^+/A^+)^2\}] \quad (2.15)$$

The starting velocity profiles for pipe flow problems where the flow is fully developed before entering the solution regime can then be easily generated. In order to obtain the starting profile for flat plate problems, the shear stress τ is assumed to be constant at the starting location and equation (2.15) is solved for u up to a point where its solution matches with a $1/7^{\text{th}}$ power law profile.

In addition to starting profiles, the enthalpy and momentum equations require one boundary condition at each of its boundaries. These will either be of known enthalpy and velocity or a known gradient. Thus, at the wall where $y = 0$,

* e.g., $U^+ = B[1 - \exp(-y^+/B - (y^+)^{1.5}/100)]$; $B = 2.5 \ln(y^+ + 1) + 5.5$.

$$u = 0; v = 0; t = t_w \text{ or } \left. \frac{\partial t}{\partial y} \right|_{y=0} = q_w .$$

At a free stream boundary,

$$u = u_\infty; t = t_\infty$$

and at an axis of symmetry,

$$\frac{\partial u}{\partial y} = 0; \frac{\partial t}{\partial y} = 0 .$$

2.6 Concluding Remarks

The present model differs from a previous two-dimensional analysis³⁴ of supercritical fluids, first by the fact that additional terms have been added to account for viscous dissipation and buoyancy and second, the governing equations were used in their full form all the way to the wall. A one-dimensional analysis at the wall which is an important feature of the numerical procedure⁴³ adopted by Sastry^{34,45}, is made possible by neglecting convection in the laminar and transitional near wall region. This assumption has been widely tested and proven to be good for constant or moderately variable property fluids. However, for supercritical fluids when the pseudo-critical temperature lies in this region it appears that rapid changes in density will make this assumption unsuitable. What effect this has on the overall flow computation has not yet been sufficiently evaluated. One difficulty with using a one-dimensional analysis for supercritical fluids is that their wall shear stress behaviour is not known adequately either through standard correlations or experimental data. In the absence of this information, wall shear stresses in one-dimensional

methods can be found only by use of iterative schemes that do not always converge easily. With a two-dimensional analysis, this problem does not arise since in that case the wall shear stress can be found in a straightforward manner from the computed velocity profiles. A higher order turbulence model that was incorporated in the analysis is discussed in the next chapter.

III. TURBULENCE MODEL

3.1 General

A major limitation in prediction of turbulent flows is an imprecise knowledge of velocity and enthalpy correlations $\rho \overline{U_i U_j}$ and $\rho \overline{h U_j}$ respectively. Several different approaches to modelling these correlations may be found in the literature. So far, the various different forms of algebraic formulations have found the widest use. However, in recent years, a different class of turbulence models has gained in popularity. These involve a simultaneous solution of differential equations for quantities such as the kinetic energy of turbulence, dissipation, and Reynolds stresses*.

Although a significant improvement over the algebraic formulations, the alternative models of turbulence considered here have their limitations as well. It should be pointed out that turbulence modelling is not a rigorous theoretical effort. Exact equations are derived as a starting point and guide to modelling, but only those terms that can be exactly defined are retained. The remaining information is supplied through approximation and empiricism. However, it is felt that further improvements in turbulence modelling will come from this direction considering the fact that these models are presently undergoing a rapid development.

As already mentioned, only the high Reynolds number form of modelling will be considered. That is, the turbulence modelling will be applicable only in the fully turbulent region of the flow. For laminar and transi-

* See for example, Launder and Spalding³⁸, Launder, Reece, and Rodi⁴⁶, and Hanjalic⁴⁷ for multi-equation approach to turbulence modelling.

tional regions, the present study makes use of the Van Driest hypothesis. This was felt justifiable since modelling in this region has as yet made little progress even for constant property fluids. As further progress takes place in low Reynolds number regions, it can be added to the methods proposed in this investigation since the remaining equations are in any case solved in the laminar and transitional regions. Of the several different turbulence models comprising the multi-equation approach, the kinetic energy-dissipation ($K - \epsilon$) model^{*} appears to be adequate for the work carried out in this investigation. It permits the analysis to stay at a reasonably simple level and appears to compare in accuracy with some of the more involved turbulence models. The kinetic energy-dissipation model has already been formulated and much used for constant property fluids. The formulation of this model was re-examined here for application to supercritical fluids. This examination starts at the Reynolds stress equation. Although this equation is not used directly, it is required for introducing thin shear flow simplifications^{**} in the turbulence kinetic energy and dissipation equations. It also provides a necessary link between the desired correlations and the turbulent properties (kinetic energy and dissipation of turbulence). Further, the turbulence kinetic energy equation then does not have to be derived separately since it is a direct consequence of the Reynolds stress equation. All exact forms of the relevant equations were re-derived in this investigation for variable property flows since so

$$^* \epsilon = \nu \frac{\partial U_i}{\partial x_k} \frac{\partial U_i}{\partial x_k}; \quad K = \frac{1}{2} \overline{U_i U_i}.$$

$$^{**} \text{Thin shear flow simplifications imply } \hat{U}_1 \gg \hat{U}_2; \frac{\partial \hat{U}_1}{\partial x_2} \gg \frac{\partial \hat{U}_1}{\partial x_1}.$$

far, the literature has been concerned primarily with constant property situations. The turbulence correlations that arise because of the fluctuations in physical properties have been neglected in the derivations of this chapter in the same manner as they were neglected in Chapter II. However, it was deduced from the computed results (as discussed in Chapter VI) that a fluctuating property correlation that arises due to buoyancy (that is, $\overline{\rho' U_j g_i}$) in the Reynolds stress equation may not be negligible under the influence of free convective effects. This correlation was neglected because the primary interest in this investigation is forced convection and also because the science of turbulent free convection still appears to be at the development state for constant property fluids.

The Cartesian tensor notation is used in this section but towards the end of this chapter, the final equations employed in the numerical solution are also expressed in the conventional notation.

3.2 Reynolds Stress Equation

A comprehensive discussion of Reynolds stress equation^{*} and its closure for constant property fluids can be found in Launder et al⁴⁶. The same equation was derived in this investigation for variable property fluids. The details are provided in Appendix B.

An equation for fluctuating motion U_i is obtained by subtracting the Navier-Stokes equation from the Reynolds equation. The resulting equation is:

* An equation for the transport of Reynolds stresses $\overline{U_i U_j}$ is often called the Reynolds stress equation.

$$\frac{\partial \bar{U}_i}{\partial T} + \hat{U}_k \frac{\partial \bar{U}_i}{\partial X_k} = - \frac{1}{\rho} \frac{\partial p'}{\partial X_i} + \frac{1}{\rho} \frac{\partial}{\partial X_k} \left(\mu \frac{\partial \hat{U}_i}{\partial X_k} \right) - \bar{U}_k \frac{\partial \hat{U}_i}{\partial X_k} + \frac{1}{\rho} \frac{\partial}{\partial X_k} \left(\rho \bar{U}_i \bar{U}_k - \rho \hat{U}_i \hat{U}_k \right) . \quad (3.1)$$

Multiplying equation (3.1) by U_j and adding to it the corresponding equation for U_j multiplied by U_i , leads after rearrangement and averaging (as shown in Appendix B) to the Reynolds stress equation:

$$\begin{aligned} \frac{D \overline{U_i U_j}}{DT} = & - \left(\overline{U_j U_k} \frac{\partial \bar{U}_i}{\partial X_k} + \overline{U_i U_k} \frac{\partial \bar{U}_j}{\partial X_k} \right) && \text{(Production)} \\ & - 2\nu \overline{\frac{\partial U_i}{\partial X_k} \frac{\partial U_j}{\partial X_k}} && \text{(Dissipation)} \\ & + \frac{p'}{\rho} \left(\frac{\partial \bar{U}_i}{\partial X_j} + \frac{\partial \bar{U}_j}{\partial X_i} \right) && \text{(Pressure-strain or Redistribution)} \\ & - \frac{1}{\rho} \frac{\partial}{\partial X_k} \left[\rho \overline{U_i U_j U_k} - \mu \frac{\partial \overline{U_i U_j}}{\partial X_k} - p' (\delta_{jk} \bar{U}_i + \delta_{ik} \bar{U}_j) \right] && \text{(Diffusion)}. \end{aligned} \quad (3.2)$$

The preceding equations account for variation in properties ρ , μ , and ν but neglect the correlations with fluctuation in properties. The titles provided in brackets on the right-hand side are the physical interpretations usually associated with these terms. Except for some differences in the diffusion term, this equation is very much like its constant property counterpart. In the latter case, diffusion is normally represented as:

$$- \frac{\partial}{\partial X_k} \left[\overline{U_i U_j U_k} - \nu \frac{\partial \overline{U_i U_j}}{\partial X_k} + \frac{p'}{\rho} (\delta_{jk} \bar{U}_i + \delta_{ik} \bar{U}_j) \right] . \quad (3.3)$$

From a purely physical argument, this difference is reasonable since variations in density from point to point in the flow should influence

the turbulent diffusion process associated with the Reynolds stresses. It is fortunate that the remaining terms are alike indicating that similar modelling practices for these terms appear suitable. Accordingly as a preliminary step, these terms were modelled as in earlier works⁴⁶.

Viscous dissipation was described using Rotta's⁴⁸ result for isotropic turbulence with the assumption that fine scale motions are isotropic:

$$2\nu \overline{\frac{\partial U_i}{\partial x_k} \frac{\partial U_j}{\partial x_k}} = \frac{2}{3} \delta_{ij} \epsilon . \quad (3.4)$$

The pressure-strain correlation has been modelled by Launder et al⁴⁶ and Naot et al⁴⁹ using different approaches but with the same result. Namely:

$$\frac{p'}{\rho} \overline{\left(\frac{\partial U_i}{\partial x_j} + \frac{\partial U_j}{\partial x_i} \right)} = \phi_{ij,1} + \phi_{ij,2} , \quad (3.5)$$

where,

$$\phi_{ij,1} = -C_1 \frac{\epsilon}{K} \overline{U_i U_j} - \frac{2}{3} \delta_{ij} K , \quad (3.6)$$

$$\begin{aligned} \phi_{ij,2} = & -\frac{(C_2+8)}{11} \left(P_{ij} - \frac{2}{3} P \delta_{ij} \right) - \left(\frac{30 C_2-2}{55} \right) K \left(\frac{\hat{\partial U_i}}{\partial x_j} + \frac{\hat{\partial U_j}}{\partial x_i} \right) \\ & - \frac{(8 C_2-2)}{11} \left(D_{ij} - \frac{2}{3} P \delta_{ij} \right) , \end{aligned} \quad (3.7)$$

where,

$$P_{ij} = - \overline{U_i U_k} \frac{\hat{\partial U_j}}{\partial x_k} - \overline{U_j U_k} \frac{\hat{\partial U_i}}{\partial x_k} \quad (3.8)$$

$$D_{ij} = - \overline{U_i U_k} \frac{\partial \hat{U}_k}{\partial X_j} - \overline{U_j U_k} \frac{\partial \hat{U}_k}{\partial X_i}, \quad (3.9)$$

and

$$P = - \overline{U_i U_k} \frac{\partial \hat{U}_i}{\partial X_k}. \quad (3.10)$$

As pointed out by Launder et al⁴⁶, one or more terms in the pressure-strain correlation³⁷ may be removed without altering the essential feature that the term as a whole be redistributive. Therefore, they proposed a simpler version of the pressure-strain correlation:

$$\phi_{ij,2} = - \gamma (P_{ij} - \frac{2}{3} P \delta_{ij}). \quad (3.11)$$

This form is convenient because of its algebraic simplicity and appears adequate for algebraic stress modelling to be discussed later. Another reason for retaining the latter proposal is that there is considerable controversy regarding the value of C_2 in equation (3.7). However, when (3.11) is used, γ is found directly from Crow's⁵⁰ result for suddenly strained isotropic turbulence*. When the full pressure-strain correlation is used, Crow's result is satisfied irrespective of the value of C_2 ⁴⁶.

Presence of a nearby wall results in additional effects on the pressure-strain correlation. This effect was not considered in the present work because it was felt to be a minor consideration in the thin shear flow model to be used. Only one of the shear stresses is of interest in this model and its transport effects are found from the turbulent kinetic energy

* Equation (3.11) satisfies Crow's result when $\gamma = 0.6$.

equation. The pressure-strain correlation drops out entirely when the Reynolds stress equation is contracted to yield an equation for the turbulent kinetic energy. This is also expected from a physical point of view since the effect of the pressure-strain correlation is to redistribute turbulent kinetic energy from one component to another without influencing the overall balance of turbulent kinetic energy.

The diffusion terms have been treated⁴⁶ by assuming that pressure and viscous diffusion are negligible; a result that has found further confirmation by Irwin's experiments⁵¹. The task then remains to model the triple correlation appearing in equation (3.2). Various proposals for approximating $\overline{U_i U_j U_k}$ are reviewed by Wolfshtein, Naoi, and Lin⁵². The task of selecting or formulating this correlation in terms of known parameters was simplified in this analysis because the area of interest in this investigation is thin shear flows. A relatively simple proposal for this correlation is due to Daly and Harlow⁵³,

$$\overline{U_i U_j U_k} = - C'_s \frac{K}{\epsilon} \overline{U_k U_l} \frac{\partial \overline{U_i U_l}}{\partial x_l}. \quad (3.12)$$

The general validity of this equation was not questioned in this investigation because the only place it found use was in the reduction of equation (3.2) to the turbulent kinetic energy equation^{*}. In that case, this equation simplifies to a gradient diffusion hypothesis. That is, the rate of transport of turbulence energy is taken as proportional to the spatial gradient of the same quantity. This hypothesis appears to be physically realistic and has been used by several investigators starting from Prandtl⁵⁴.

* During the algebraic stress modelling simplifications, an explicit statement of diffusion is not required.

Therefore, equation (3.12) is retained here for the time being. Equation (3.12) has been used with just about equal success in thin shear flow computations as compared to another considerably more complex expression for diffusion by Launder et al⁴⁶.

Putting all these proposals together, the Reynolds stress equation can be written as:

$$\begin{aligned} \frac{D \overline{U_i U_j}}{DT} = & - \overline{U_j U_k} \frac{\partial \hat{U}_i}{\partial X_k} + \overline{U_i U_k} \frac{\partial \hat{U}_j}{\partial X_k} - \frac{2}{3} \delta_{ij} \epsilon - C_1 \frac{\epsilon}{K} (\overline{U_i U_j} - \frac{2}{3} \delta_{ij} K) \\ & + (\phi_{ij,1} + \phi_{ij,2}) + \frac{C'_s}{\rho} \frac{\partial}{\partial X_R} \left(\rho \frac{K}{\epsilon} \overline{U_k U_\ell} \frac{\partial \overline{U_i U_j}}{\partial X_\ell} \right). \end{aligned} \quad (3.13)$$

3.3 Turbulence Dissipation Equation

An equation for the dissipative correlation ϵ was obtained by the following procedure. Equation (3.1) is first differentiated by the operator $\frac{\partial}{\partial X_\ell}$ () and then multiplied by $\frac{\partial U_i}{\partial X_\ell}$. After some rearrangement and averaging, this results in the desired equation. Details of this derivation are shown in Appendix B. The dissipation equation is then:

$$\nu \frac{D(\epsilon/\nu)}{DT} = - \frac{\nu}{\rho} \frac{\partial}{\partial X_k} \left[\frac{\rho}{\nu} \overline{U_k \epsilon'} - 2 \frac{\partial U_i}{\partial X_\ell} \frac{\partial}{\partial X_\ell} \left(\overline{\frac{\partial U_i}{\partial X_\ell}} \right) \right] \quad (I)$$

$$+ 2\nu \frac{\partial U_i}{\partial X_\ell} \frac{\partial}{\partial X_\ell} \left(\frac{1}{\rho} \frac{\partial p'}{\partial X_i} \right) \quad (II)$$

$$- 2\nu \frac{\partial \hat{U}_i}{\partial X_k} \left(\overline{\frac{\partial U_i}{\partial X_\ell} \frac{\partial U_k}{\partial X_\ell}} + \overline{\frac{\partial U_\ell}{\partial X_i} \frac{\partial U_\ell}{\partial X_k}} \right) \quad (III) \quad (3.14)$$

$$- 2\nu \overline{u_k \frac{\partial u_i}{\partial x_\ell} \frac{\partial^2 u_i}{\partial x_k \partial x_\ell}} \quad (\text{IV})$$

$$- 2\nu \left[\overline{\frac{1}{\rho} \frac{\partial}{\partial x_k} \frac{\partial u_i}{\partial x_\ell} \frac{\partial}{\partial x_\ell} \left(\mu \frac{\partial u_i}{\partial x_k} \right)} \right] \quad (\text{V})$$

$$+ 2\nu \overline{\frac{\partial u_i}{\partial x_\ell} \frac{\partial}{\partial x_\ell} \frac{1}{\rho} \frac{\partial}{\partial x_k} \left(\mu \frac{\partial u_i}{\partial x_k} \right)} \quad (\text{VI})$$

$$- 2\nu \overline{\frac{\partial u_i}{\partial x_k} \frac{\partial u_i}{\partial x_\ell} \frac{\partial u_k}{\partial x_\ell}} \quad (\text{VII}) \quad (3.15)$$

The most outstanding difference between the present and constant property case is that it was possible to derive an equation for the ratio of dissipation to kinematic viscosity, ε/ν , rather than ε by a derivation procedure that is essentially similar to the constant property case.

Of the terms involving source and sink terms III and IV in equation (3.15) are the same as in the corresponding constant property dissipation equation. These have been shown to be negligible by Tennekes and Lumley⁵⁵. For the case of constant property fluids terms V and VI of equation (3.15) become equal to

$$- 2 \overline{\left(\nu \frac{\partial^2 u_i}{\partial x_k \partial x_\ell} \right)^2}.$$

Term VII is similar to its constant property form.

The source and sink terms were modelled collectively by Hanjalic and Launder⁵⁶ as follows:

$$- 2\nu \overline{\frac{\partial U_i}{\partial X_k} \frac{\partial U_i}{\partial X_\ell} \frac{\partial U_k}{\partial X_k}} - 2 \overline{\left(\nu \frac{\partial^2 U_i}{\partial X_k \partial X_\ell} \right)^2} = (C_{\epsilon 1} \frac{P}{\epsilon} - C_{\epsilon 2}) \frac{\epsilon^2}{K}. \quad (3.16)$$

The same expression was adopted in this investigation for terms V, VI, and VII of equation (3.15). Since the right-hand side of equation (3.16) does not contain any differential operators, it is difficult to conceive a different result for variable property fluids. A more rigorous treatment of the source-sink combination is difficult here because the modelling of equation (3.16) is a result of empirical information.

Terms I and II of equation (3.15) contribute towards the diffusion process. In these terms, the viscous diffusion and pressure diffusion were assumed to be negligible by Hanjalic and Launder⁵⁶ and the following formula was derived for $\overline{U_k \epsilon'}$:

$$\overline{U_k \epsilon'} = -C_\epsilon \frac{K}{\epsilon} \overline{U_k U_\ell} \frac{\partial \epsilon}{\partial X_\ell}. \quad (3.17)$$

For the case of thin shear flows, this equation reduces to a simple gradient diffusion hypothesis essentially similar to the gradient diffusion hypothesis for turbulent energy. However, equation (3.17) is not compatible with equation (3.15) since the variable under consideration is ϵ/ν rather than ϵ . Therefore, if equation (3.16) is modified to include the gradient of (ϵ/ν) rather than ϵ , the modelled dissipation equation for variable property fluids could be written as:

$$\nu \frac{D(\epsilon/\nu)}{Dt} = \frac{\nu}{\rho} \frac{\partial}{\partial X_k} \left(\rho C_\epsilon \frac{K}{\epsilon} \overline{U_k U_\ell} \frac{\partial \epsilon/\nu}{\partial X_\ell} \right) + (C_{\epsilon 1} \frac{P}{\epsilon} - C_{\epsilon 2}) \frac{\epsilon^2}{K}. \quad (3.18)$$

This compares with the constant property dissipation equation, which is

$$\frac{D}{DT}(\epsilon) = \frac{\partial}{\partial X_k} \left(C_\epsilon \frac{K}{\epsilon} \overline{U_k U_\ell} \frac{\partial \epsilon}{\partial X_\ell} \right) + \left(C_{\epsilon_1} \frac{P}{\epsilon} - C_{\epsilon_2} \right) \frac{\epsilon^2}{K} . \quad (3.19)$$

Without further examination, the additional modifications embodied in equation (3.18) must be tentative. A choice had to be made in this investigation between equations (3.18) and (3.19). The task of numerical computation is essentially similar in both cases and if the variations of kinematic viscosity are neglected in equation (3.18), it too becomes an equation for the transport of the dissipative correlation ϵ . In supercritical fluids, the properties μ and ρ vary rapidly around the critical point but fortunately the variations of ν is comparatively moderate as illustrated in Figure 7*. Therefore, as a first step variations in ν were neglected in equation (3.18). The variations in density however are still maintained inside the differential operation. Equation (3.19) has already been used successfully in moderately varying property situations**.

3.4 Algebraic Stress Modelling and Thin Shear Flow Simplifications

An attractive simplification of the Reynolds stress equation is a procedure termed algebraic stress modelling by Rodi⁵⁸. This simplification is effected in the Reynolds stress equation by introducing the assumption that variations in $\overline{U_i U_j}/K$ are small compared to variations in $\overline{U_i U_j}$ itself. Therefore, since

$$\frac{DK}{DT} - \Gamma(K) = P - \epsilon , \quad (3.20)$$

Hence,

* Dotted lines in Figure 7 arise because of uncertainty in precise values of viscosity (see Appendix A).

** See for example Khalil and Whitelaw⁵⁷.

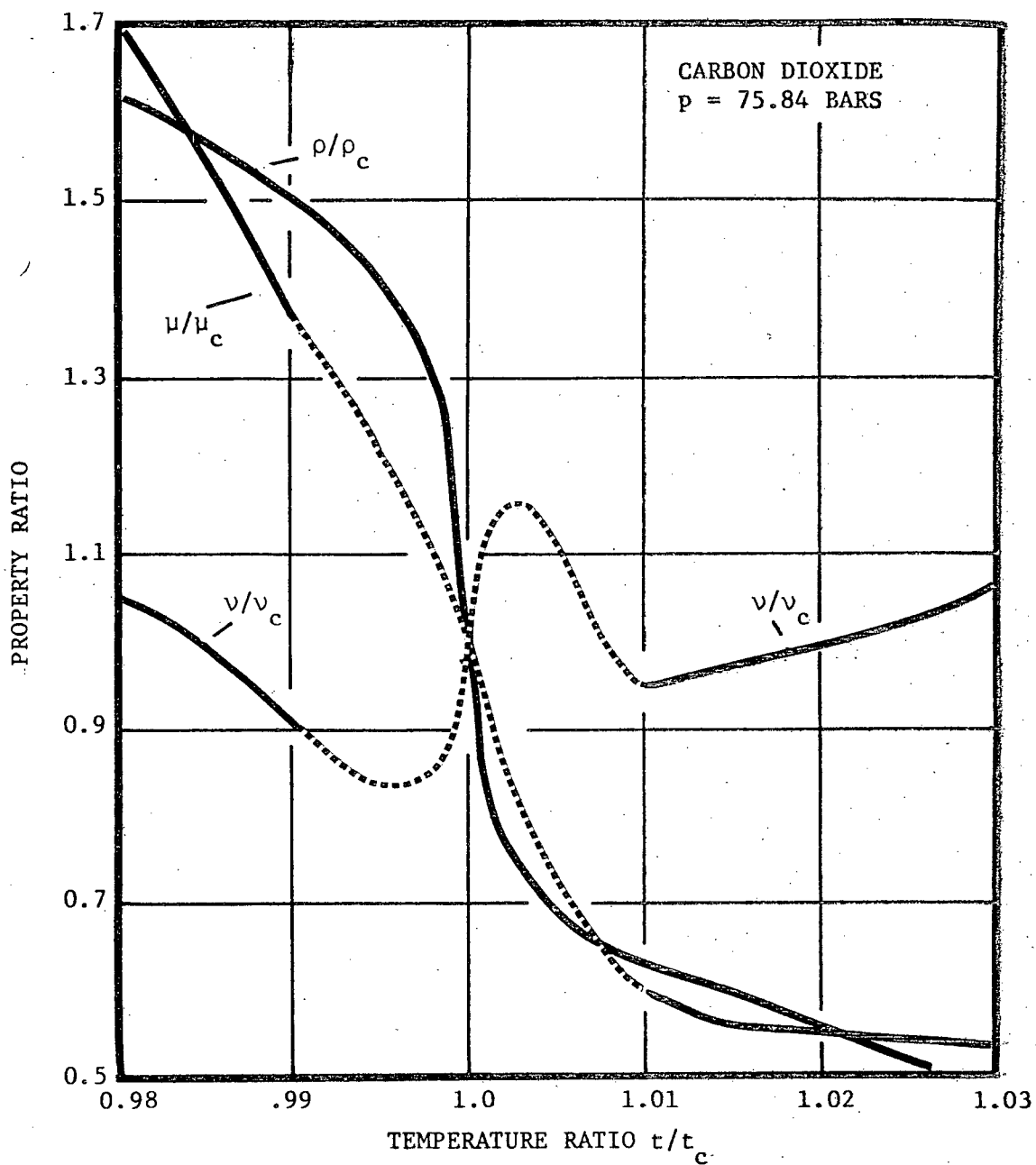


FIGURE 7. Properties of Carbon Dioxide Near the Pseudocritical Temperature.

$$\frac{D}{DT}(\overline{U_i U_j}) - \Gamma(\overline{U_i U_j}) = \frac{\overline{U_i U_j}}{K} (P - \epsilon) . \quad (3.21)$$

Introducing equation (3.21) in equation (3.13) yields an algebraic expression for the Reynolds stresses $\overline{U_i U_j}$,

$$\frac{\overline{U_i U_j} - \frac{2}{3} \delta_{ij} K}{K} = \frac{\Lambda}{E} (P_{ij} - \frac{2}{3} P \delta_{ij}) , \quad (3.22)$$

where

$$\Lambda = \frac{1 - \gamma}{(P/\epsilon - 1 + C_1)} .$$

In obtaining equation (3.22), the simpler version of the pressure-strain correlation equation (3.11) was used. Further simplifications for thin shear flows yields:

$$-\overline{U_1 U_2} = f(P/\epsilon) \frac{K^2}{\epsilon} \frac{\partial \hat{U}_1}{\partial x_2} , \quad (3.23)$$

where

$$f(P/\epsilon) = \frac{2}{3} (1 - \gamma) \frac{(C_1 - 1 + \gamma P/\epsilon)}{(C_1 - 1 + P/\epsilon)^2} . \quad (3.24)$$

Equation (3.23) makes possible the definition of an effective viscosity type of hypothesis. In the present study, a similar equation was derived using the full pressure-strain correlation. The final result bears the same features as equation (3.22) but in this case the function $f(P/\epsilon)$ is somewhat more complicated:

$$f(P/\epsilon) = \frac{1}{1815} \frac{f_2}{(P/\epsilon - 1 + C_1)^2}, \quad (3.25)$$

where,

$$f_2 = \left[33(30 C_2 - 2)(P/\epsilon - 1 + C_1) + 10\{(12 - 15 C_2)P/\epsilon + 11C_1 - 11\}(5 - 9C_2) \right]. \quad (3.26)$$

Details of the derivation are provided in Appendix B.

Equation (3.23) is the basis of the kinetic energy-dissipation model described by Launder and Spalding⁵⁹. In this model (which was at first probably conceived through physical arguments rather than through algebraic stress modelling), the function $f(P/\epsilon)$ is replaced by a constant. At first sight, this appears to be a drastic simplification of the algebraic stress model proposals. However, in actual practice, it does not make a significant difference whichever procedure is used. Preliminary calculations were made in this investigation using a constant value of $f(P/\epsilon)$ (equal to 0.09) as well as with equation (3.24). In the latter case, C_1 was assigned a value equal to 2.4863 so that $f(P/\epsilon)$ will be equal to 0.09 when the production to dissipation ratio is equal to unity. Computed results showed that there was no significant difference between the calculated velocity and temperature profiles. The reason for this is that in near wall flows, production to dissipation ratio retains a value close to unity in most of the calculation regions. However, towards the edge of the boundary layer it rapidly drops to zero but here the velocity gradients are very small and therefore errors in effective viscosity do not reflect in the calculated

results. Therefore, for the sake of simplicity, all calculations reported in this investigation were made with a constant value of $f(P/\epsilon)$ (equal to 0.09).

A knowledge of turbulence energy K and the dissipation ϵ is necessary before the required Reynolds stress can be computed through equation (3.23). These quantities are determined through differential equations which can be obtained in the following manner.

By a contraction of the tensor and introducing thin shear flow simplifications in equation (3.14), leads directly to the turbulence energy equation for such flows:

$$\frac{DK}{DT} = - \overline{U_1 U_2} \frac{\partial \hat{U}_1}{\partial X_2} - \epsilon + \frac{C'_s}{\rho} \frac{\partial}{\partial X_2} \left(\rho \frac{K}{\epsilon} \overline{U_2^2} \frac{\partial K}{\partial X_2} \right). \quad (3.27)$$

Now substituting $\overline{U_2^2}$ in accordance with algebraic stress model proposals and using a new constant σ'_K , equation (3.27) becomes:

$$\frac{DK}{DT} = \frac{1}{\rho} \frac{\partial}{\partial X_2} \left(\frac{\rho}{\sigma'_K} \frac{K^2}{\epsilon} \frac{\partial K}{\partial X_2} \right) - \overline{U_1 U_2} \frac{\partial \hat{U}_1}{\partial X_2} - \epsilon. \quad (3.28)$$

Similarly, the dissipation equation becomes

$$\frac{D\epsilon}{DT} = \frac{1}{\rho} \frac{\partial}{\partial X_2} \left(\frac{\rho}{\sigma'_\epsilon} \frac{K^2}{\epsilon} \frac{\partial \epsilon}{\partial X_2} \right) + (C_{\epsilon 1} \frac{P}{\epsilon} - C_{\epsilon 2}) \frac{\epsilon^2}{K}. \quad (3.29)$$

Or in line with the notation used in Chapter II, equations (3.28) and (3.29) can be rewritten as:

$$u \frac{\partial K}{\partial x} + v \frac{\partial K}{\partial y} = \frac{1}{\rho r^\alpha} \frac{\partial}{\partial y} \left(r^\alpha \rho \frac{K^2}{\epsilon \sigma'_K} \frac{\partial K}{\partial y} \right) - \overline{u'v'} \frac{\partial u}{\partial x} - \epsilon, \quad (3.30)$$

and

$$u \frac{\partial \epsilon}{\partial x} + v \frac{\partial \epsilon}{\partial y} = \frac{1}{\rho r^\alpha} \frac{\partial}{\partial y} \left(r^\alpha \rho \frac{\kappa^2}{\epsilon \sigma'_\epsilon} \frac{\partial \epsilon}{\partial y} \right) + (C_{\epsilon 1} \frac{P}{\epsilon} - C_{\epsilon 2}) \frac{\epsilon^2}{K} \quad (3.31)$$

Equations (3.30) and (3.31) involve four empirical constants. These are found by reference to standard sets of experimental data. They must necessarily have the same values as for constant property fluids if these equations are to have general validity. A recent study by Stephenson⁶⁰ for turbulent pipe flow uses the following values for the empirical constants:

$$\sigma'_K = 1.0/C_\mu, \quad \sigma'_\epsilon = 1.0/C_\mu, \quad C_{\epsilon 2} = 1.9, \text{ and } C_\mu = 0.09.$$

These values were also used in the present study. The function $f(P/\epsilon)$ is written as C_μ since it is regarded as a constant for the purpose of computations. Constant $C_{\epsilon 1}$ is then found by reference to near wall data in plane flows which yields the relationship,

$$\kappa^2 = \sigma'_\epsilon (C_{\epsilon 2} - C_{\epsilon 1}) C_\mu^{3/2} \quad (3.32)$$

In the present work, equation (3.32) was replaced by another similar equation. This is discussed in the next section. Equations (3.23), (3.30), and (3.31) comprise the kinetic energy-dissipation model of turbulence used for computations in this investigation.

3.5 Boundary Conditions for the Kinetic Energy-dissipation Model of Turbulence

Wall boundary conditions for the turbulence kinetic energy and dissipation equations are derived by noting that close to a wall convection and diffusion of turbulent kinetic energy can be neglected³⁸, and production

and dissipation of this quantity are nearly in balance. This leads to the following relation:

$$\epsilon = C_{\mu}^{1/2} K \frac{\partial u}{\partial y} . \quad (3.33)$$

In the laminar and transitional region close to the wall, use is made of the Van Driest hypothesis but at the point where the turbulence model takes over, the two regions are matched by equating the respective effective viscosities. This leads to the relation for this region,

$$C_{\mu} \rho \frac{K^2}{\epsilon} = \rho K^2 y^2 \frac{du}{dy} . \quad (3.34)$$

The point at which the two solutions are matched is sufficiently removed into the fully turbulent region so the exponential damping term was not necessary in equation (3.34). The region of matching was between $y^+ = 75$ and $y^+ = 150$ for most computations carried out in this investigation. Another relation that applies in this region is

$$\tau = \rho K^2 y^2 \left(\frac{\partial u}{\partial y} \right)^2 . \quad (3.35)$$

Equations (3.33), (3.34), and (3.35) can be combined to yield

$$\tau = C_{\mu}^{1/2} \rho K . \quad (3.36)$$

Further, to ensure complete consistency between the near wall and fully turbulent region, the practice in the past has been to use equation (3.32) for obtaining the numerical value of constant $C_{\epsilon 1}$. However, occasional instabilities in the solution caused a re-examination of equation (3.32) in the present study. It is possible that the problem never arose before

because of a different type of numerical solution procedure. Equation (3.32) was obtained with reference to plane flows where the shear stress close to a wall is nearly constant in the absence of a pressure gradient.

The relationship between the two empirical constants $C_{\epsilon 1}$ and $C_{\epsilon 2}$ was reformulated in the present study with reference to fully developed pipe flow. In this case, the shear stress distribution can be expressed as

$$\tau = \tau_w r/R . \quad (3.37)$$

Using this shear stress distribution and the results expressed in equations (3.33), (3.34), (3.35), and (3.36) in the relevant dissipation equation for constant property, fully developed pipe flow yields

$$\kappa^2 \left[1 + \frac{3y}{R} + \frac{3y^2}{R^2} \right] = \sigma'_\epsilon (C_{\epsilon 2} - C_{\epsilon 1}) C_\mu^{3/2} . \quad (3.38)$$

The procedure of obtaining equation (3.38) is given in Appendix B. There was no indication during the modelling of the dissipation equation that it is not generally valid for both plane and axisymmetric flows. Therefore, the differences between equation (3.32) and (3.38) appear contradictory. The most likely cause of this difference should then not be the dissipation equation itself but equations (3.34) and (3.35) which follow from the near wall algebraic formulation.

Let us therefore suppose that the near wall mixing length type distributions are different in plane and pipe flow and that in pipe flow it is expressed through

$$-\overline{u_1 u_2} = \kappa^2 y^2 \left(\frac{du}{dy} \right)^2 f(y)^2 , \quad (3.39)$$

where $f(y)$ is some unknown function. Now if the preceeding derivation is repeated using equation (3.39), then the value of $f(y)$ could be recovered. This would strictly involve solving a cumbersome differential equation. Fortunately, this does not have to be done. The value of $f(y)$ can be deduced approximately by an examination of equation (3.38). It should be

$$f(y) = \frac{1}{\sqrt{1 + \frac{3y}{R} + \frac{3y^2}{R^2}}} . \quad (3.40)$$

Therefore, the near wall mixing length distribution for pipe flow can then be expressed approximately as

$$\ell/R = \frac{\kappa y/R}{\sqrt{1 + 3y/R + 3y^2/R^2}} . \quad (3.41)$$

Equation (3.41) is compared with a well known empirical result due to Nikuradse for fully developed pipe flow,

$$\ell/R = 0.14 - 0.08(1 - y/R)^2 - 0.06(1 - y/R)^4 . \quad (3.42)$$

Table 3.1 compares some calculated values from three different proposals in the near wall region. The last column of Table 3.1 contains values according to the standard plane flow proposal. Equation (3.41) reduces to the plane flow equation when the radius R is large. The close agreement between the values contained in the first two columns of Table 3.1 appears to validate the argument presented in this section.

TABLE 3.1 Mixing Length Distribution in Turbulent Pipe Flow

y/R	ℓ/R Equation (3.41) (This Investigation)	ℓ/R Equation (3.42) Nikuradse	$\ell/R = 0.4 \ y/R$
0.01	0.0039	0.0039	0.0040
0.015	0.0059	0.0059	0.0060
0.02	0.0078	0.0078	0.0080
0.05	0.0186	0.0189	0.020
0.07	0.0253	0.0259	0.0280

A further comparison for the full pipe is illustrated in Figure 8. The close agreement almost throughout the pipe is surprising since the discussion and derivations of this section were only intended for the near wall region.

The procedure used for obtaining equation (3.41) may be of significance in other investigations where a mixing length distribution is required in flows of arbitrary but known shear stress variation. However, for this work, the main consideration was formulating consistent constants for the dissipation equation. In line with the previous argument, this can be done by using either of the following procedures:

- a) by using equation (3.42) as the near wall algebraic formulation for pipe flows and equation (3.32) for obtaining the value of $C_{\epsilon 1}$;
- b) by continuing the use of plane flow algebraic formulation but using equation (3.38) for obtaining the value of $C_{\epsilon 1}$.

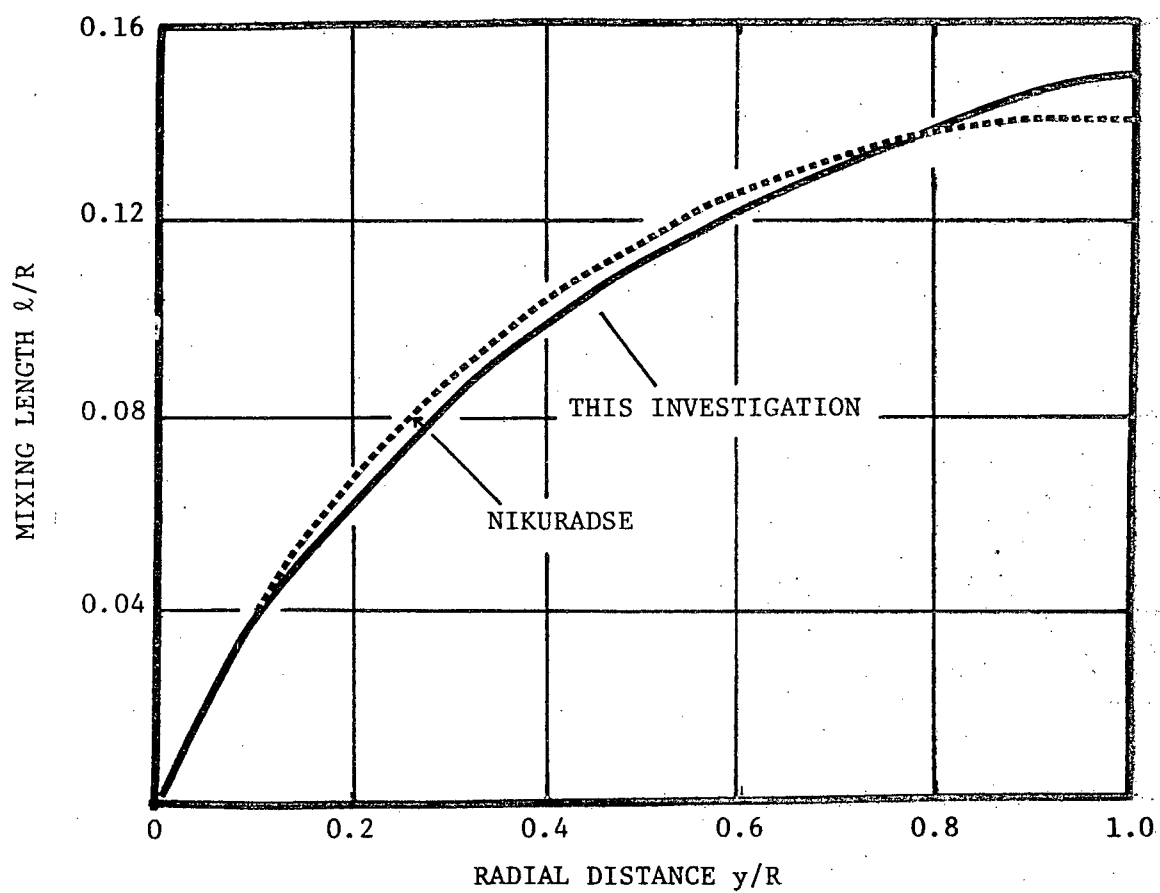


FIGURE 8. Mixing Length Distribution in Pipe Flow.

The first procedure has the advantage that it appears to be more correct. However, this is not a significant advantage since the value of y/R at the point where the two solutions are normally matched is small (about 0.05) and therefore the value of $C_{\epsilon 2}$ and the subsequent computed results should not be significantly different. The second procedure which is an approximation is computationally simpler. While developing the numerical solution procedure, computations were initially made with both equations (3.32) and (3.38) and the results were found to be of comparable accuracy. The latter procedure was finally selected for numerical solution because of its computational simplicity. Figure 9 shows the various possible values of $C_{\epsilon 1}$.

Starting profiles for the turbulent kinetic energy equation were found by fitting an arbitrary but smooth monotonic function between a known value close to the wall (equation (3.36)) and another at the axis of symmetry found by reference to Laufer's experimental data⁶¹. Starting dissipation profiles are then found through equation (3.32). There appears to be as yet no standard procedure for obtaining these profiles. However, the downstream computations are not normally very sensitive to inaccuracies in the starting profiles. This is illustrated in the next chapter in the section on preliminary results. It may be pointed out that in formulating the boundary conditions, the primary consideration was to obtain a workable procedure and that this area bears further inquiry.

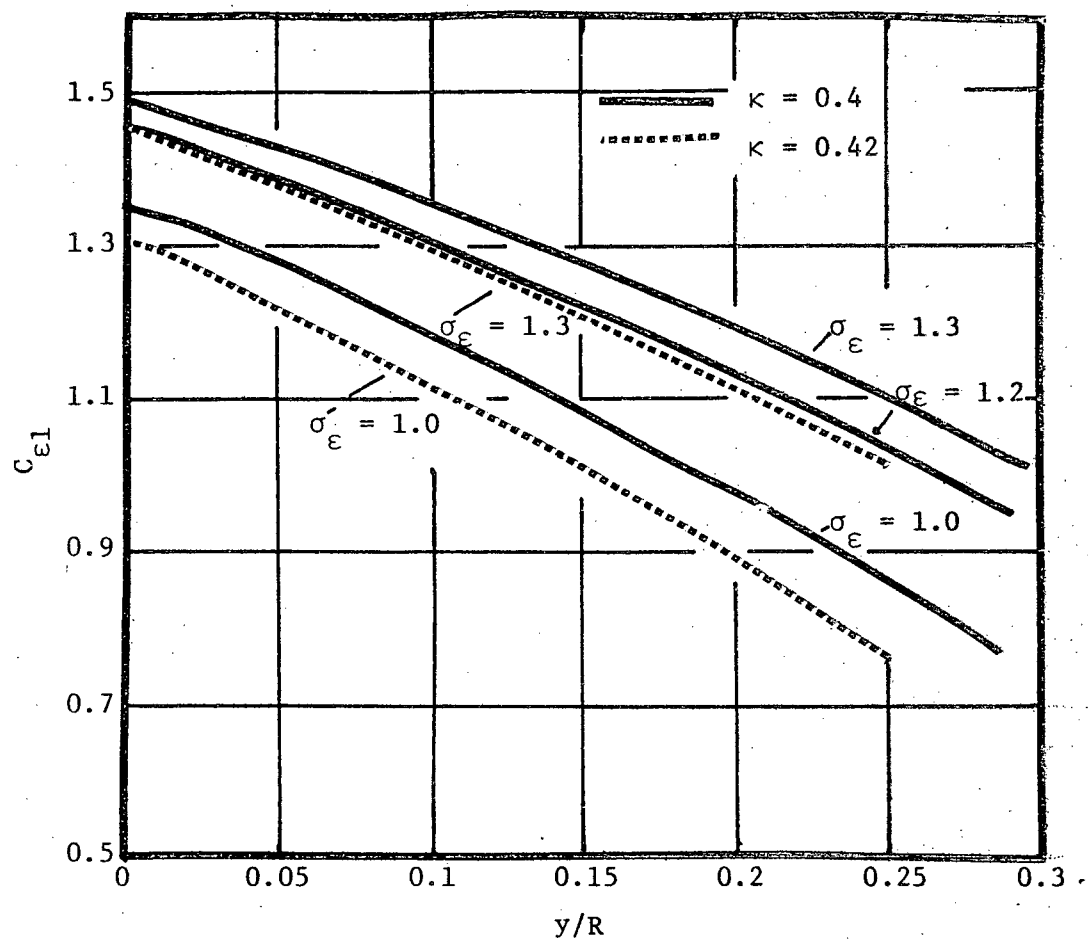


FIGURE 9. Constant $C_{\epsilon 1}$ for the Dissipation Equation.

3.6 Summary of Mathematical Formulation

TABLE 3.2 Summary of Mathematical Formulation

PRINCIPAL UNKNOWNNS	RELEVANT EQUATION IF ANY
v , cross-stream velocity	Equation (2.1)
u , stream-wise velocity	Equation (2.2)
h , enthalpy	Equation (2.3)
$\rho \overline{u'v'}$, turbulent shear stress	Equation (2.10) in the near wall region and equation (3.23) in the fully turbulent region
$\rho \overline{h'v'}$, turbulent heat flux	Equations (2.7) and (2.8)
p , pressure	Equation (2.9)
K , kinetic energy of turbulence	Equation (3.30)
ϵ , dissipation of turbulence energy	Equation (3.31)
ρ , density	Tabulated property data
C_p , specific heat	Tabulated property data
μ , viscosity	Tabulated property data
k , thermal conductivity	Tabulated property data

Chapters II and III describe the mathematical formulation used in the present study. The primary unknowns have been collected together in Table 3.2 along with the relevant relationships for these variables.

3.7 Concluding Remarks

It is apparent in review of this chapter that the multi-equation approach to turbulence modelling relies to a great extent on empiricism and approximation. Nevertheless, it was decided to make use of this approach in preference to the algebraic formulations for the following reasons:

- a) this approach is an improvement over the algebraic formulations, particularly so when abnormal phenomenon are encountered^{*};
- b) it is felt that this approach holds good prospects of future improvement;
- c) since this approach involves empiricism and approximation, an important test of its usefulness is its ability to predict known experimental results. So far in constant property situations, the agreement between predicted and measured results has been surprisingly good. It appeared worthwhile to test the same methods under the influence of severe property variations.

A number of different proposals are available for adoption in this area of turbulence modelling. Here the selection was governed by practical considerations. It was felt that the selected approach should be reasonably simple, at least as a first attempt of introducing this approach to an already complex phenomenon.

* An abnormal phenomenon encountered in supercritical heat transfer is the existence of maximas in velocity away from the axis of symmetry. In such situations, the mixing length type algebraic formulations imply zero turbulent fluxes at the location of the maximas. A heat flux equal to zero does not appear to be realistic.

IV. THE NUMERICAL PROCEDURE

4.1 General

Partial differential equations governing turbulent supercritical flows are non-linear and intricately coupled. The velocity u occurs in all the equations. The density ρ (which is a function of enthalpy) is also featured in all the equations. The dissipation ϵ appears in the turbulence energy equation K and vice versa, while the turbulent viscosity depends on both. Besides this simultaneity, there is no obvious equation from which pressure can be extracted. In such a situation, approximate analytical methods cannot be profitably employed and only numerical procedures appear to have any hope of success. In the past decade a certain number of numerical schemes have proven to be successful in handling two-dimensional turbulent flow problems. A review of the various methods available for the analysis of turbulent flow heat transfer has been made by Patankar and Spalding⁴³. The approach in this investigation was to select an existing numerical scheme and adapt its formulation for the problem being investigated.

4.2 Required Capabilities of the Numerical Procedure

Any numerical scheme for the problem must meet the following requirements:

- a) it should be applicable to two-dimensional turbulent flows and preferably allow for the treatment of both axisymmetric and plane flows;

- b) it should permit calculation of confined flows;
- c) it should be applicable to variable property flows;
- d) it should be efficient in terms of computer time usage so as to be a practically useful tool for both research and engineering design.

The procedure selected to satisfy these requirements is based on the DuFort-Frankel explicit finite difference formulation⁶². It has been developed and used for two-dimensional turbulent flows by Pletcher⁶³, and Pletcher and Nelson^{40,41}. It was selected in preference to the better known Patankar-Spalding procedure⁴³. The Patankar-Spalding procedure normally makes use of a one-dimensional analysis close to the wall which does not appear to be suitable for supercritical fluids. The Pletcher scheme has the advantage that it is very flexible and permits easy modification for testing a variety of different proposals. Being based on an explicit formulation, it permits an easier development of a computer code. An important point to note while selecting a numerical scheme is that existing computer codes cannot easily be used or modified and the only reasonable course is to develop a new code. In this regard, a simpler formulation is useful since already the problem is a complex one because of the fact that five partial differential equations and several auxiliary relationships constitute the physical model.

A point in favor of the Patankar-Spalding procedure was that it has already been tested on the kind of turbulence model being employed. However, this was not considered to be a major criterion for selection since it was felt that if a scheme is successful with the mixing length

type of algebraic formulations (such as the ones employed in Pletcher's scheme), it would also be successful with higher order turbulence models.

The numerical scheme selected has very good stability performance. Further, it does not make use of iterative or matrix-type solutions and is therefore reasonably efficient in computer time usage. A more complete treatment of the finite difference scheme can be found in the literature already quoted; only the important points are covered in this chapter.

4.3 Finite Difference Formulation

The grid selected was orthogonal. Spacing between consecutive grid lines in either x or y direction was varied but only gradually. If a central node is denoted as (I, J), remaining nodes around it are denoted as shown in Figure 10. Numbers next to each node are used to denote these points and were used in the computer program as consistently as possible. In order to solve for information at node 5, all information about the flow has to be known at nodes 1, 2, 3, and 4 and some at nodes 6 and 7 (density and velocities).

The finite difference formulation for the energy equation is as follows:

$$\begin{aligned} & \rho_{I,J} u_{I,J} \frac{(h_{I+1,J} - h_{I-1,J})}{\Delta x_+ + \Delta x_-} + \rho_{I,J} v_{I,J} \frac{(h_{I,J+1} - h_{I,J-1})}{\Delta y_+ + \Delta y_-} \\ &= u_{I,J} \frac{(p_{I+1} - p_{I-1})}{\Delta x_+ + \Delta x_-} + \frac{1}{R_J} \frac{2}{\Delta y_+ + \Delta y_-} \left[\frac{(R_{J+1} + R_J)}{4} \left\{ \frac{k_{eff\ I,J+1}}{C_{p\ I,J+1}} \right. \right. \\ & \quad \left. \left. + \frac{k_{eff\ I,J}}{C_{p\ I,J}} \right\} \left\{ \frac{h_{I,J+1} - 0.5(h_{I+1,J} + h_{I-1,J})}{\Delta y_+} \right\} \right] \end{aligned}$$

$$\begin{aligned}
& - \frac{(R_J + R_{J-1})}{4} \left\{ \frac{k_{\text{eff } I,J}}{C_{p \text{ } I,J}} + \frac{k_{\text{eff } I,J-1}}{C_{p \text{ } I,J-1}} \right\} \left\{ \frac{0.5(h_{I+1,J} + h_{I-1,J}) - h_{I,J-1}}{\Delta y_-} \right\} \\
& + \mu_{\text{eff } I,J} \left(\frac{u_{I,J+1} - u_{I,J-1}}{\Delta y_+ + \Delta y_-} \right)^2. \quad (4.1)
\end{aligned}$$

The convective and diffusion terms in the momentum and turbulence equations are described in a manner similar to that in the energy equation (4.1). The remaining terms in those equations are either algebraic or only contain first-order partial derivatives. Therefore, the finite difference formulations for the momentum and turbulence equations are constructed similarly. The momentum equation is:

$$\begin{aligned}
& \rho_{I,J} u_{I,J} \frac{(u_{I+1,J} - u_{I-1,J})}{\Delta x_+ + \Delta x_-} + \rho_{I,J} v_{I,J} \frac{(u_{I,J+1} - u_{I,J-1})}{\Delta y_+ + \Delta y_-} \\
& = - \frac{(p_{I+1} - p_{I-1})}{\Delta x_+ + \Delta x_-} + \frac{1}{R_J} \frac{2}{\Delta y_+ + \Delta y_-} \left[\frac{(R_{J+1} + R_J)}{4\Delta y_+} (\mu_{\text{eff } I,J+1} \right. \\
& \quad + \mu_{\text{eff } I,J}) \{ (u_{I,J+1} - 0.5(u_{I+1,J} + u_{I-1,J})) \} - \frac{(R_J + R_{J-1})}{4\Delta y_-} (\mu_{\text{eff } I,J} \\
& \quad + \mu_{\text{eff } I,J-1}) \{ 0.5(u_{I+1,J} + u_{I-1,J}) - u_{I,J-1} \} \left. \right] + g\rho_{I,J}. \quad (4.2)
\end{aligned}$$

The finite difference formulation for the turbulence kinetic energy equation is:

$$\begin{aligned}
& \rho_{I,J} u_{I,J} \frac{(K_{I+1,J} - K_{I-1,J})}{\Delta x_+ + \Delta x_-} + \rho_{I,J} v_{I,J} \frac{(K_{I,J+1} - K_{I,J-1})}{\Delta y_+ + \Delta y_-} \\
& = \frac{1}{R_J} \frac{2}{\Delta y_+ + \Delta y_-} \left[\frac{(R_{J+1} + R_J)}{4\Delta y_+} (\mu_{K \text{ } I,J+1} + \mu_{K \text{ } I,J}) \{ K_{I,J+1} \right. \\
& \quad - 0.5(K_{I+1,J} + K_{I-1,J}) \} - \frac{(R_J + R_{J-1})}{4\Delta y_-} (\mu_{K \text{ } I,J} + \mu_{K \text{ } I,J-1}) \{ 0.5(K_{I+1,J}
\end{aligned}$$

$$+ K_{I-1,J} - K_{I,J-1}) \} \Big] + \mu_{K I,J} \frac{(u_{I,J+1} - u_{I,J-1})^2}{\Delta y_+ + \Delta y_-} - \rho_{I,J} \epsilon_{I,J} , \quad (4.3)$$

and the dissipation equation

$$\begin{aligned} & \rho_{I,J} u_{I,J} \frac{(\epsilon_{I+1,J} - \epsilon_{I-1,J})}{\Delta x_+ + \Delta x_-} + \rho_{I,J} v_{I,J} \frac{(\epsilon_{I,J+1} - \epsilon_{I,J-1})}{\Delta y_+ + \Delta y_-} \\ &= \frac{1}{R_J} \frac{2}{\Delta y_+ + \Delta y_-} \left[\frac{(R_{J+1} + R_J)}{4\Delta y_+} (\mu_{K I,J+1} + \mu_{K I,J}) \{(\epsilon_{I,J+1} - 0.5(\epsilon_{I+1,J} \right. \\ & \quad \left. + \epsilon_{I-1,J})\} - \frac{(R_J + R_{J-1})}{4\Delta y_-} (\mu_{K I,J} + \mu_{K I,J-1}) \{0.5(\epsilon_{I+1,J} + \epsilon_{I-1,J}) \right. \\ & \quad \left. - \epsilon_{I,J-1}\} \right] + \left[c_{\epsilon 1} \mu_{K I,J} \frac{(u_{I,J+1} - u_{I,J-1})^2}{(\Delta y_+ + \Delta y_-) \rho_{I,J} \epsilon_{I,J}} - c_{\epsilon 2} \right] \frac{\epsilon_{I,J}^2 \rho_{I,J}}{K_{I,J}} , \quad (4.4) \end{aligned}$$

where the parameter $\mu_K = 0.09 \rho \frac{K^2}{\epsilon}$. The finite difference formulation for the continuity equation is:

$$\begin{aligned} & \frac{R_{J+1} + R_J}{4\Delta x_+ + \Delta x_-} \left[(\rho u)_{I+1,J+1} - (\rho u)_{I-1,J+1} + (\rho u)_{I+1,J} - (\rho u)_{I-1,J} \right] \\ & \quad + \frac{(\rho v R)_{I+1,J+1} - (\rho v R)_{I+1,J}}{\Delta y_+} = 0 . \quad (4.5) \end{aligned}$$

To obtain a pressure equation to be used in conjunction with the partial differential equations, the method devised by Pletcher and Nelson⁴¹ was used. In this method, the momentum equation is rearranged to yield $u_{I+1,J}$ explicitly and then multiplied by $\rho_{I,J}$. This equation is then integrated over the cross-section of the pipe or channel and equated to the known mass flow rate. Since the pressure is only a function of the axial location, it can be factored out of the integration to yield a

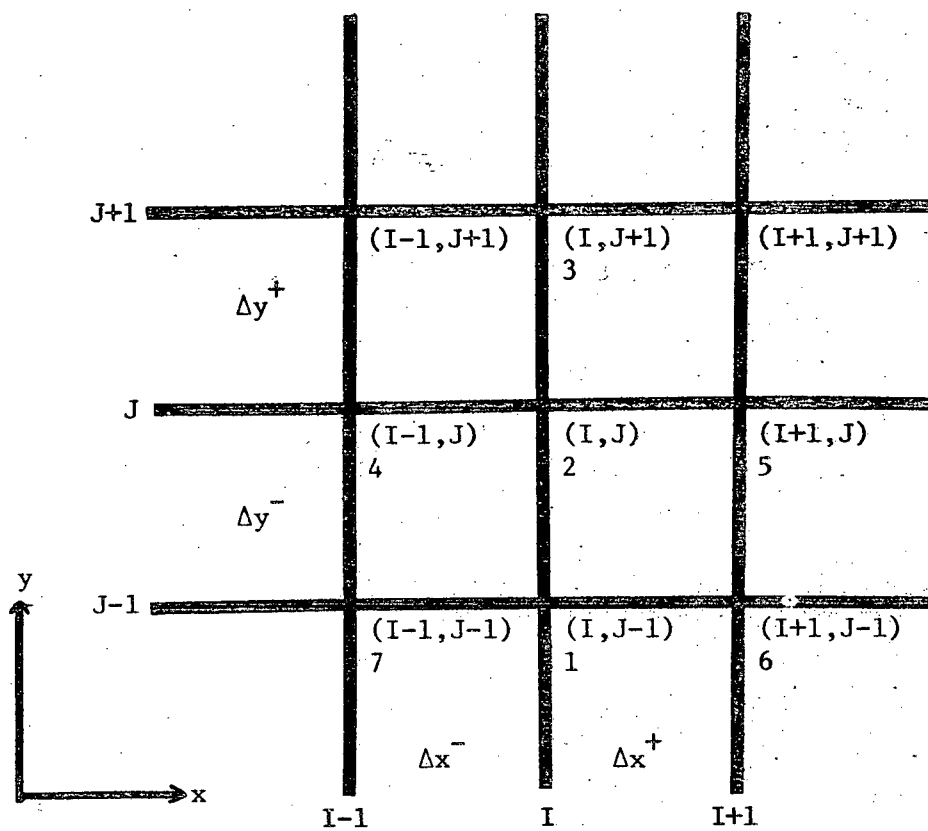


FIGURE 10. The Finite Difference Grid.

pressure equation,

$$G = \int_A \rho_{I,J} u_{I+1,J} dA = \int_A \frac{PB}{PA} dA + (p_{I+1} - p_{I-1}) \int_A \frac{PC}{PA} dA, \quad (4.6)$$

where: $PA = 4\rho_{I,J} u_{I,J} R_J (\Delta y_+ + \Delta y_-) \Delta y_+ \Delta y_-$

$$+ (\Delta x_+ + \Delta x_-) \Delta y_- (R_{J+1} + R_J) (\mu_{eff\ I,J+1} + \mu_{eff\ I,J})$$

$$+ (\Delta x_+ + \Delta x_-) \Delta y_+ (R_J + R_{J-1}) (\mu_{eff\ I,J} + \mu_{eff\ I,J-1}), \quad (4.7)$$

$$PB = -4\rho_{I,J}^2 R_J \Delta y_+ \Delta y_- (\Delta x_+ + \Delta x_-) v_{I,J} (u_{I,J+1} - u_{I,J-1})$$

$$+ 2\rho_{I,J} (\Delta x_+ + \Delta x_-) \Delta y_- (u_{eff\ I,J+1} + u_{eff\ I,J})$$

$$+ (u_{I,J+1} - 0.5 u_{I-1,J}) (R_{J+1} + R_J)$$

$$+ 2\rho_{I,J} (\Delta x_+ + \Delta x_-) \Delta y_+ (\mu_{eff\ I,J} + \mu_{eff\ I,J-1}) (u_{I,J-1}$$

$$- 0.5 u_{I-1,J}) (R_J + R_{J-1})$$

$$+ 4\rho_{I,J}^2 u_{I-1,J} u_{I,J} R_J (\Delta y_+ + \Delta y_-) \Delta y_+ \Delta y_-$$

$$+ 4\rho_{I,J}^2 R_J (\Delta x_+ + \Delta x_-) (\Delta y_+ + \Delta y_-) \Delta y_+ \Delta y_- \quad (4.8)$$

and $PC = -4\rho_{I,J} R_J (\Delta y_+ + \Delta y_-) \Delta y_+ \Delta y_- \quad (4.9)$

In equation (4.6), $u_{I+1,J}$ is multiplied with $\rho_{I,J}$ instead of $\rho_{I+1,J}$ because the latter quantity remains unknown until ρ_{I+1} is determined. Once $\rho_{I+1,J}$ is determined, an iterative correction for the mass flow rate can be carried out. However, this is not necessary because the finite difference formulation requires a fine grid for convergence so the errors incurred by the use of $\rho_{I,J}$ in equation (4.6) are negligible.

4.4 Method of Solution

It should be pointed out that although the preceeding finite difference formulations were written for axisymmetric configurations, they are also valid for plane flows when all R's are assigned a value equal to unity.

Briefly, the method of solution was as follows. First, all the equations were rearranged to exhibit the relevant unknown variable explicitly. Thus for example, equation (4.1) was rearranged so that only the unknown enthalpy $h_{L+1,J}$ was on the left-hand side. In this form, the equations are ready for a solution. Once all the variables are known at two previous grid lines (i.e., at I and I-1 locations), then the equations can be solved one at a time to yield the required information for all J's at an 'I+1' location. The order in which the equations are solved is pressure equation, momentum equation, energy equation, continuity equation, turbulence kinetic energy equation, and finally dissipation equation. The turbulent fluxes are formulated through algebraic relationships prior to the solution of these equations. Property values are computed at each 'I+1' location after the solution of the energy equation but prior to the solution of the continuity equation since the continuity equation requires the value of density at the 'I+1' grid location. The solution then progresses to the next grid line. More description about the solution procedure is provided in Appendix C and D.

It may be noted that information about the flow is required at two previous grid lines. Normally such information is available, but if it is not (as sometimes may be the case at a starting location), then a standard explicit formula that requires information at only one previous loca-

tion was used at the first step. Standard explicit formulations are also embodied in the computer program but their use was minimised because they have poor stability performance as compared to the DuFort-Frankel formulation.

Properties are stored in tabular form at each pressure. The property tables were divided in equal increments of enthalpy rather than at equal temperature intervals. The former procedure is superior because it permits for greater number of divisions around the pseudo-critical temperature where the property variation is steep. Property values at known enthalpies or temperature are found by linear interpolation.

Once all variables are computed at internal nodes along an $I+1$ grid line, wall values are found by imposing the appropriate boundary conditions. These are mostly of the gradient type for the energy equation. Wall values in that case are found by,

$$t_{I,1} = t_{I,2} - \frac{\Delta y q_w}{k_{I,1}} \quad (4.10)$$

This simple relationship was felt to be sufficient since whenever any of the partial differential equations contain a gradient type boundary condition, the y grid has to be very fine close to the wall (with y^+ equal to about unity) in order to secure convergence.

Starting velocity and enthalpy profiles are found through relationships described in Chapter II in the section on boundary conditions. Equation (2.15) is solved through a forward difference formula in order to obtain the starting velocity profile in pipe flow problems. For the starting turbulence kinetic energy profile, certain empirical relationships

were tried^{*}, but finally a simpler practice was adopted:

$$K = A_1 U + A_2. \quad (4.11)$$

The constants A_1 and A_2 are found by a knowledge of the kinetic energy at two locations. Near the wall, kinetic energy is known through equation (3.35) and at the center of a pipe with fully developed flow conditions, it was assigned a value equal to $0.84 \tau_w / \rho$, found by reference to Laufer's experimental data⁶¹. Equation (4.11) automatically satisfies the symmetry boundary condition and follows the correct trend. This simpler practice was felt to be adequate since downstream results are not very sensitive to starting profiles in turbulent flow problems. In the next section, the results of a computation are illustrated in which the starting K profile was intentionally kept somewhat inaccurate. The starting dissipation profile is found through equation (3.32), a practice that has often been used in other studies (e.g., Laufer et al⁴⁶). It may be recalled that the fluid is unheated before entering the solution region and as a result behaves like a constant property fluid at the starting location.

The present solution procedure is applicable to both laminar and turbulent flows. For laminar flows, the only change that has to be made is to equate the turbulent component of effective viscosity to zero. The main difference in solving various types of problems is the way in which grid spaces are arranged. If an extremely fine grid were to be used, various different kinds of grid spacings would yield convergence. This would be a

* An approximate empirical relationship designed in this investigation to describe Laufer's experimental data⁶¹ for fully developed pipe flows is:

$$K / \frac{\tau_w}{\rho} = 3.9 + 3.6(y/R) - 7.9(y/R)^2 + 4.72(y/R)^3 - 3.5(y/R)^{0.56}.$$

costly procedure. Therefore, grids lines are arranged in a manner so as to secure convergence with the coarsest possible grid. The spacing between the grid lines is varied in such a way that the flow regions with the steepest variations (such as near wall regions in turbulent flows) contain the most nodes. The particular manner in which this is done for different types of flows is indicated alongside the preliminary results discussed next.

4.5 Preliminary Results

The computer program was developed in stages and verified thoroughly at each step. The program development can be approximately categorized in three steps:

- a) development of subroutines for solution of momentum, continuity, and energy equations;
- b) addition of a turbulence viscosity subroutine based on algebraic formulations;
- c) addition of subroutines for solution of pressure, kinetic energy, and dissipation equations.

Several tests were conducted during the development of the program. Some of the more important ones are reported here. During most of the preliminary testing, variation of properties was suppressed by using constant values through the property subroutine.

4.5.1 Laminar Flow Along a Flat Plate

In order to test the formulation of the continuity and momentum equations, boundary conditions were simulated to correspond with the

Blasius flat-plate problem. The leading edge of the plate was at $x=0$, the plate being parallel to the x -axis. A solution was attempted starting from the leading edge and uniform streamwise velocities were imposed at the starting location.

Before grid spacings can be decided, some idea of the length scales involved is necessary. In most boundary layer problems, this scale is taken to be of the order of the boundary layer thickness at the starting location and then the grid lines in both x and y directions are spaced in some proportion of the boundary layer thickness. However, the flat plate problem is unique because the starting location is the leading edge where boundary layer thickness is zero. Therefore, an alternative length scale was devised by reference to laminar boundary layer theory. This length scale was taken to be equal to the thickness of the boundary layer at a downstream distance equal to the boundary layer thickness. Such a situation occurs only once very close to the leading edge during the development of the boundary layer and occurs at a distance of approximately $25 \nu/U_\infty^*$. Having obtained a length scale, the next step was to devise the grid spacing. Equal divisions in the cross-stream direction were adopted as suggested by Pletcher⁴¹. The grid lines in the cross-stream direction were spaced at distances equal to $6 \nu/U_\infty$. For the streamwise divisions, most of the previous numerical studies have suggested a step size proportional to the boundary layer thickness ($\Delta x = A_x \delta$). The constant of proportionality in this example was assigned a value equal to 0.5, although this rule does not apply at the leading edge. At the leading edge, a step size equal to $9 \nu/U_\infty$ was

* Since $\delta \sim 5 \sqrt{\frac{\nu x}{U_\infty}}$, the length scale is found from $x \sim 25 \frac{\nu}{U_\infty}$ or $x \sim 25 \frac{\nu}{U_\infty}$.

selected. The main criterion for obtaining these divisions was to ensure that at least one nodal point lies within the boundary layer at the first grid line downstream from the leading edge. The manner of obtaining the final grid spacings was this: what was believed to be a conservative grid division along the X-axis was decided first, then the spacing along the Y-axis was narrowed successively until convergence was secured some distance downstream from the leading edge. The final grid spacing thus found worked well for widely different values of free-stream velocity and fluid properties. The solution found in this way was in error by about 10% at the first step away from the leading edge and then progressively improved in the downstream direction until the Blasius velocity profile was achieved.

Figure 11 compares the computed values with the results due to L. Howarth^{*}. The agreement here can be seen to be satisfactory. Hence, it was concluded that the continuity and momentum equations are properly formulated and that the program was functioning well up to this stage.

A subroutine for solving the energy equation was then introduced in the computer program. Thermal boundary conditions in this case were a uniform initial temperature profile and an isothermal wall. The previous grid spacing was retained in this case. The results are shown in Figure 12. The agreement here too was surprisingly good. The next step was to try the program for turbulent flows.

4.5.2 Turbulent Flow Along a Flat Plate

It will be noted in Chapter II that the general form of the

^{*} See Schlichting⁶⁴.

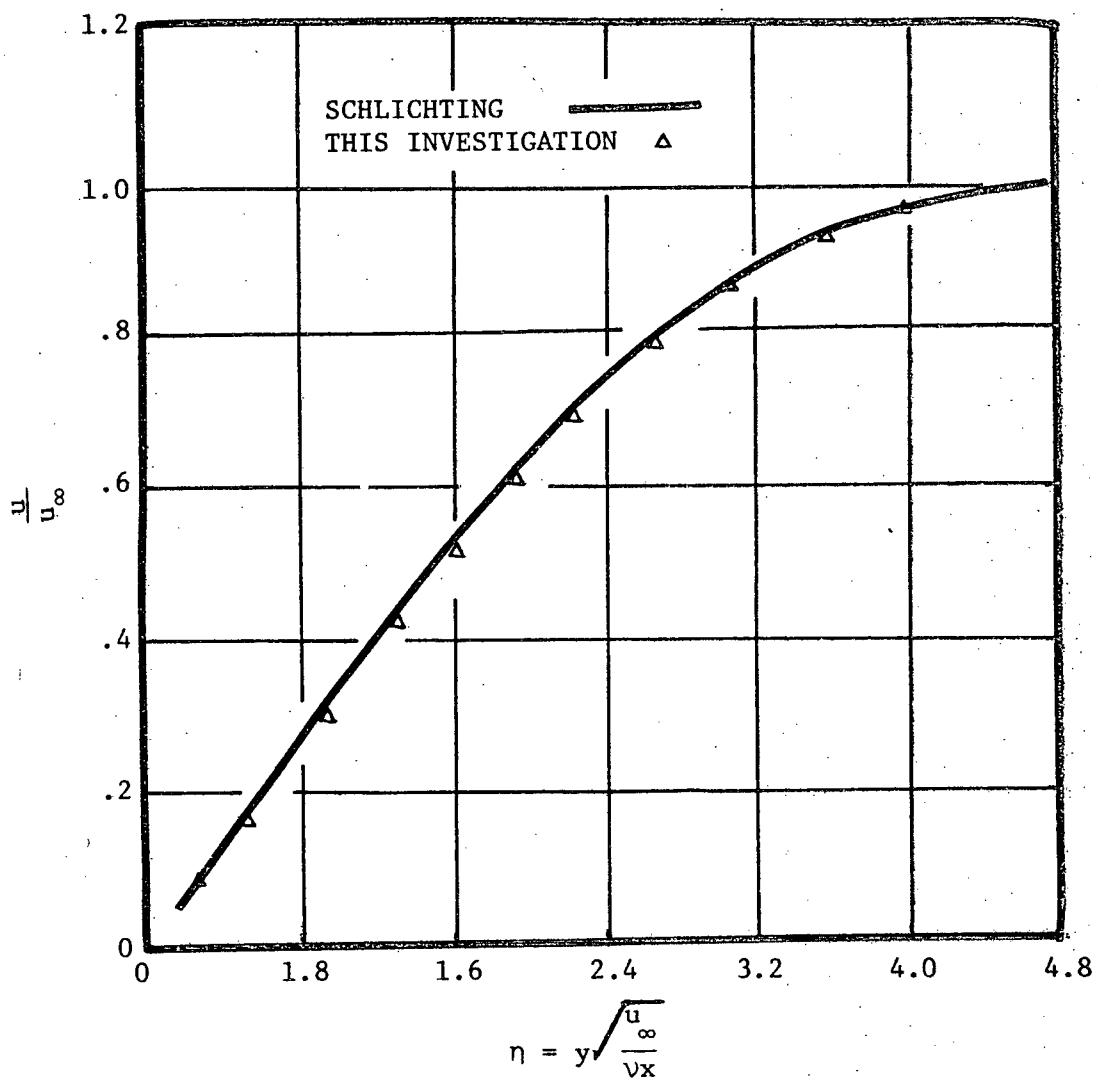


FIGURE 11. Blasius Velocity Distribution in the Boundary Layer Along a Flat Plate.

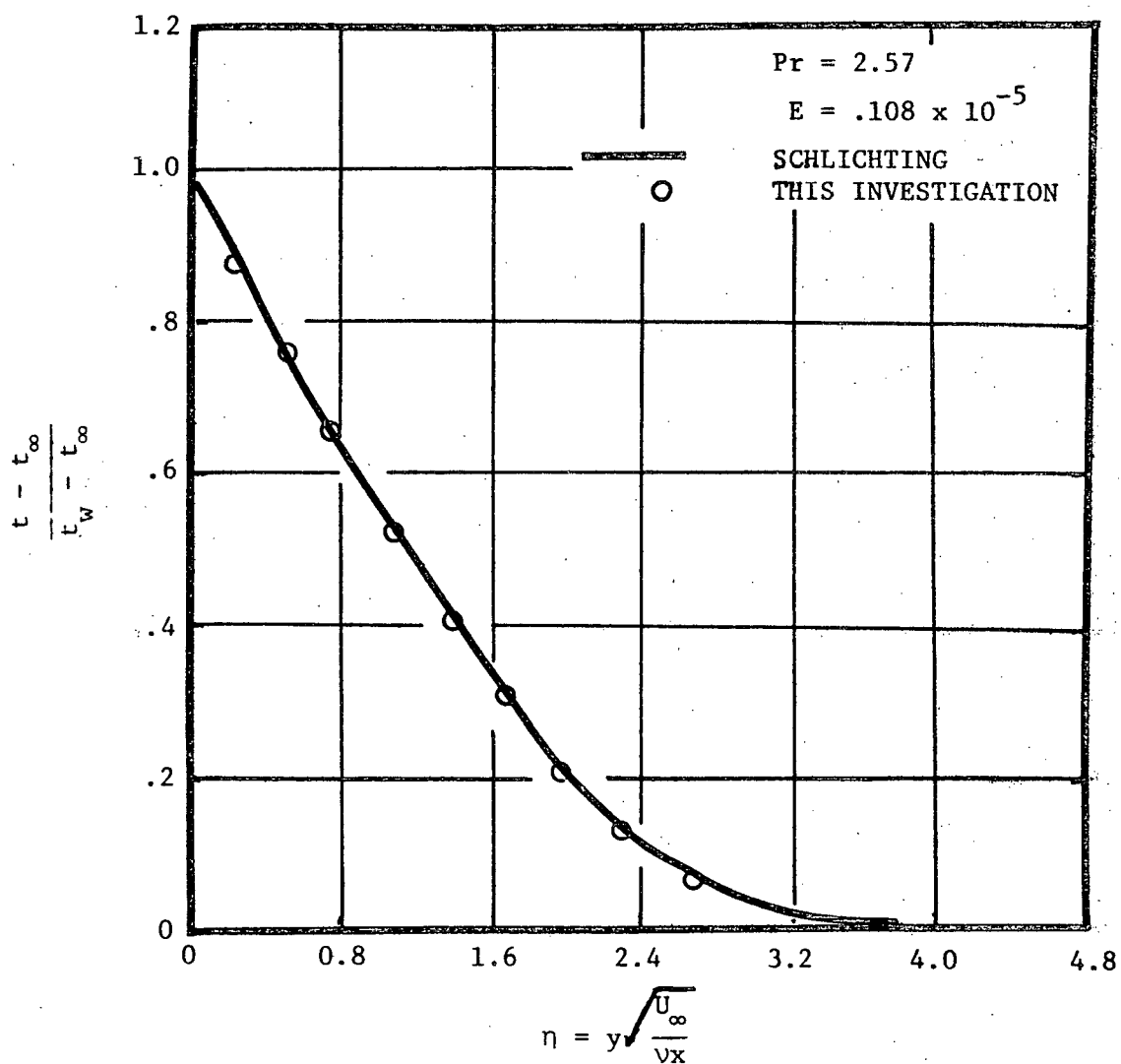


FIGURE 12. Temperature Distribution on a Heated Flat Plate at Small Eckert Number for $Pr = 2.57$.

governing equations is the same in both laminar and turbulent flows. The only change is in the values of the effective viscosity. Accordingly, a subroutine based on the algebraic formulations of Chapter II was added to the program for computing the turbulent viscosity.

The problem attempted was flow over a smooth flat plate. In this case, however, the solution was started some distance downstream from the leading edge. Starting profiles of velocity, u were found as discussed in Chapter II. The normal velocity v at the starting location was computed through the use of the standard explicit formulation used in conjunction with the starting u profiles.

Since the variation of velocity near the wall is very steep in turbulent flows, the grid spacings in the y direction are normally kept in geometric progression rather than equal divisions as in the laminar case. The nodal points in the y direction are found from the relation⁶³:

$$y_{I,J} = A_y y_{I,J-1} \quad (4.12)$$

A_y was prescribed a value of 1.1 in this case. It is also necessary to ensure that the first node nearest the wall lies within the laminar sub-layer ($y^+ < 5$). Grid spacing in the streamwise direction were found in the same way as in the laminar flow problem,

$$\Delta x = A_x \delta_x \quad (4.13)$$

A value of .65 for A_x was found to be adequate in this case. At the starting location about thirty nodal points lay within the boundary layer. These increased progressively with the growth of the boundary layer in a manner implied by equation (4.12). The universal velocity profile given by

Kays⁶⁵ was chosen as a reference for comparison. The universal velocity profile is given by:

$$\begin{aligned} u^+ &= y^+ \text{ for } y^+ < 5, \\ u^+ &= -3.05 + 5.0 \ln y^+ \text{ for } 5 \leq y^+ \leq 30, \\ u^+ &= 5.5 + 2.5 \ln y^+ \text{ for } y^+ \geq 30. \end{aligned} \quad (4.14)$$

The profile obtained from equation (4.14) is compared with the computed profile in Figure 13. It can be seen that the result is satisfactory.

Wall shear stress values and the growth of the boundary layer were also checked to see that they satisfied the following relationships approximately (Figure 14):

$$\frac{\delta}{\delta_o} = \left(\frac{x}{x_o} \right)^{0.8}, \quad (4.15)$$

$$\frac{\tau_o}{\tau} = \left(\frac{x}{x_o} \right)^{0.2}. \quad (4.16)$$

The next stage was to add a subroutine for the pressure equation and test the program on confined flows.

4.5.3 Turbulent Flow in a Pipe

At this stage, a subroutine for the solution of the pressure equation (4.6) was introduced in the computer program. After some initial runs with the algebraic formulations for effective viscosity subroutines for the solution of kinetic energy and dissipation were added to the computer program. This completed the development of the solution procedure as

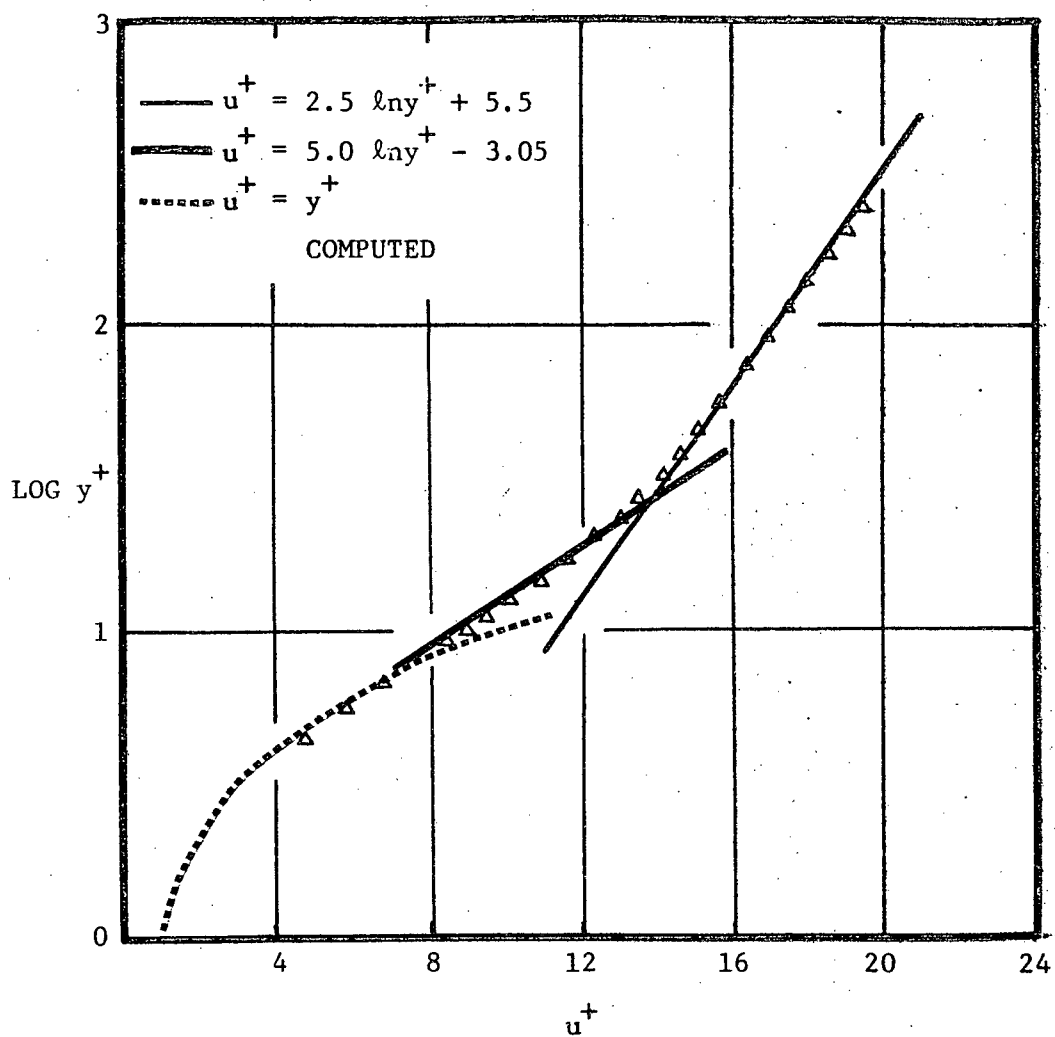


FIGURE 13. Velocity Distribution in a Turbulent Boundary Layer Along a Flat Plate.

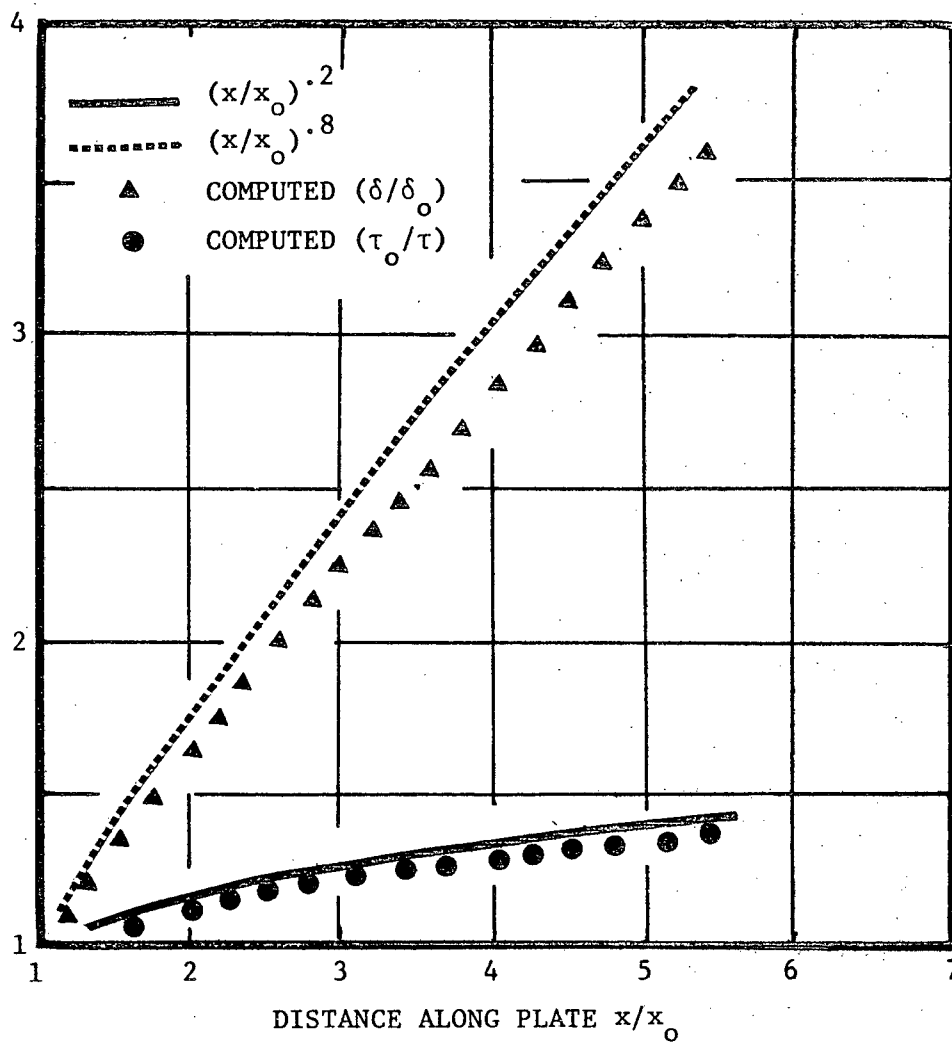


FIGURE 14. Growth of a Turbulent Boundary Layer and Decline of Shear Stress Along a Plate.

required in this investigation. Some examples from constant property pipe flow computations are described next.

Starting profiles in this case corresponded to hydrodynamically fully-developed flow conditions and constant starting enthalpy profiles. A constant wall heat flux boundary condition was imposed.

Grid lines in the cross-stream direction were divided according to equation (4.12). The only difference in this case is that the constant A_y is determined in such a way that the prescribed number of nodes cover the entire pipe. In most problems covered in this investigation, about 100 nodes along a diameter of the pipe were found to be adequate. The numerical solution has to be carried out at only half of these nodal points since the rest follow from symmetry. Divisions in the streamwise direction were found in accordance with equation (4.13). The value of A_x in pipe flow problems was kept between 0.3 and 0.65 depending on the particular problem. High heat flux cases require lower values of A_x . However, in the initial portion of the thermal entry length, A_x was kept much smaller and increased gradually in a geometric progression. This is necessary because of a rapid change in wall temperature close to the starting location. For the particular example illustrated in this section, A_x was equal to 0.5. The first streamwise step was kept equal to $y_{1,2}$ and increased in ratios of 1.2 until the streamwise step became equal to a value indicated by equation (4.13).

An expression for Nusselt numbers due to Bankston and McEligot as reported by Sastry⁴⁵ was used as a reference for comparison. They recommended the following equation for air:

$$\text{Nu}_\infty = 0.259 \text{ Re}^{0.725} \text{ Pr}^{0.4} . \quad (4.17)$$

This comparison is illustrated in Figure 15. The computed values of Nu_∞ are lower than that indicated by equation (4.17). However, it appears that in this range of Reynolds numbers, equation (4.17) overpredicts the Nusselt number by about 6%. Experimental data of Kays⁶⁵ as well as Mills⁶⁶ suggest a value of Nusselt number approximately equal to 177 at $\text{Re} = 1.026 \times 10^5$. The computed value of Nu_∞ is about 173. Similarly, at a Reynolds number of 50,000, equation (4.17) appears to slightly overpredict the data (by about 3.5%)⁶⁵. Therefore, it was concluded that the computed results are as satisfactory as can be expected.

Next, a test run was made with a somewhat inaccurate starting profile of turbulence kinetic energy. The starting profile was determined in this manner: in order to find the values of constants A_1 and A_2 of equation (4.11), the kinetic energy at the axis of symmetry was assigned a value equal to $0.1 \tau_w / \rho$ instead of the usual $0.84 \tau_w / \rho$. Strictly if the program is functioning well, the correct values of kinetic energy K should be achieved at a downstream location starting from any arbitrary values. However, the starting profile should not be such that it causes large instabilities in the solution procedure. Figure 16 shows that the inaccuracies in the starting profile appear to be corrected at thirteen diameters downstream from the starting location.

The final result included in this section is the velocity distribution in pipe flow. Equation (4.11) was again used as a reference for comparison. The results are shown in Figure 17. A correct prediction of the velocity distribution is essential because in a way, it plays a controlling

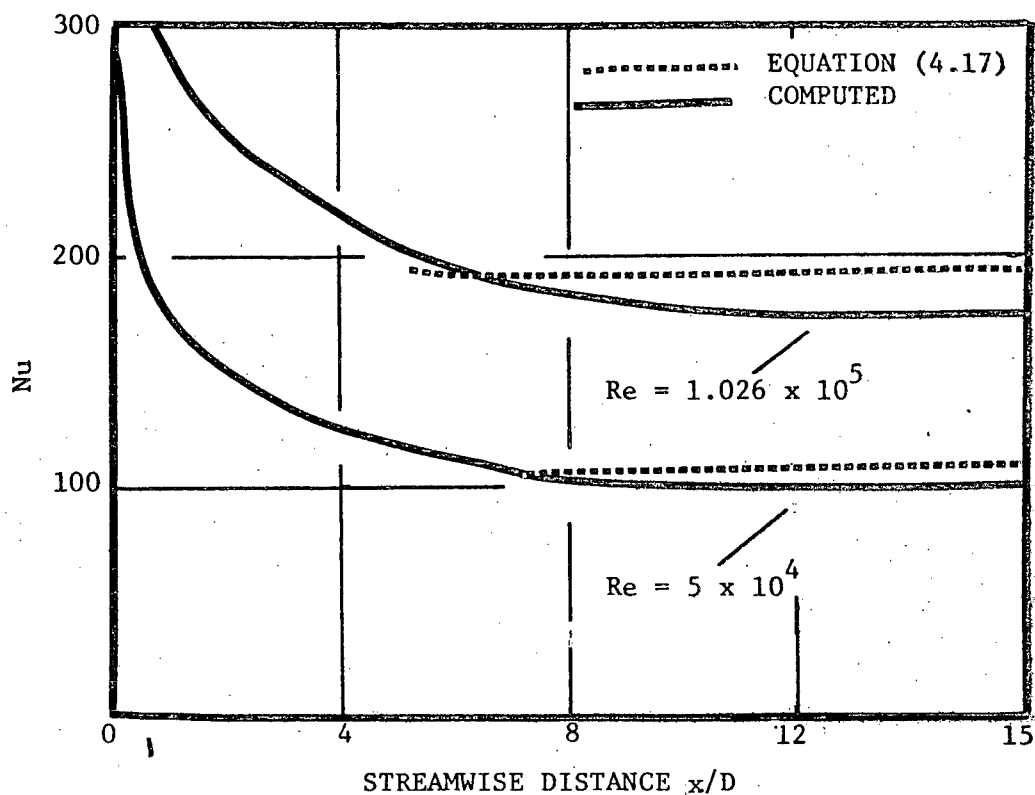


FIGURE 15. Nusselt Number in Pipe Flow.

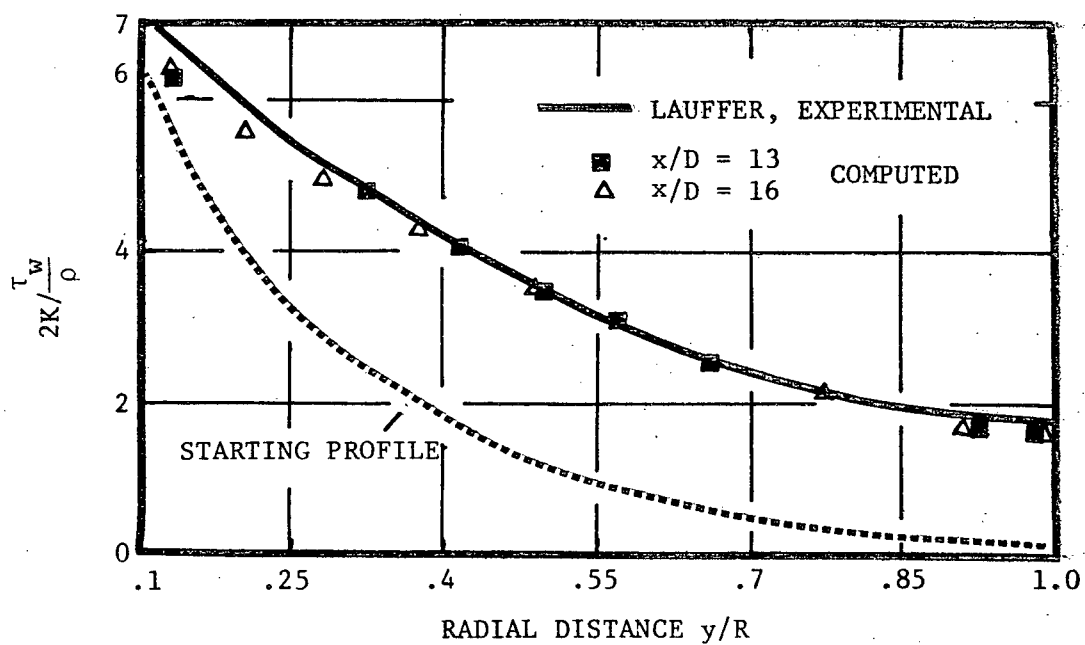


FIGURE 16. Turbulence Kinetic Energy in Pipe Flow.

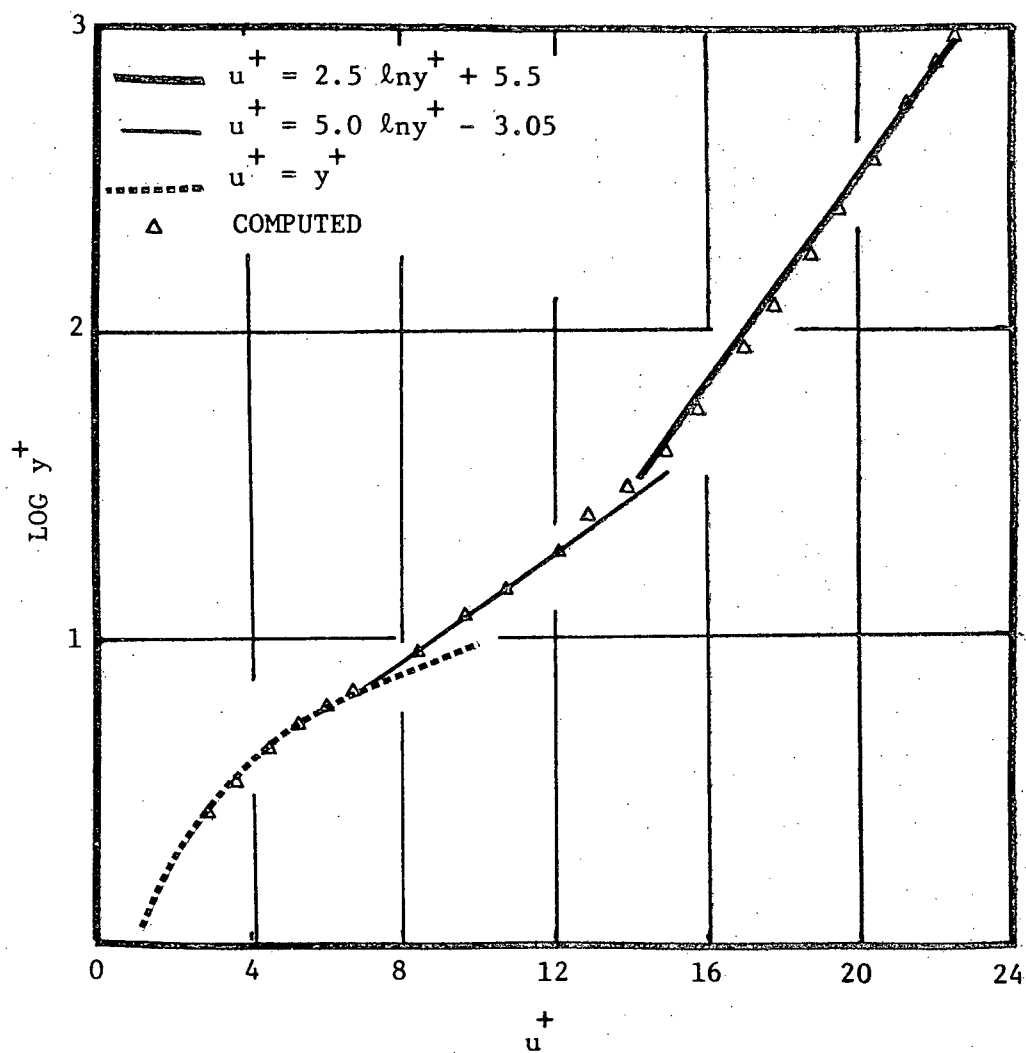


FIGURE 17. Velocity Distribution in Turbulent Pipe Flow.

role in all of the partial differential equations comprising the physical model.

From these results, it was ascertained that the program is functioning well. In the next chapter, this solution procedure is applied to supercritical carbon dioxide.

V. RESULTS AND DISCUSSION

5.1 General

Heat transfer predictions for supercritical carbon dioxide made with the procedure developed in this investigation are compared with previous experimental data in this chapter. Computations were carried out in the reduced pressure range 1.0037 to 1.098. Although numerical predictions in this range of pressures are comparatively difficult because of the proximity of the critical point, heat transfer within this range of pressures is the least understood. A completely general prediction scheme should be able to make realistic predictions at these pressures.

A comparison was made between measured and calculated temperature and velocity profiles^{*} in pipe flow, followed by a comparison of wall temperature distributions. The discussion of results in this chapter mainly focuses attention on specific features as related to the flow under consideration. Approximations and assumptions of a general nature have already been stated. The most influential of these are discussed in greater detail in the next chapter.

Calculations were made for pipes because that is where most of the experimental data and practical applications exist. There is one investigation by Hauptmann⁷ for supercritical carbon dioxide flowing on a flat plate^{**}. Part of that study was an optical examination of the flow

* For brevity, radial velocity and radial temperature profiles are referred simply as velocity and temperature profiles.

** A flat plate study for supercritical nitrogen is due to Simoneau¹⁷.

which served to establish flow mechanisms. However, it is not very convenient for comparison because temperatures were reported at only one location on the plate and the flow was partly laminar with transition occurring on the plate. However, if need arises in a future investigation to make such computations, the procedure presented in this investigation can be adapted for such problems since both the numerical procedure and physical model is applicable to plane flows as well.

5.2 Velocity and Temperature Profiles

Compared to wall temperature measurements, experimental data for velocity and temperature profiles is scant. However, Wood¹⁶ has devoted an entire thesis to the measurement of such profiles and use is made of his data here in order to test the theoretical model.

Wood conducted experiments in an Inconel pipe with an inside diameter of 0.0229 m and total length of 1.435 m. It was mounted vertically and the flow was upward. The heated section of the pipe was .7645 m long. The tube upstream of the heated section served to establish a fully developed velocity profile. He conducted his tests at two general conditions: a pressure of 74.12 bars with a constant wall heat flux of 117350 W/m^2 ; a pressure of 75.84 bars with a heat flux of 92744.45 W/m^2 . A series of runs were conducted by varying mass flow rates and inlet bulk temperatures. Temperature profiles were measured throughout, but velocity profiles were measured only during runs conducted at the lower pressure. Profile measurements were made at one location (30.7 diameters downstream from the beginning of the heated section) only.

Conditions corresponding to four of his experimental runs were

selected for computations. Fully developed velocity profiles and constant bulk enthalpies were used as starting conditions and computations were carried out in step-by-step fashion up to a point where profiles were measured.

Calculated and experimental temperature profiles are compared in Figure 18 at a pressure of 75.84 bars ($p/p_c = 1.027$, $t_c = 305.6^\circ\text{K}$). Inlet temperature in case (a) is 293.15°K and for (b), it is 298.7°K . Both results compare within 0.5% with experimental data (within 8% based on wall-centerline temperature differences). The centerline temperatures are predicted well with approximately correct amounts of temperature drops to various radial locations. Most of the temperature drop, however, takes place in the near wall region which cannot be shown on such a graph. It was not felt necessary to draw another graph on an expanded or logarithmic scale for the near wall region since there were no measurements in that region for comparison. However, Wood measured the temperature of the wall and these can be used as an indication of the accuracy of prediction in the near wall region. The measured and computed wall temperatures for case (a) are 305.04°K and 304.4°K respectively. The same quantities for case (b) are 306.1°K and 305.55°K . The close agreement here suggests that the predictions are good in the entire flow region from wall to centerline.

Figure 19 compares results at 74.12 bars ($p/p_c = 1.0037$, $t_c = 304.3^\circ\text{K}$). The inlet temperature in this case is 299.81°K . Property variations in this run were more severe due to the proximity to the critical point as well as higher heat flux, but agreement is still good. Inaccuracies in the property data probably increase with the proximity of the critical state, but if this has influenced the results, it is in the near wall region. Deviations (by about 10%) in velocity profile can be seen close to the wall.

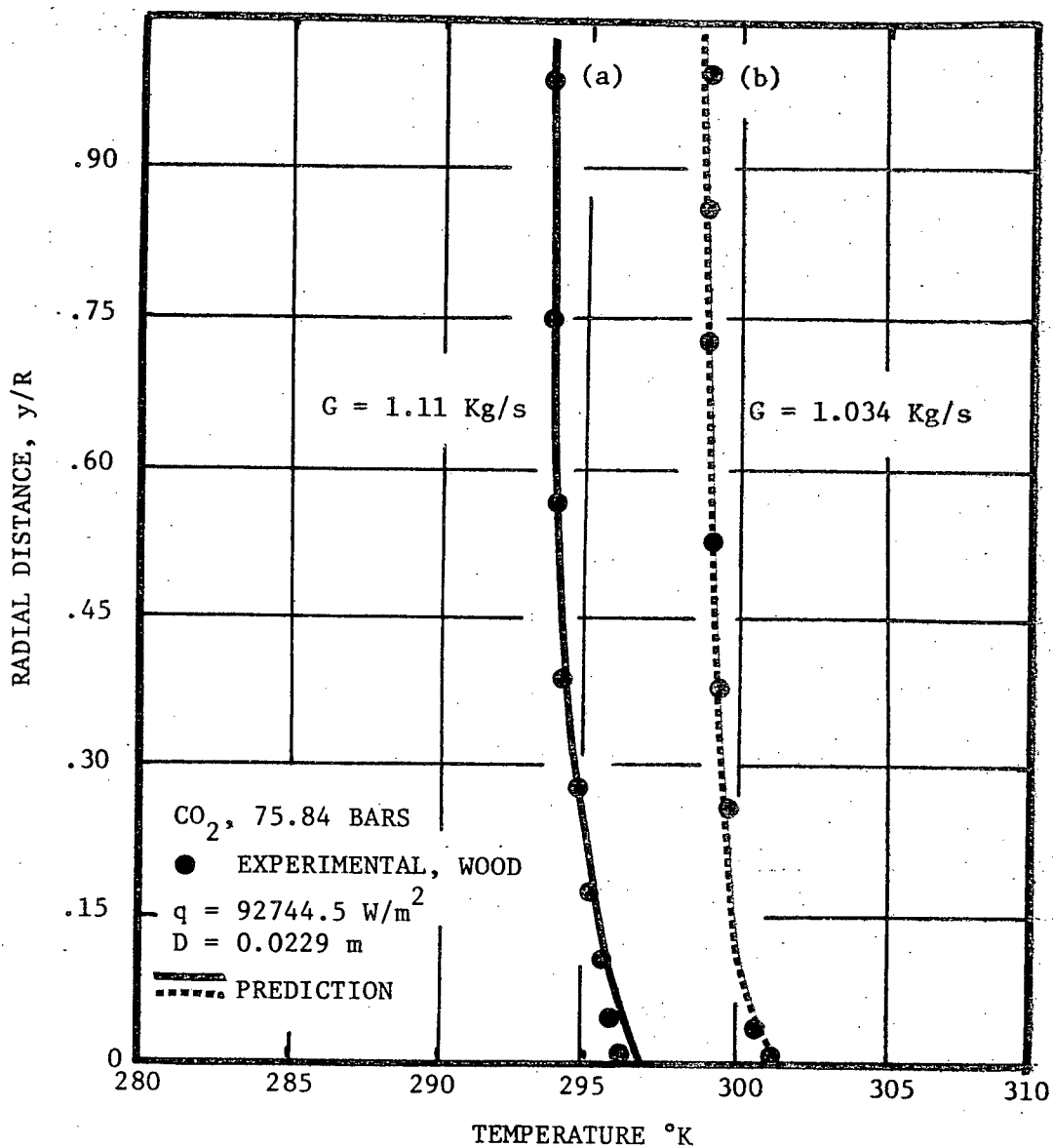


FIGURE 18. Temperature Profiles for Supercritical Carbon Dioxide.

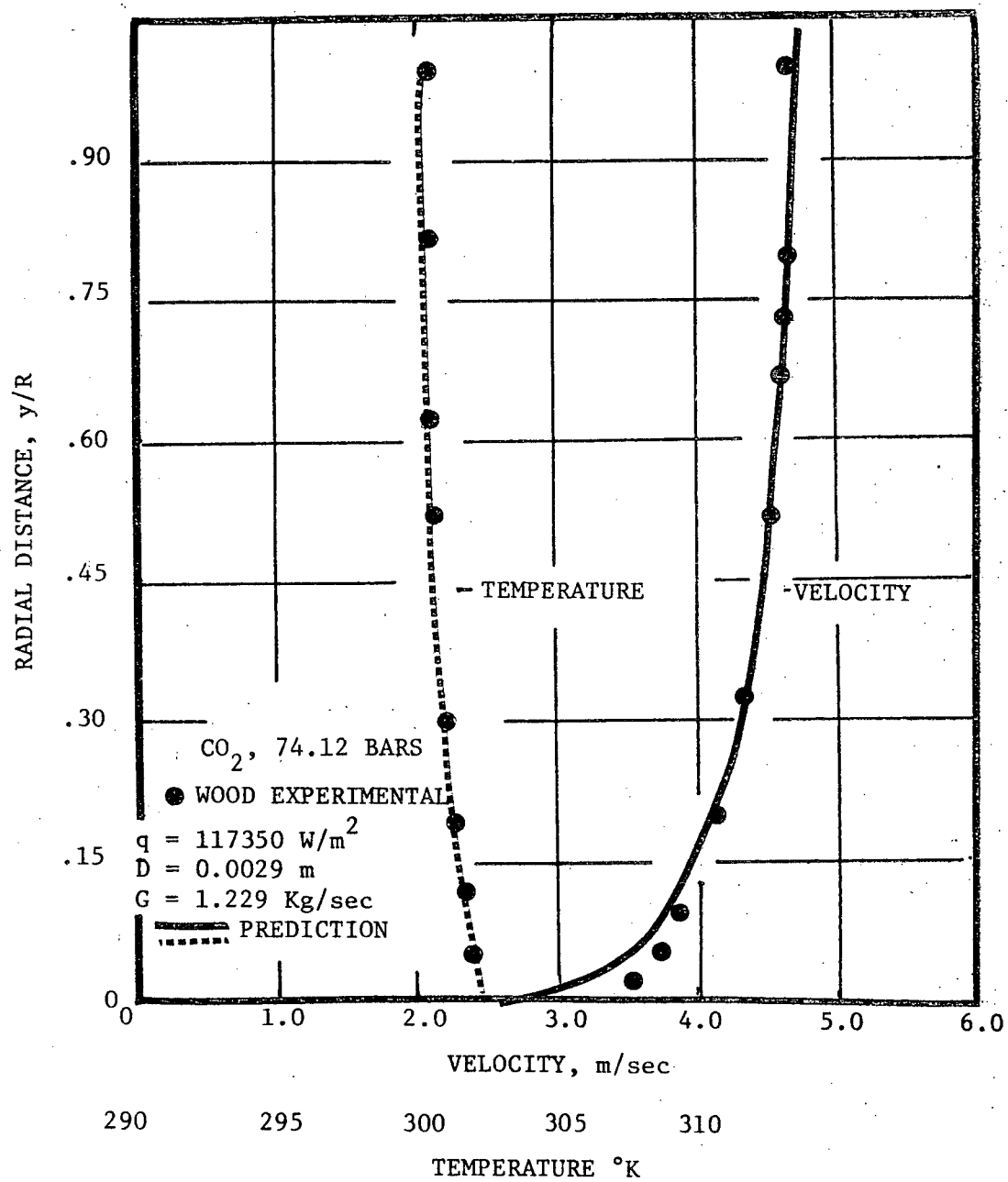


FIGURE 19. Velocity and Temperature Profiles for Supercritical Carbon Dioxide.

Wall velocity in both cases is zero, therefore, the deviation in the velocity profile should start reducing in the near wall region. No such helpful constraint is available for the prediction of temperature profiles. There was some difference between measured (306.372) and computed (305.01) wall temperature in this case. However, the agreement here is still close enough to indicate that the prediction procedure has worked well under the conditions considered. A detailed comparison of the entire near wall region is not possible because of lack of measurements for this part of the flow.

In his measurements of temperature profile, Wood noted that they become less 'round' as inlet bulk temperatures approached the pseudocritical temperature. The total temperature span from centerline to wall is indicative of the overall 'roundness' of temperature profiles. The same feature has been predicted computationally as well. This effect occurs because specific heat variations play an important role in determining the precise shape of temperature profiles. In constant property fluids, a similarity can often be noticed between temperature and velocity profiles when Prandtl number is close to unity. This happens because equations for conservation of energy (with temperature as independent variable) and momentum have a similar form. The analogous situation for variable property fluids is approximately a similarity between enthalpy and velocity profiles. In the present case, C_p peaks at the pseudocritical temperature. Consequently, temperature varies gradually with enthalpy in the vicinity of the pseudocritical temperature. Therefore the temperature profiles look flatter. While developing heat transfer correlations for supercritical fluids, it may be worthwhile investigating the possibility of a number based on enthalpy difference

rather than the usual practice of employing temperature difference. An attempt to develop such correlations was not made in this investigation because it was felt that the prediction procedure is not yet sophisticated enough to be sufficiently reliable and accurate for this purpose.

The final set of data due to Wood that were compared showed several interesting features. Computations corresponding to this data are shown in Figure 20. The trend appears to be approximately correct, but actual magnitudes are in error up to 15% at some locations. The unusual shape of the velocity profile here is a consequence of buoyancy force with varying density. It appears that a variety of different shapes of velocity profiles are possible in supercritical fluids. Figure 21 illustrates some of the formations that the velocity profile undergoes as the fluid progresses along the pipe. This profile could have been modified further at conditions of higher heat fluxes or if the pipe had been longer as is illustrated later in Figure 30. At the time when Wood made these measurements, he found this to be a surprising discovery and had to argue in several different ways before he accepted them as a fact, even though their existence had been postulated early by Hsu³⁰. The term 'unusual profiles' was coined by him and it is used here although these are now widely accepted. The entire range of shapes and their development in a pipe was however probably not known until this investigation. Unusual profiles have been predicted before^{30,35,36} by several investigators using a one-dimensional analysis but in that case, although a profile can be predicted in which velocity first rises and then falls towards the axis of symmetry leading to a global maxima away from center. A profile such as in Figure 20 in which velocity rises, falls, and rises again cannot be predicted by previous methods. In practice, a profile must transform gradually from its

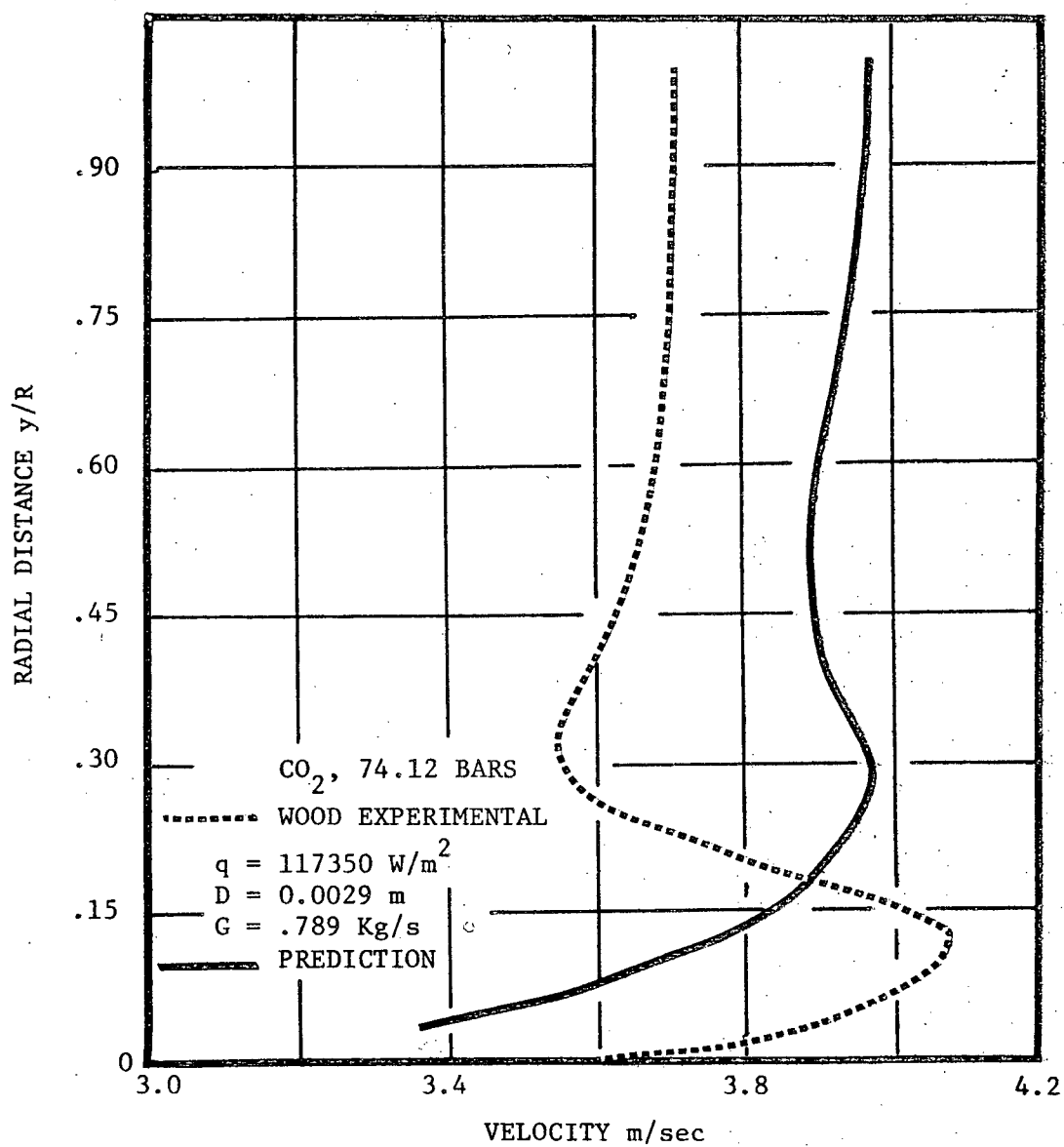


FIGURE 20. 'Unusual' Velocity Profile in Supercritical Carbon Dioxide.

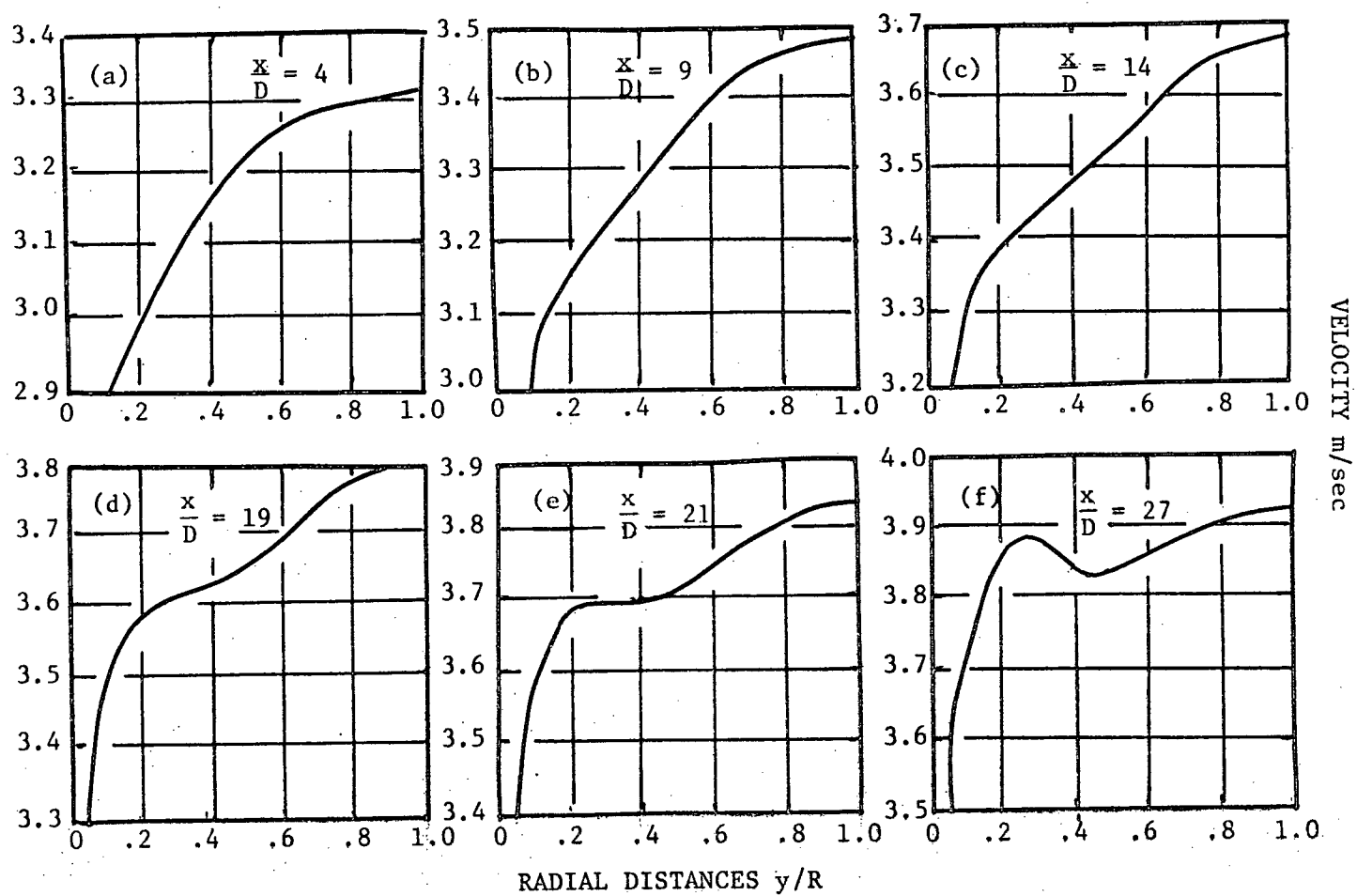


FIGURE 21. Development of 'Unusual' Velocity Profiles in Supercritical Carbon Dioxide.

usual constant property form to an approximately one-dimensional form. This gradual transformation (Figure 21) can be predicted by a two-dimensional analysis accounting for buoyancy. The actual profile in Figure 20 has not yet attained its one-dimensional shape which it could have had the pipe been long enough.

The encouraging feature in this computation is the correct prediction of trend in a flow where a variety of different types of velocity profiles are possible (Figures 22 and 30). The discouraging feature is that actual magnitudes of velocity were not well predicted. Although an error of 15% can sometimes be considered commonplace when predicting wall temperature distributions, better agreement was expected between measured and computed velocity profiles. The main reason why a better agreement could not be achieved in this flow is the extreme proximity of the pseudocritical temperature which led to uncertainties in both calculated and experimental results. In order to attain an unusual profile, Wood had to take inlet temperatures within 0.005% of the pseudocritical temperature. This is not a general requirement for unusual profiles (which can occur with lower inlet temperatures as well if Q/G ratios are higher). However, due to experimental limitations, the value of Q/G was not raised further in Wood's experiments. At his particular operating conditions, the result was that the fluid travelled down the pipe without a significant change in temperature. At this temperature, density variations are very steep which means that the slightest errors in temperature will result in significant errors in density. This effect is shown in Figure 22. In most supercritical flows, similar differences normally occur over smaller regions and therefore effect the computation to a smaller degree. The slight difference in

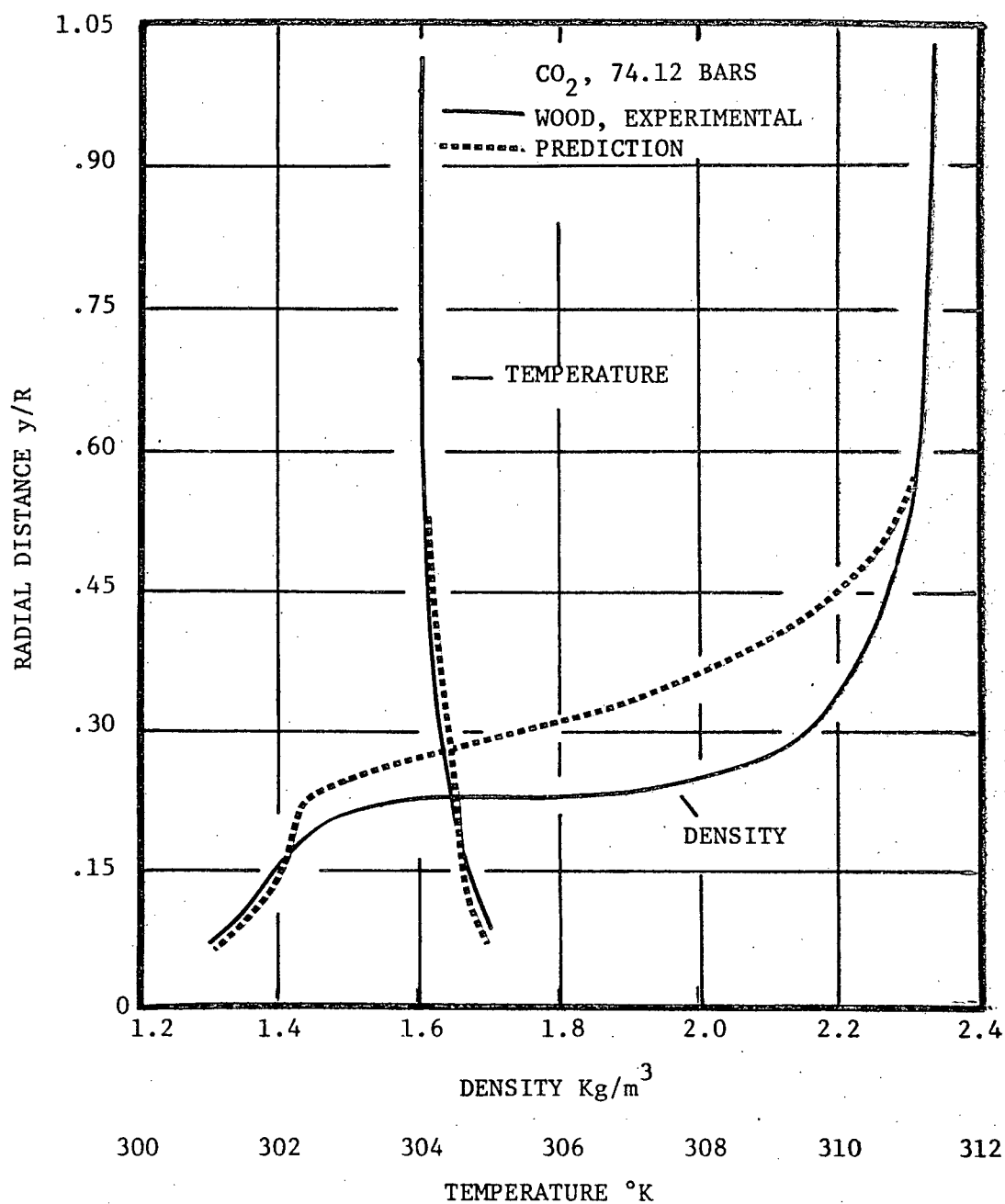


FIGURE 22. Temperature and Density Profile in Supercritical Carbon Dioxide Corresponding to Data in Figure 20.

temperature in Figure 22 could easily have been rectified by redesignating certain empirical constants* that go into the mathematical model, but this was not done since the entire set of computations in this investigation should be made with fixed values of such parameters.

Another important source of error in the present computation is the possible inaccuracies in property data caused as a result of the proximity of critical pressure and pseudocritical temperature**. The same difficulty was faced by Wood in reducing his experimental data. He found that when the profile in Figure 20 was numerically integrated, it did not yield correct mass flow rate. The computed profile has this in its favour. Given the density, it yields the correct mass flow rate since mass flow constraint is an integral part of the mathematical procedure.

5.3 Comparison of Wall Temperature Distributions

As mentioned in Chapter I, supercritical fluids can produce a variety of different wall temperature distributions varying from the enhancement regimes, where wall temperature rises less slowly than bulk temperature to deterioration regimes characterised by local peaks in wall temperature. A realistic theoretical model must be able to predict both these regimes.

Wall temperature measurements have been carried out in a greater

* These are empirical constants such as Von Karman's constant for which values like 0.4 and 0.42 have been suggested.

** Computations made after raising the pressure from 78.84 bars to 76.75 bars showed that velocity profiles were again normal.

number of investigations because it is relatively easier to measure. From a computational point of view, it is somewhat more difficult to predict wall temperatures accurately compared to velocity and temperature profiles because they require an accurate near-wall analysis. In the case of temperature and velocity profiles, inaccuracies of the near-wall region do not always influence predictions in the rest of the flow. Moreover, temperature profiles must always have the same general shape, that is, decreasing towards the axis of symmetry. There is no such helpful characteristic when predicting wall temperatures for supercritical fluids.

A. Wood's Data

Wood's experimental procedure has already been discussed. He also measured wall temperatures at various axial locations by soldering copper constantan thermocouples to the outer wall of his test section. Assuming uniform heat generation and no heat loss to the surroundings, he used the following equation relating inside and outside wall temperatures:

$$t_e - t_w = \frac{q_w R}{2k} \left[\frac{\beta^2 - \ln(\beta^2) - 1}{1 - \beta^2} \right] \quad (5.1)$$

where β is the ratio of inside diameter to outside diameter. Since much of Wood's data consists of outside wall temperatures, the same relation was used for calculating inside wall temperatures. The first assumption involved in equation (5.1) was satisfied by the low thermal resistivity of inconel and the second was checked by a heat balance (which indicated a loss of less than 0.3%). His measurements indicated that some thermocouples always read high and others always read low. This apparently happens because it is not possible to attach all the thermocouples in the same

fashion. Therefore, he drew a smooth curve through the data for finding wall temperatures. His smoothed values of inside wall temperatures were used in the previous section but here the raw data reduced by equation (5.1) is used in Figures 23 to 25.

Figures 23 to 25 show computed and experimental values of wall temperatures corresponding to graphs (a) and (b) of Figure 18; Figure 25 corresponds to the operating conditions in Figure 19. The agreement can be seen to be satisfactory at 75.84 bars, but at 74.12 bars, it is comparatively poor. A possible reason for this was mentioned earlier that is uncertainty of property data. Figures 24 and 25 display enhancement regimes found in supercritical fluids at moderate heat fluxes. It can be seen in these figures that after an initial length (about 9 diameters in Figure 24 and 12 diameters in Figure 25), the wall temperatures are almost constant whereas the bulk temperatures rise linearly.

The remaining computations of wall temperature in this investigation are all in which deterioration (local peaks in wall temperatures) was observed.

B. Data of Jackson and Lutterodt

Jackson and Lutterodt⁶⁷ conducted their experiments at a pressure of 75.8 bars ($p/p_c = 1.026$) in a stainless steel tube ($D = .01897$ m). The tube was mounted vertically and consisted of 64 diameters of entry length followed by a heated length of 129 diameters. Besides thermocouples at various axial locations, thermocouples were also attached around the tube to check for circumferential variations.

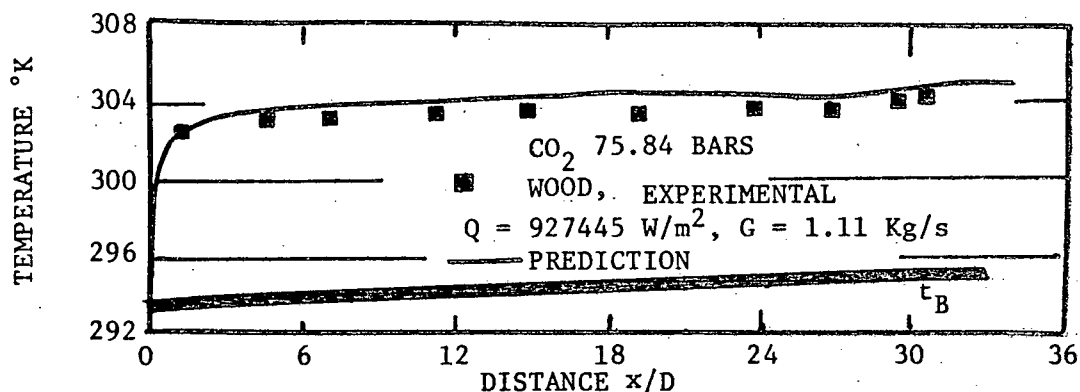


FIGURE 23. Wall Temperatures in Supercritical Carbon Dioxide.

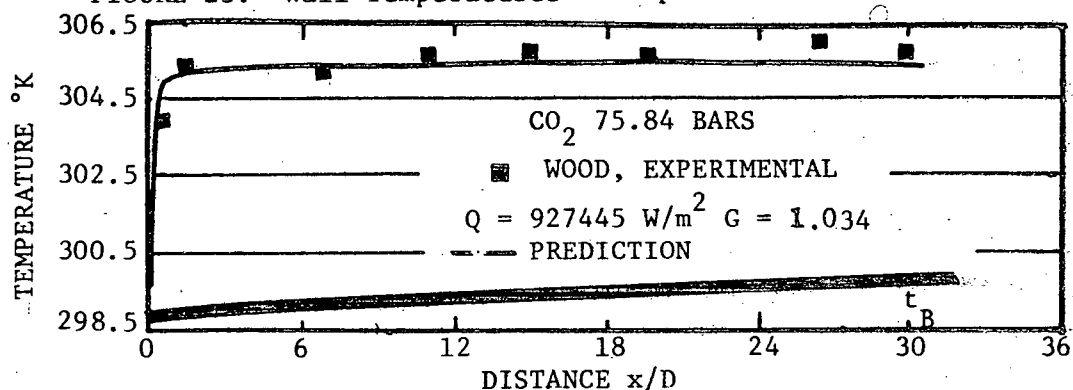


FIGURE 24. Wall Temperatures in Supercritical Carbon Dioxide.

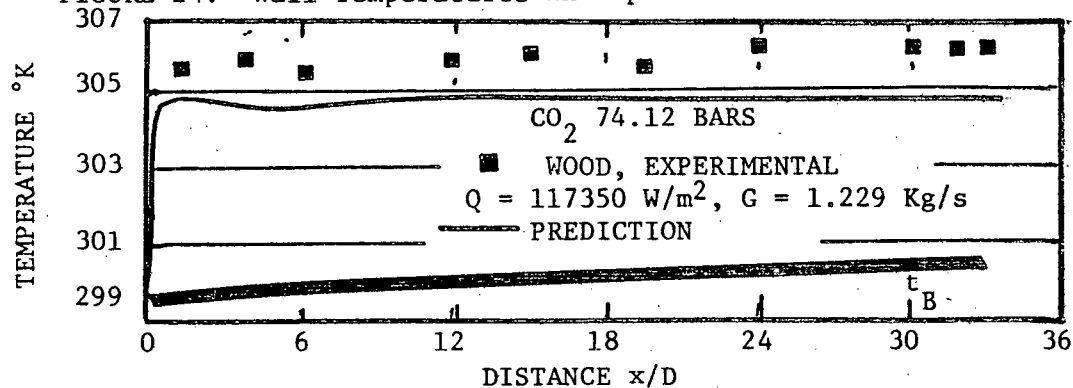


FIGURE 25. Wall Temperatures in Supercritical Carbon Dioxide.

Figure 26 compares computed and experimental data from their work. The shaded area shows the extent of circumferential variations of temperature. The shading was done in this investigation by joining the original data points. Computed results are approximately within this zone. Correct behaviour is predicted in the thermal entrance length where wall temperature rises quickly. Buoyancy force was included corresponding to vertical upflow, although in this particular flow, buoyancy plays a minor role. (Jackson and Lutterodt confirmed this by changing the direction of flow and noting that there was no significant change in wall temperature distributions.) Strictly because of axial symmetry, there should not be any circumferential variation of temperature in this flow. In practice, this seems difficult to achieve due to unsymmetry in tube wall thickness and variation of inlet conditions. These may cause significant circumferential variations because heat transfer behaviour close to the critical region is very sensitive to inlet and boundary conditions. It may be pointed out that an even tube wall thickness is necessary in order to obtain a uniform heat flux boundary condition, because heating in this type of experimental set-up is provided by means of resistance heating. The measurements of circumferential variations has not been given enough attention in most of the other investigations concerned with wall temperature measurements and could at least partly be responsible for observed differences between computed and experimental results in those cases.

C. Data of Schnurr

Schnurr⁶⁸ conducted his experiments in a 0.0034 m outer diameter stainless steel tube with a 0.00038 m thick wall. An entrance length of 127 diameters was followed by an 82 diameter test length. Local tube wall

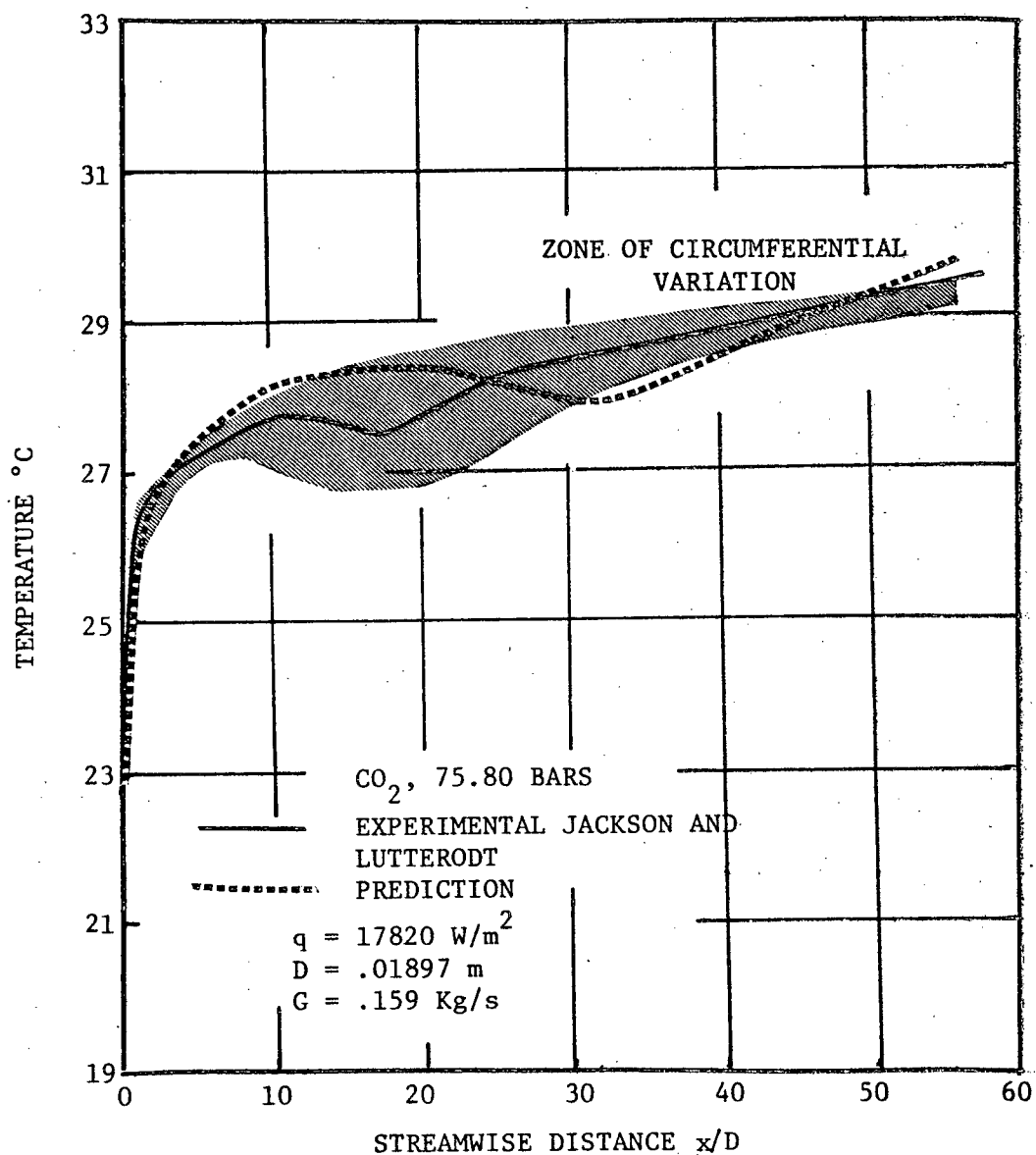


FIGURE 26. Wall Temperatures in Supercritical Carbon Dioxide.

temperatures were measured by chromel-alumel thermocouples. Schnurr did not make an explicit statement about the orientation of the tube but from his references to the top and bottom surfaces, it is inferred that the tube was horizontal, accordingly buoyancy force was dropped from the governing equations. Computations corresponding to his operating conditions at 75.29 bars ($p/p_c = 1.012$) are shown in Figure 27. The agreement here is not good in several respects. First, the temperatures are too low (by about 7%) at the beginning of the thermal entrance length. Second, a slight peak in wall temperature observed both experimentally and computationally has shifted considerably to the right. This is probably a consequence of the former error since fluid temperatures must reach a certain level before deterioration is affected. Last, at the termination of deterioration, temperatures are too high.

It appears that a major part of the error is due to neglected buoyancy effects. Heat flux is fairly high in this case and density gradients in the vertical direction are large. Therefore, as pointed out by Schnurr, buoyancy forces must play an important role in this flow. The computation of this three-dimensional effect has not been taken up in the present investigation. Nevertheless, this computation shows that this could be a worthwhile point to investigate in future work.

D. Data of Ikaynnikov and Petukhov

Ikaynnikov and Petukhov conducted their experiments in a stainless steel tube of 29 mm inside diameter with a wall thickness of 1.5 mm, 78 diameters of the tube served as the test length. This was preceded by 25 diameters (calming section according to their terminology) for allowing

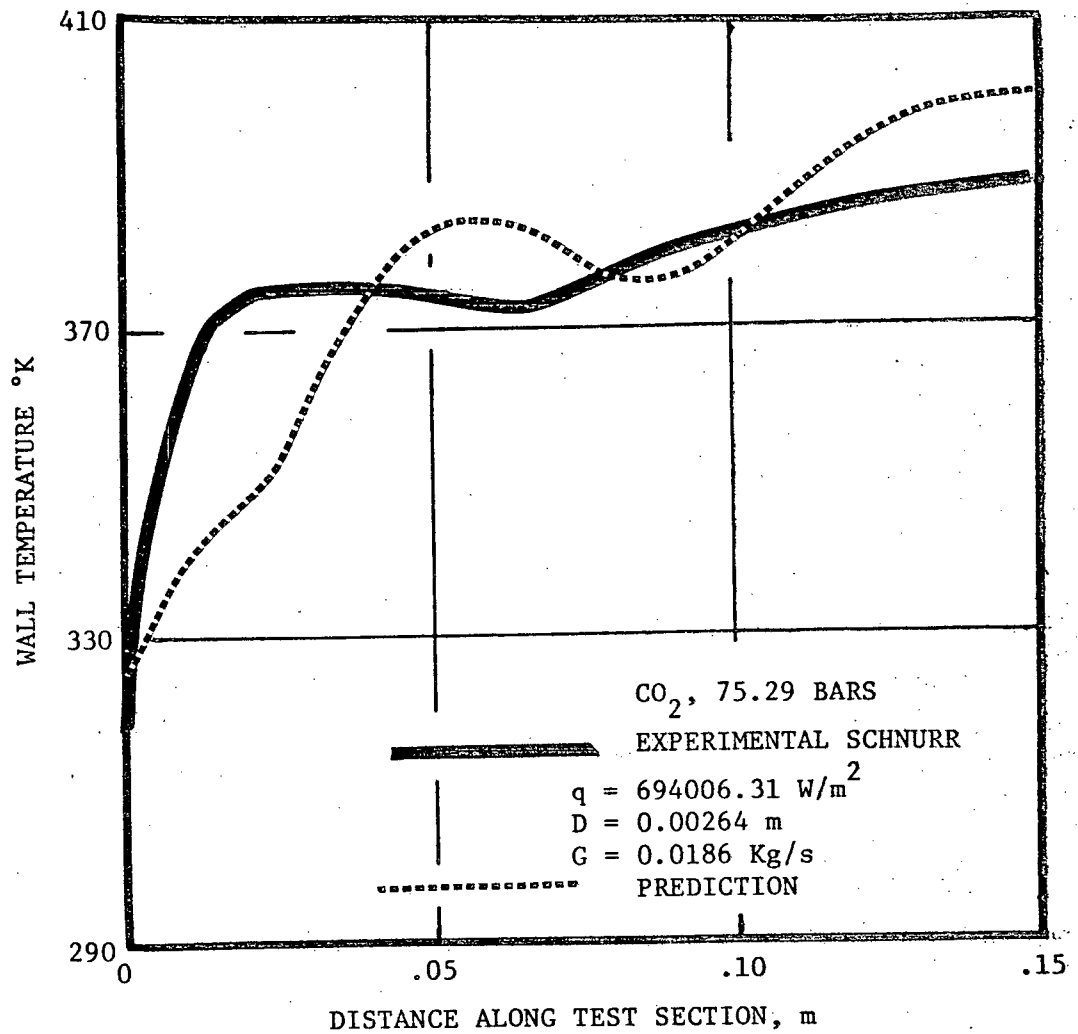


FIGURE 27. Wall Temperatures in Supercritical Carbon Dioxide.

the flow to get fully developed. Wall temperatures were measured by chromel-alumel thermocouples and the tube was oriented vertically with the flow upward.

They used relatively low mass flow rates and high heat fluxes. Therefore, deterioration as well as buoyancy effects are significant. Computations corresponding to their data shows the development of unusual velocity profiles. Results for measured and computed wall temperature are plotted in Figures 28 and 29. Inlet temperatures for both runs are 15°C .

Figure 28 compares results at the lower heat flux. Although computed temperatures are somewhat lower (by up to about 12%), the trend is predicted well. This flow is quite sensitive to inlet conditions. Computations corresponding to the same conditions but with an inlet temperature of about 5°C higher (not plotted here) resulted in a double peak instead of the single peak found in this case.

Figure 29 shows a plot of another result from their investigation at a heat flux approximately nine times as high. Here the correct level of temperature peak is predicted as well as the location of deterioration (within 10%). However, computed wall temperatures drop far below predicted temperatures at the conclusion of deterioration. A reason for this appears to be a free convective effect that was excluded in this analysis and is discussed in the next chapter. Its effect is to lower predicted temperatures for vertical upflow whenever it becomes dominant. A second cause which could be partially responsible is circumferential variations of temperature which can be large* just at the conclusion of such a deterioration.

* See Jackson and Lutterodt⁶⁷.

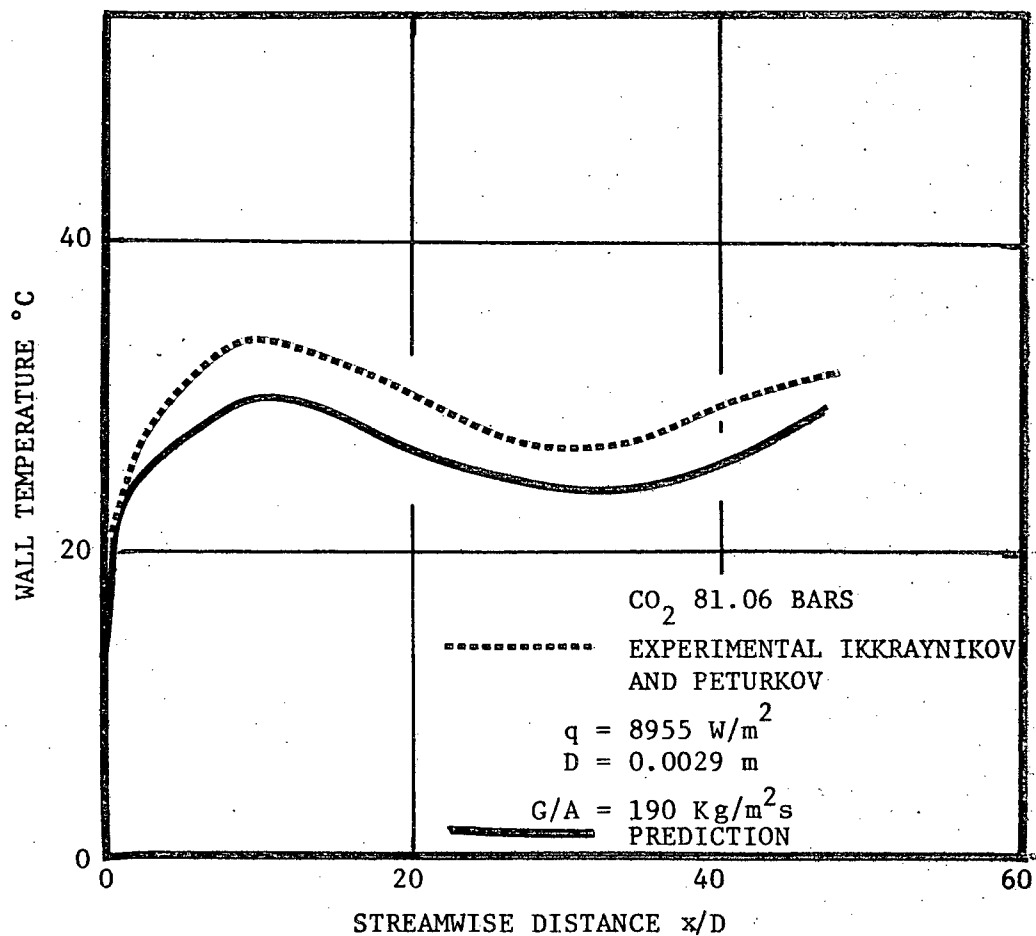


FIGURE 28. Wall Temperatures in Supercritical Carbon Dioxide.

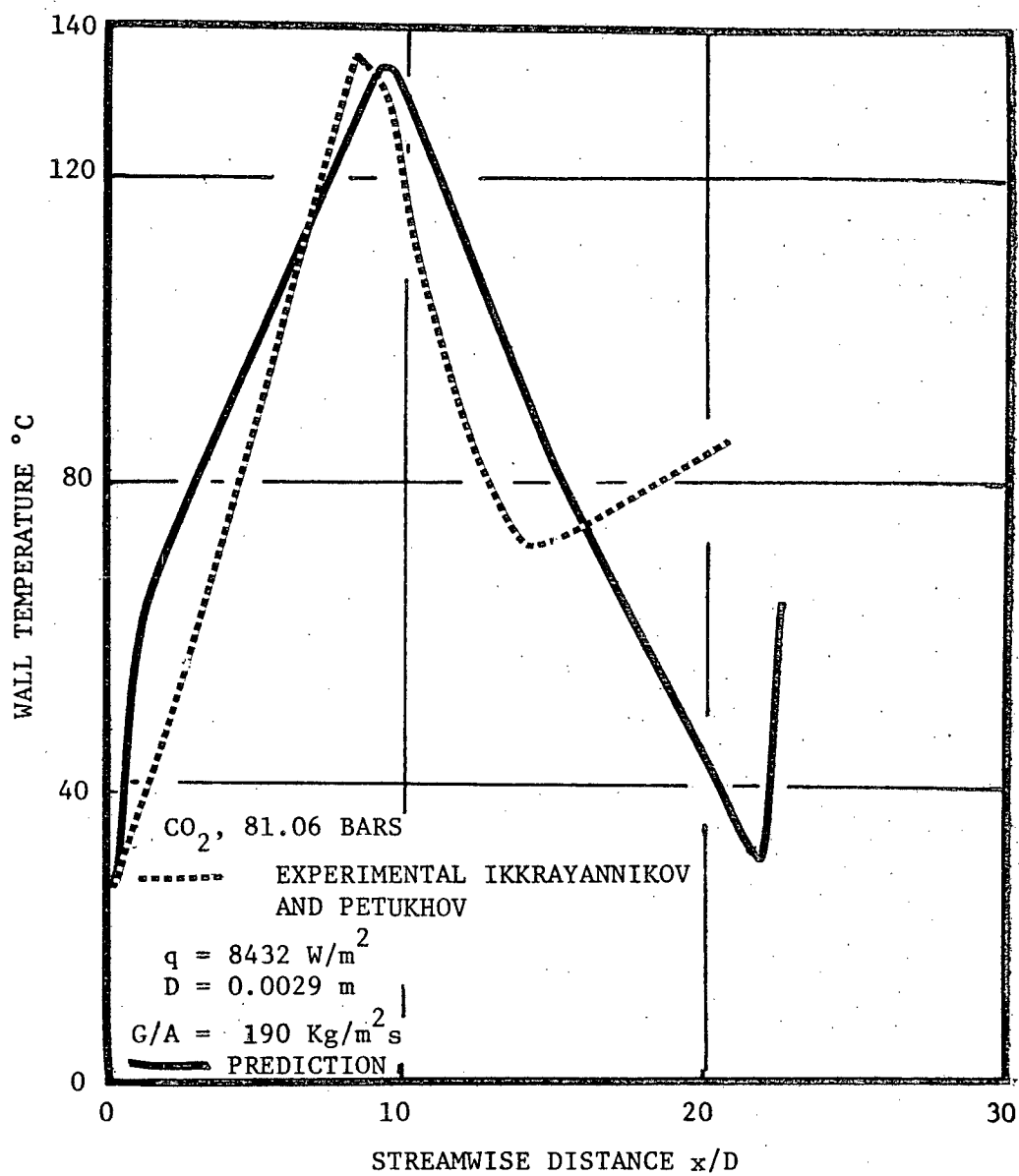


FIGURE 29. Wall Temperatures in Supercritical Carbon Dioxide.

Computed velocity profiles for this flow shown in Figure 30 demonstrate how the buoyancy forces modify the velocity profiles in this flow. These modifications are much severer as compared to those in Figure 21 because of strong heating at the walls. The near wall regions are not shown in Figure 30 for the sake of clarity. Since the velocity at the wall is zero and since there is no back flow or recirculation in any of the problems considered here, the velocity always increases with radial distance in the near wall region in this investigation. Figure 30(f) indicates the first signs of a return to a normal velocity profile. If the pipe is long enough, the flow eventually heats itself out of the critical region and behaves like a constant property fluid.

5.4 Scope for Further Results

This chapter was mostly restricted to a discussion of wall temperature distributions and radial velocity and temperature profiles. The calculation of other flow properties that comprises the mathematical formulation is also a necessary part of each computation (such as those in Figure 31). The necessity of recording such data was not felt primarily because experimental data on these quantities is not available for comparison. Further, it is felt that an adequate reliability cannot be placed on all the data at the present stage. It should be pointed out that the fact that some of the data compares well with experimental data is not a sufficient criterion that all the associated data is equally accurate.

Another important point that deserves restating concerns the type of computations made. These were restricted to conform to the operating conditions in previous experimental studies. However, for the purpose of practical design work, several other operating conditions (such

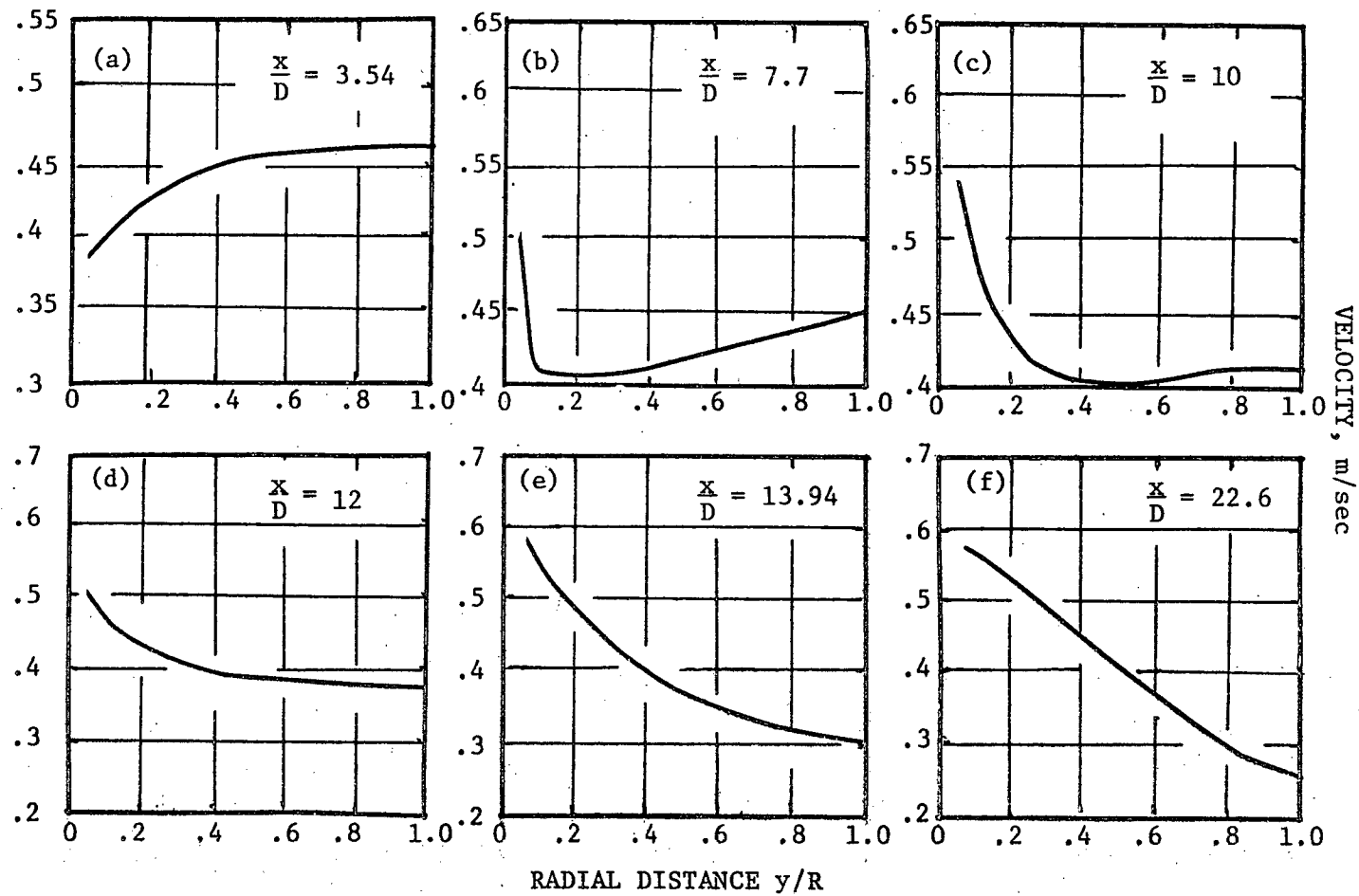


FIGURE 30. Development of Unusual Velocity Profiles in Supercritical Carbon Dioxide.

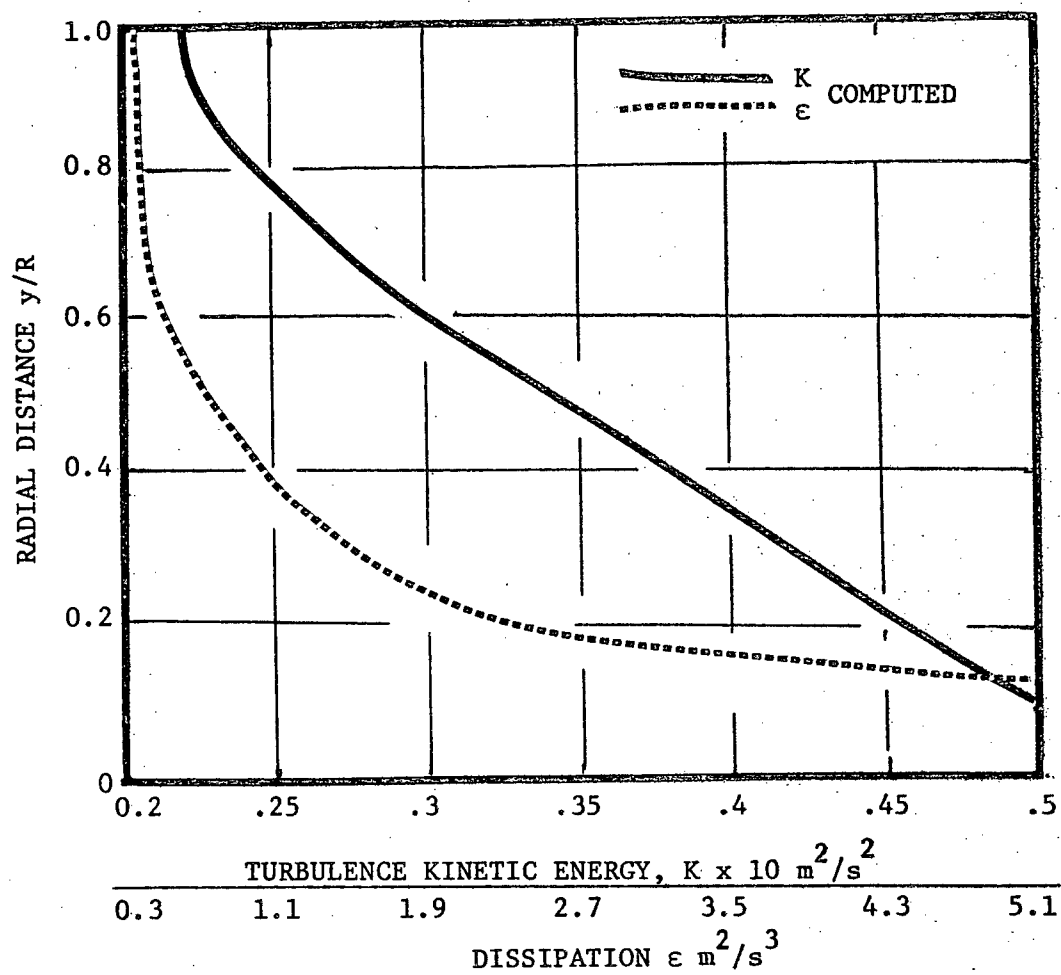


FIGURE 31. Turbulence Kinetic Energy and Dissipation Profile Corresponding to Computations Illustrated in Figure 19.

as variable wall heat fluxes) will probably be of interest. It is hoped that the present procedure will prove amenable to further extensions. It is felt that in the present form, the full potential of the present procedure can be exploited only when used in conjunction with experimental data. Whenever an adequate agreement can be reached between experimental and predicted results, the present procedure can be used for generating similar results at other related operating conditions. Alternatively, the present procedure can be used for carrying out preliminary feasibility studies before undertaking an actual experimental study.

5.5 Concluding Remarks

To conclude, calculations made in this chapter indicate that there are several ways in which the theoretical analysis is not completely satisfactory. However, overall agreement is considered reasonable for the calculations illustrated. Predictions made in this chapter, though broadly covering the range of forced convection heat transfer phenomenon occurring in supercritical fluids are not exhaustive, more over computations in some cases were not carried out for the full range of the heated section. For example, measurements corresponding to Figure 26 extend to 130 diameters, but calculations were terminated after 60 diameters. The only reason for doing so was to efficiently utilize the available computer time. Computer time usage is directly proportional to the number of diameters covered and therefore computations were terminated as soon as what was felt to be the important range was covered.

VI. FURTHER DISCUSSION

6.1 General

Variations in turbulent Prandtl number, contribution of fluctuating property correlations, and the influence of free convective effects in the turbulence model are three major areas leading to uncertainty in the formulation of the theoretical model. It was felt that these should be discussed more fully since the further development of the theoretical procedure presented in this investigation will probably depend on the clarification of these issues.

6.2 Turbulent Prandtl Number

The turbulent Prandtl number was assigned a constant value equal to 0.9 in the present work. In actual practice, turbulent Prandtl number varies with molecular Prandtl number Pr and also with geometric location in the flow. A better practice was not adopted because there is as yet no definite procedure for doing so, even in constant property fluids. A large number of proposals, however, can be found. Reynolds⁷⁰ has examined more than thirty different ways of predicting turbulent Prandtl number. Calculations were made using some of these in order to study their effect on calculated heat transfer behaviour.

A. Graber's Proposal

Graber⁷¹ took no account of the position within the flow but allowed for the dependence of molecular Prandtl number through the formula

$$\text{Pr}_t^{-1} = 0.91 + 0.13 \text{Pr}^{0.545} . \quad (6.1)$$

The illustration of Figure 32 shows the calculated Prandtl number using equation (6.1) for a supercritical flow. This flow is the same as that in Figure 26 of Chapter V. The result shows the low sensitivity of turbulent Prandtl number to its molecular counterpart. This is also apparent directly from equation (6.1). Even though values calculated from equation (6.1) are slightly lower than 0.9, calculated temperatures do not differ significantly (See Figure 33). Equation (6.1), however, indicates that the practice of using a value less than unity for supercritical carbon dioxide appears to be better founded than that of other investigations which employ a value of unity.

B. Quaramby and Quirk's Proposal

In view of the scatter in their data, Quaramby and Quirk⁷² felt that it was impossible to isolate the dependence of turbulent Prandtl number on molecular properties. However, they proposed a relation for variation across the pipe and represented it by

$$\text{Pr}_t = (1 + 400^{-y/R})^{-1} . \quad (6.2)$$

This gives $\text{Pr}_t = 1/2$ near the wall and $\text{Pr}_t = 1$ in the core (Figure 32). Scatter around this result is ± 0.1 in the core and more in the wall layer. A value of 0.5 at the wall is much lower than that suggested by other investigations and leads to lower calculated wall temperatures as seen in Figure 32.

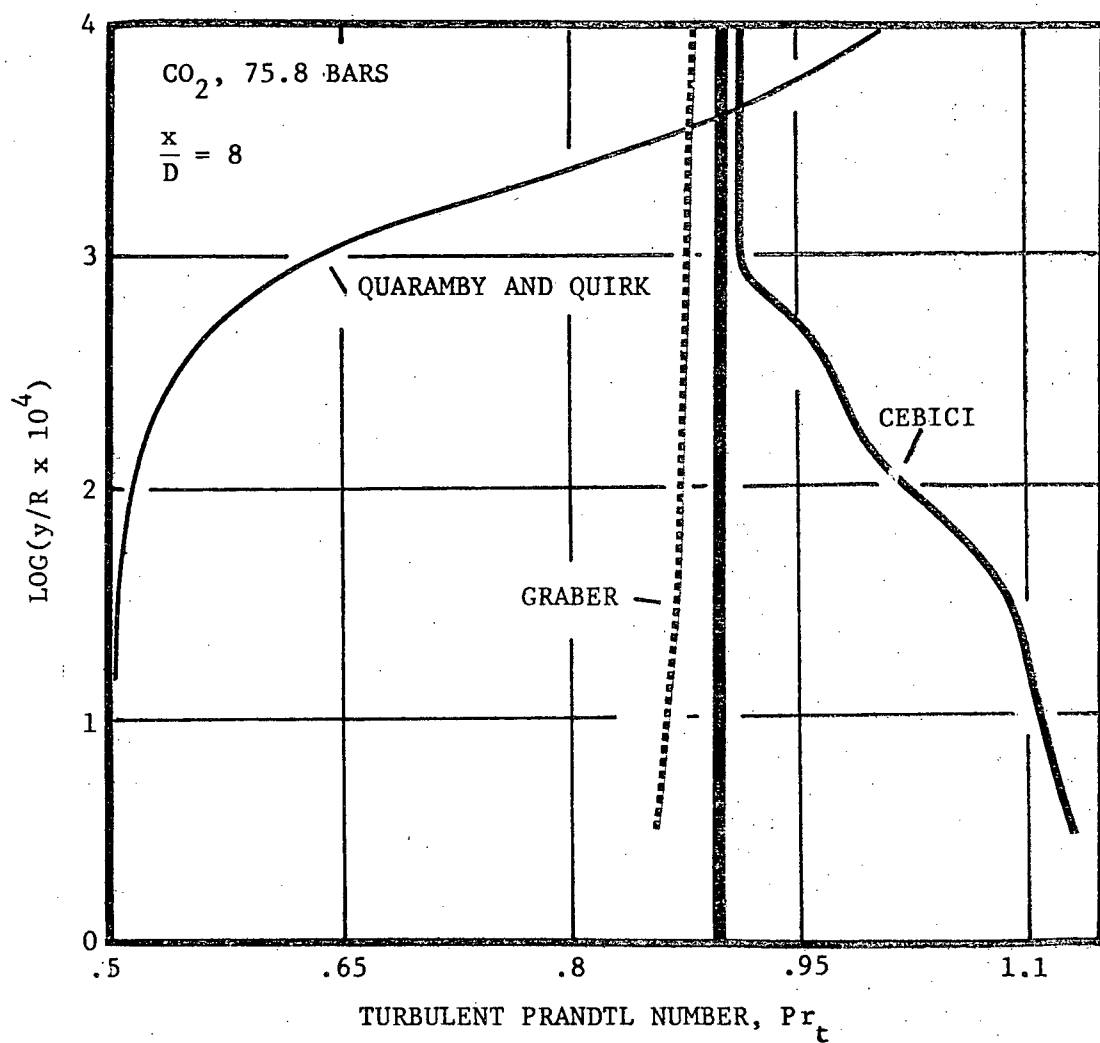


FIGURE 32. Turbulent Prandtl Number Variation Across a Pipe.

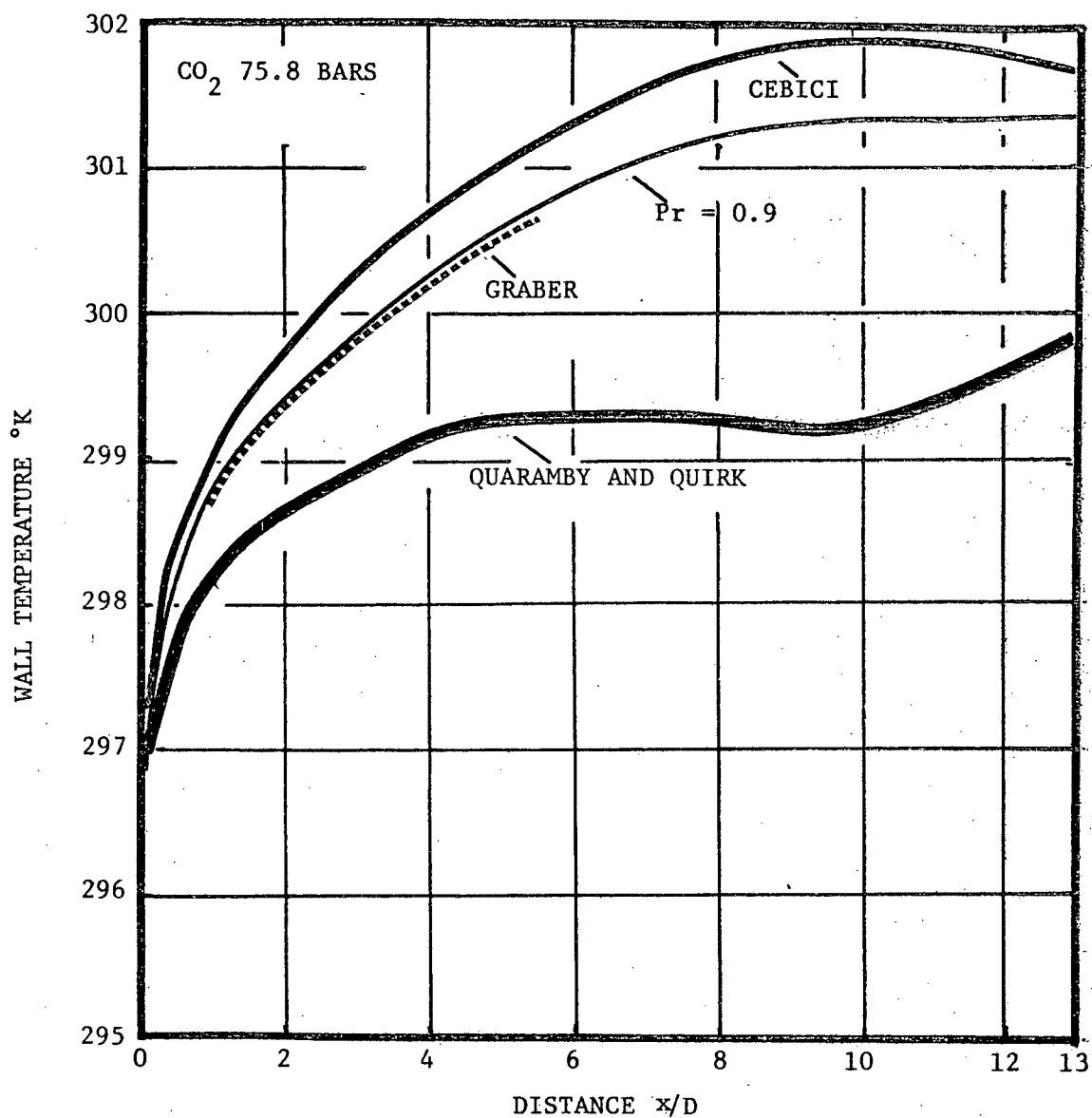


FIGURE 33. Wall Temperature Variations with Different Turbulent Prandtl Numbers.

C. Cebici's Proposal

Cebici⁷³ extended Van Driest's mixing length representation near a wall to turbulent heat fluxes. His arguments lead to the result

$$Pr_t = \frac{\kappa [1 - \exp(-y^+/A^+)]}{\kappa_h [1 - \exp(-y^+/B^+)]} \quad (6.3)$$

At the wall, Pr_t is given by

$$Pr_t = \frac{\kappa}{\kappa_h} \frac{B^+}{A^+} \quad (6.4)$$

As y becomes larger, the exponential terms in equation (6.3) rapidly approach zero, leading to

$$Pr_t = \frac{\kappa}{\kappa_h} \quad (6.5)$$

Cebici's proposal and its later modification by Na and Habib⁷⁴ allow for dependence of constants in equation (6.3) on molecular Prandtl number. Therefore, it combines both molecular and geometric effects. Molecular effects, however, are small in this flow as indicated already. Therefore, calculations were made with equation (6.3) assigning constant values of $\kappa_h = 0.44$ and $B^+ = 35$ (suggested by Cebici). Calculations made with equation (6.3) are shown in Figures 32 and 33. Calculated wall temperatures are higher because of higher Pr_t near the wall.

Trends of variation in the last two proposals are completely opposite. A decreasing Pr_t with radial distance in the wall layer is in agreement with Rotta's⁷⁵ proposal, whereas a trend of increasing Prandtl number in the high Reynolds number region is in agreement with turbulence

modelling theory⁷⁶. A rigorous evaluation of the two proposals cannot be made because of a paucity of experimental data for this quantity. Further, all proposals discussed here were made for constant property fluids. Additional effects due to variable properties cannot be ruled out. However, until more is known about the turbulent Prandtl number, the use of a constant value seems to be a reasonable practice since it is fairly successful in predicting experimental behaviour.

6.3 Enhancement Factors

As stated earlier, the fluctuating property correlations were neglected during the formulation of the mathematical model. Nevertheless, it is felt that in future investigations, the need may arise to question this assumption further. Probably many of the questions connected with these effects can be answered precisely only when experimental information on these quantities becomes available. At the present time, it is possible to make rough estimates of some of these additional terms in the following manner.

A strict averaging of the Navier-Stokes equations yield for the turbulent shear stress:

$$\tau_t = \rho \overline{u'v'} + \underbrace{u \overline{\rho'v'}}_I + \underbrace{v \overline{\rho'u'}}_{II} + \underbrace{\overline{u'\rho'v'}}_{III} . \quad (6.6)$$

Terms I, II, and III in equation (6.6) are additional fluctuating property correlations that arise in the momentum equation. Term I is the most amenable to an estimate. It is also probably the largest of three because term II contains \bar{v} as a product and term III is a triple correlation.

Therefore, approximating equation (6.6) as:

$$\tau_t = \rho \overline{u'v'} + u \overline{h'v'}, \quad (6.7)$$

where,

$$\phi = \left(\frac{\partial \rho}{\partial h} \right)_p.$$

The additional assumptions embodied in equation (6.7) are: density fluctuations due to pressure fluctuations are negligible and that higher order effects are small (These involve $\partial^2 \rho / \partial h^2$ and $\overline{h'^2 v'}$). Equation (6.7) can now be rearranged as:

$$\tau_t = \rho \overline{u'v'} \left[1 + \phi \frac{u}{\rho Pr_t} \frac{\partial h / \partial y}{\partial u / \partial y} \right] \text{ or,} \quad (6.8)$$

$$\tau_t = \rho \overline{u'v'} \left[1 + \frac{u}{\rho Pr_t} \left(\frac{\partial \rho}{\partial u} \right)_x \right]. \quad (6.9)$$

The factor inside the bracket may be regarded as an enhancement factor. Equation (6.9) is equal in magnitude to an enhancement factor proposed by Hsu and Smith³⁰ when Pr_t is equal to unity*. The similarity here is surprising because Hsu and Smith obtained their expression through physical arguments based on an extension of the Prandtl's mixing length concept in order to account for density derivatives.

Similar considerations for the energy equation will lead to an analogous enhancement factor for the turbulent heat flux as was done by Hsu and Smith. Here the simpler procedure of regarding both these enhance-

* See Section 1.2.

ment factors as equal is adopted in order to effect a calculation. The two enhancement factors should have the same order of magnitude on appeal to an analogy between velocity and enthalpy fields. A further simplification used here is to regard Pr_t as unity in (6.9) for similarity with Hsu and Smith's proposal. The test flow chosen for computations is the same as in the section on turbulent Prandtl numbers. Figure 34 illustrates computed values of enhancement factor. Calculations were effected by multiplying turbulent fluxes throughout by the enhancement factor. This factor has a value of unity at the wall since the velocity there is zero and unity near the core because density gradients there are zero. Velocity gradients are also zero at the centre, but this fact did not cause any complication in this flow because density falls to zero faster than velocity. Calculated results showed less than 1% alteration in computed wall temperatures. This is because enhancement is nowhere greater than 6% and influence on calculated results must be much smaller. Of all calculated results, wall shear stresses were most effected as shown in Figure 35. Wall shear stresses are slightly lower than the unenhanced case at most points because normally it tends to compensate for increases in shear stress away from the wall. Although in this particular flow, enhancement is not large, it may be larger whenever heat fluxes or flow rates are larger. This factor was not used in this investigation because it is felt that it involves uncertainties and also because in the present work, its effect is probably outweighed by other approximations. However, as prediction methods improve further in accuracy, the need for an investigation in this area may arise.

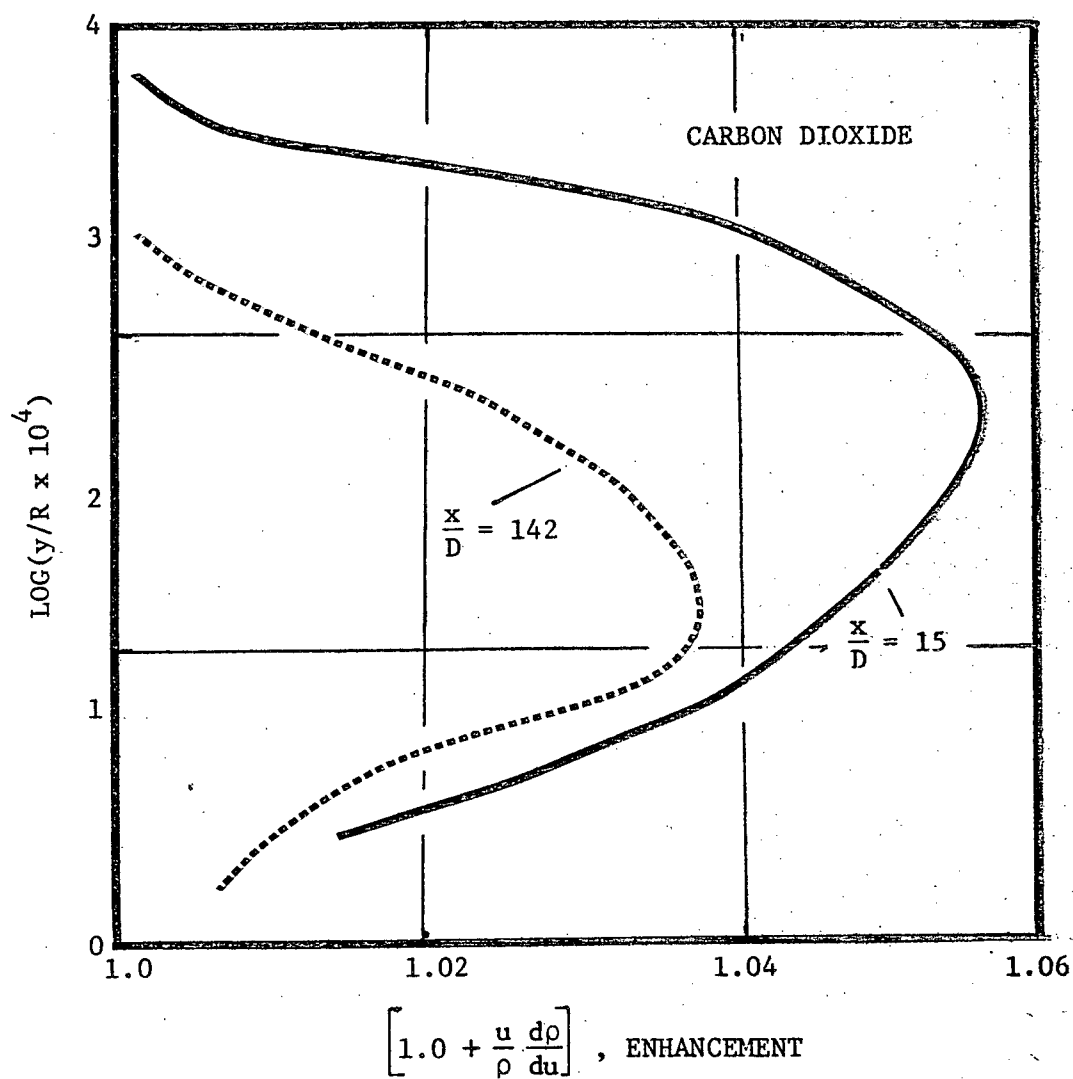


FIGURE 34. Enhancement Factors in Supercritical Carbon Dioxide.

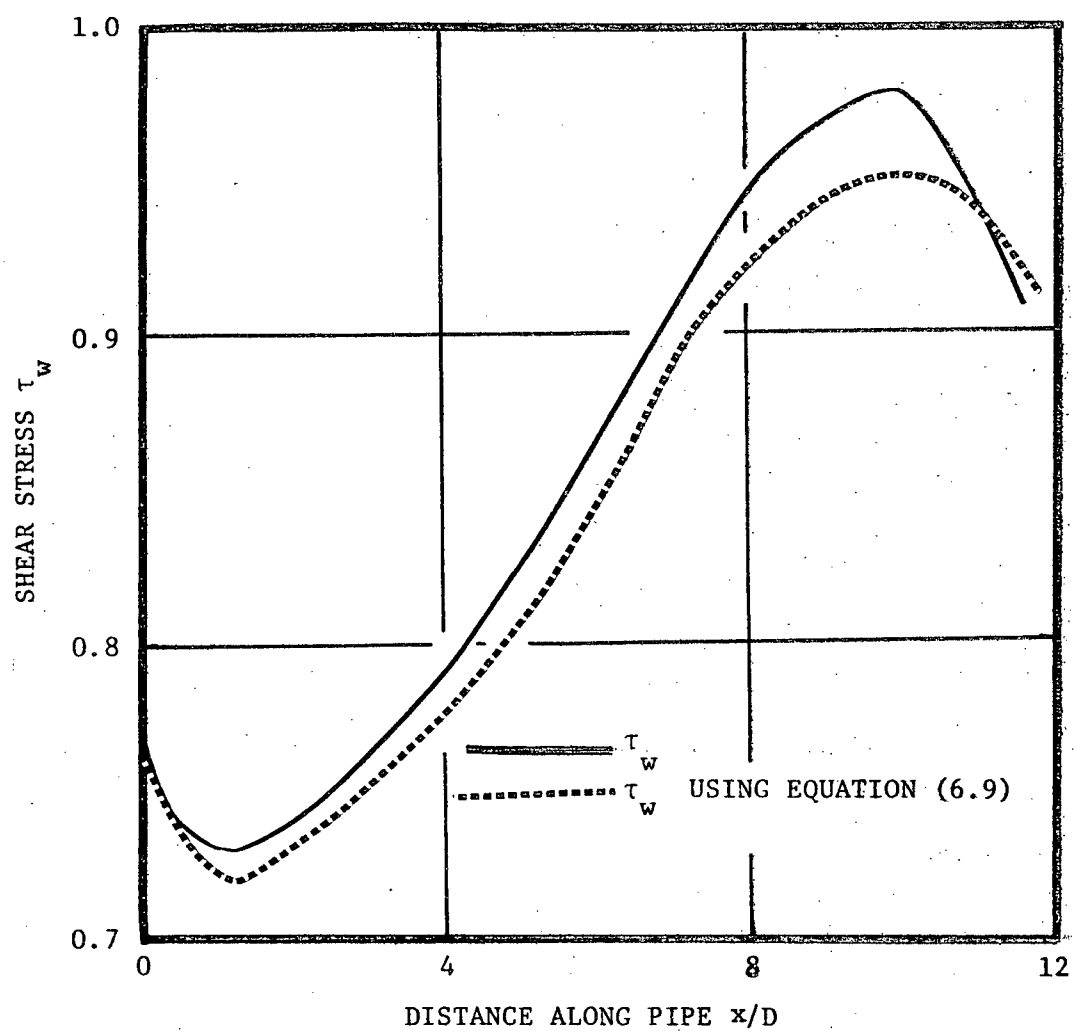


FIGURE 35. Wall Shear Stress Variation.

6.4 Free Convective Influences

The influence of free convective (or buoyant) effects in forced convection situations of supercritical fluids can clearly be determined when experiments are carried out in pipe flow by changing the orientation of the flow with respect to gravity, all other conditions remaining the same. Such experiments have been carried out by Jackson and Lutterodt⁶⁷. It was found that, as buoyant effects become significant, observed upflow wall temperatures are higher than downflow wall temperatures. Further experimental confirmation of these results has been provided by Bourke, Pulling, Gill, and Denton⁷⁷.

The prediction of the correct differences between upflow and downflow wall temperatures should strictly be outside the capability of this investigation since the sole cause of this difference is free convective effects. However, the possibility of predicting this effect was investigated in this analysis because of a hypothesis due to Hall^{36,78}. According to this hypothesis, buoyancy forces in upflow modify the shear stress distribution in such a way as to result in flatter velocity profiles in upflow. Thereby the shear generated turbulence is inhibited. This leads to higher wall temperatures in upflow. Therefore, the implication here is that if calculations are made accounting for such a modification in shear stress behaviour, then the correct differences between upflow and downflow temperatures can be predicted. This hypothesis was supported by approximate one-dimensional calculations. Hall's contribution is considered invaluable in this investigation in so far as emphasis and stimulation into the study of free convective effects is concerned. However, recently a closer look at the problem has become possible due to the

availability of two-dimensional analytical methods as is explained next and it appears that an important free convective effect may have been either overlooked or de-emphasized.

It may be pointed out that the difference between upflow and downflow temperatures is not a phenomenon unique to supercritical fluids. It has also been noted in constant property fluids. Accordingly, Bates et al⁷⁹ in response to the preceeding hypothesis, accounted for buoyancy in the mean momentum balance and computed wall temperatures in constant property fluids for both upflow and downflow through a two-dimensional numerical procedure. Their results showed a complete reversal of observed behaviour. Calculated wall temperatures in downflow were higher than in upflow.

Such a calculation for supercritical fluids was also made in this investigation. Figure 36 shows calculated results for carbon dioxide. Predicted wall temperature differences are again reversed from observed behaviour. That is, wall temperatures are lower for upflow. In this flow, unusual velocity profiles associated with negative shear stresses were noted for upflow. Figure 37 compares the radial shear stress distribution in this flow at a location ($x/D = 30$) downstream from the start of heating. Although the shear stress is lower at some points in upflow as expected, the wall shear stresses are higher. The wall shear stresses dominate heat transfer here and result in lower wall temperatures for upflow. Therefore, the conclusion drawn here is that modified radial shear stress distribution is not a sufficient criterion for obtaining the correct temperature differences and another explanation must be found. It should further be pointed out that due to a constantly changing velocity profile and the contribution of the thermal entrance length, this flow is clearly not

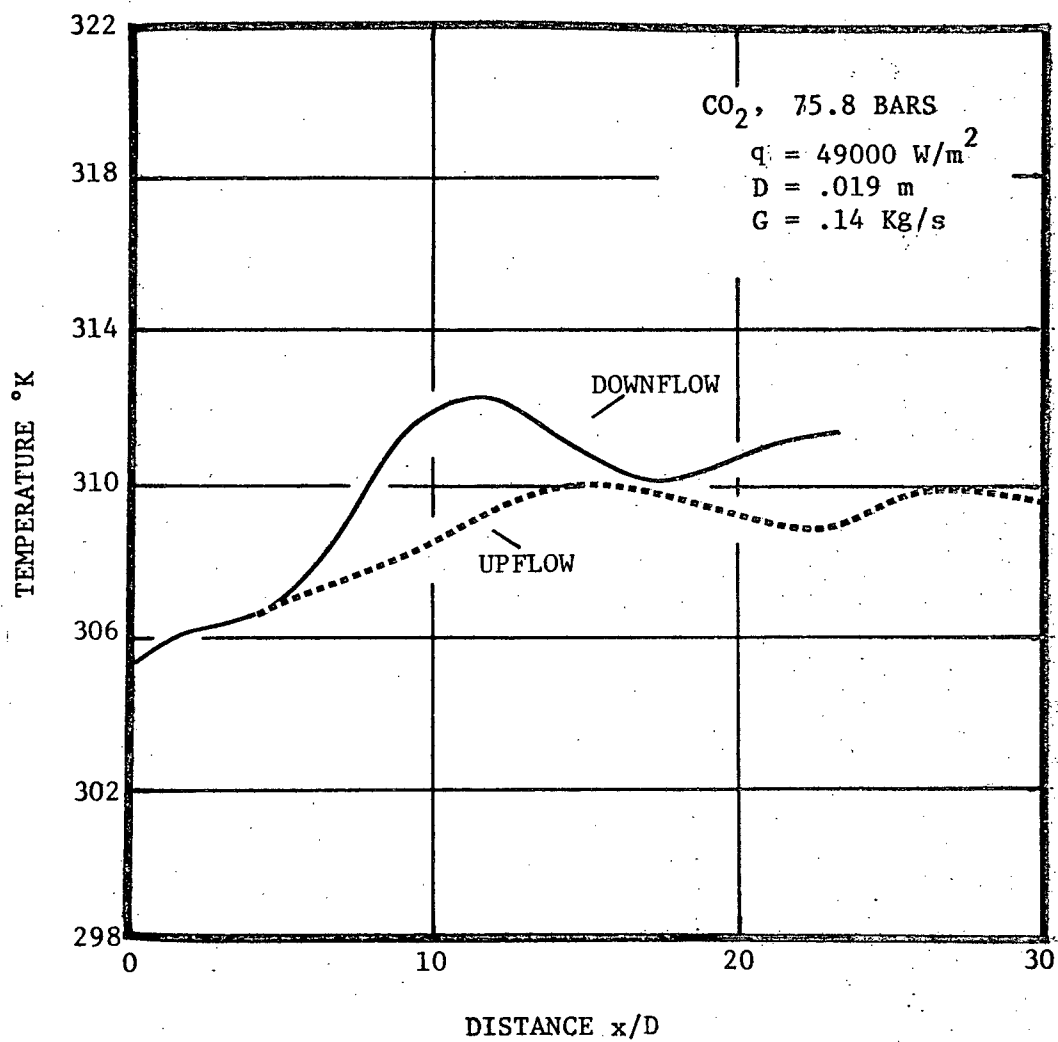


FIGURE 36. Wall Temperatures for Upflow and Downflow.

one-dimensional and therefore a one-dimensional calculation procedure that neglects flow acceleration cannot be expected to be correct. Figure 38 illustrates the computed turbulence kinetic energy profiles for this flow (at a location $x/D = 15$). However, such data was not used to deduce any conclusions here because the phenomenon under consideration appears to be dominated by the near wall region.

Buoyancy forces may be regarded as influencing the flow in two ways. First, by a contribution to the mean-momentum balance, and second, by influencing turbulence generation^{*}. Unless this second effect is included in an analysis, it is believed that calculation procedures may continue to underpredict upflow wall temperatures and overpredict downflow temperatures solely because of this effect. Upward heated flows are stably stratified and therefore, turbulence is suppressed in such flows. In downward flow, stratification is unstable and turbulent production enhanced. Stratification in vertical flows is in a direction perpendicular to the predominant heat flow direction and is therefore not very obvious. It is probably because of this reason that it has not received sufficient attention before. Recent Russian literature^{80,81}, however, indicates that the role of stratification-induced turbulence in vertical confined flows (both constant property and supercritical) is now being studied.

An adequate analytical treatment of free convective effect will

* In the momentum equation, buoyancy forces appear as $+\rho g_i$ when g_i and U_i are in the same direction. If this term is retained during the derivation of the Reynolds stress equation, the corresponding contribution in that equation is $[\overline{U_i \rho' g_j} + \overline{U_j \rho' g_i}]$ or approximately $\beta [\overline{U_i h' g_j} + \overline{U_j h' g_i}]$. This would further result in an additional production term in the kinetic energy equation equal to $+\beta \overline{U_i h' g_i}$.

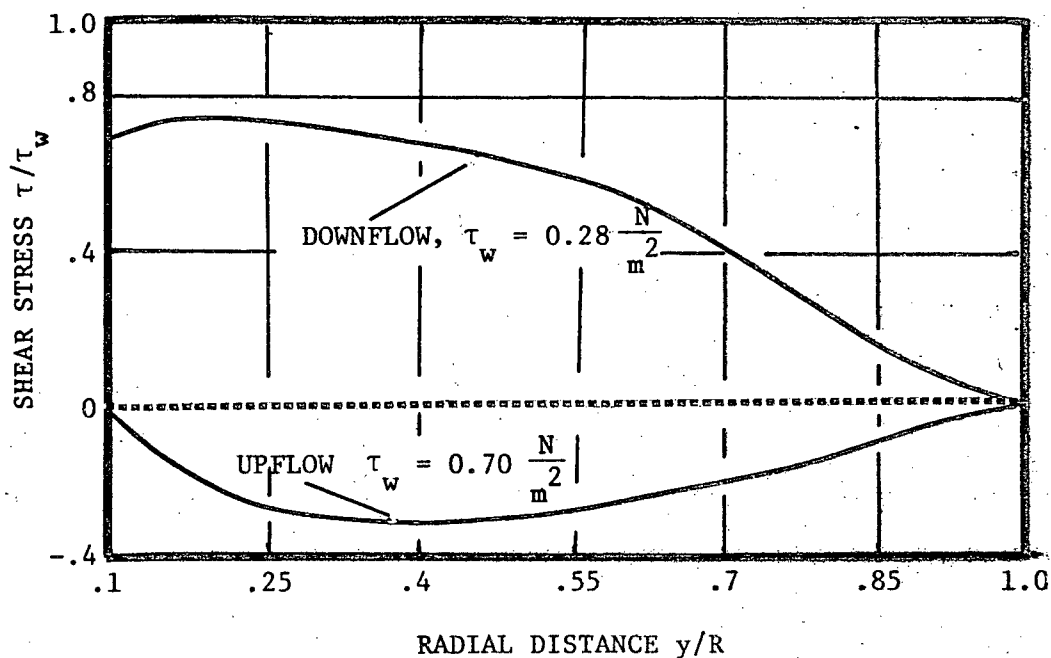


FIGURE 37. Computed Radial Shear Stress Profiles for Carbon Dioxide at $P/P_c = 1.027$ at a Location $x/D = 30$.
(Data Corresponding to Figure 36.)

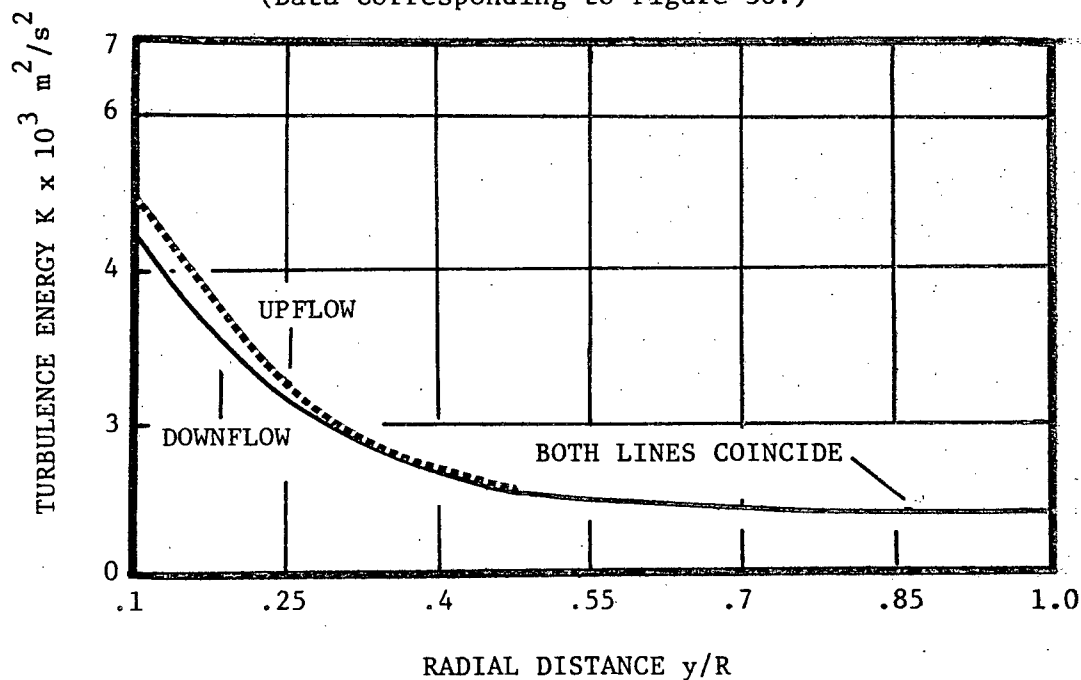


FIGURE 38. Computed Values of Turbulence Kinetic Energy K for Carbon Dioxide at $P/P_c = 1.027$ at a Location $x/D = 15$. (Data Corresponding to Figure 36.)

probably depend on the progress in handling the same problem in constant property fluids*. The analytical treatment of such effects may be the principle interest of a future investigation on supercritical fluids.

* See Launder⁸² and Gibson and Launder⁷⁶ for recent methods in constant property free shear flows.

VII. CONCLUSIONS AND RECOMMENDATIONS

Conclusions and recommendations of a specific nature will be found interspersed throughout this dissertation. Therefore, this section has been used for touching upon the broader points concerned with this work.

It is concluded from the computed results that both the physical modelling as well as the numerical solution procedure of the present work are viable procedures but in need of further development. A change was made from previous investigations by introducing the use of a completely two-dimensional solution procedure and a two-equation model of turbulence in the fully turbulent region of the flow. The mixing length type of algebraic formulations have been used in the past, mainly on the basis of how well they can predict experimentally determined behaviour. Although this still remains the criterion for testing the viability of the present method, an additional advantage of physical realism and broader generality can be achieved with the multi-equation models of turbulence. The methods and approximations of the present work, though physically realistic, can only be regarded as a beginning to apparently promising extensions. A logical extension of the physical model presented in this investigation, appears to be the use of low Reynolds number modelling (in the near wall region). In fact, many of the improvements such as extension to combined free and forced convection (refer to Chapter VI) appear to be dependent upon such physical modelling. However, it may be realized that in view of its complexity, supercritical heat transfer is not the ideal phenomenon to select for any new radical changes in forced convection theories. Rather, it is felt that new theories

should first be thoroughly verified at the constant property level before being considered for supercritical heat transfer. The kind of turbulence model employed in this investigation appears to be receiving the attention of several investigations at precisely such a level (that is, constant property level), and it may be worthwhile to make use of this progress with perhaps only minor modifications for application to supercritical fluids.

It is further concluded that the consideration of buoyancy in the mean momentum balance is a useful method of predicting unusual velocity profiles but not entirely sufficient to account for all of the free convective effects such as observed differences between upflow and downflow temperatures.

The use of fully two-dimensional numerical procedure was felt necessary in this investigation in order to account for the thermal entrance length and the near wall behaviour in supercritical fluids. The numerical procedure used in this work will probably prove amenable to further extensions.

REFERENCES

1. Hall, W.B.; HEAT TRANSFER NEAR THE CRITICAL POINT, Advances in Heat Transfer, VOL. 7, Academic Press, pg. 1 (1971).
2. Hendricks, R.C., Simoneau, R.J., and Smith, R.V.; "Survey of Heat Transfer to Near Critical Fluids", Advances in Cryogenic Engineering, VOL. 15, pg. 197, Plenum Press, New York (1970).
3. Hsu, Y.Y. and Graham, R.W.; TRANSPORT PROCESSES IN BOILING AND TWO-PHASE SYSTEMS INCLUDING NEAR-CRITICAL FLUIDS", Hemisphere Publishing Corporation (1976).
4. Schmidt, E., Eckert, E., and Grigull, U.; "Warmetransport durch Flüssigkeiten in der Nahe ihres Kritischen Zustandes", Jb. Dtsch. Luft, VOL. 2, pg. 53 (1939).
5. Schmidt, E.; "Warmetransport durch Naturliche Konvektion in Stoffen bei Kritischem Zustrand", Int. J. Heat Mass Transf., VOL. 1, pg. 92 (1960).
6. Powell, W.B.; "Heat Transfer to Fluids in the Region of the Critical Temperature", Jet Propulsion, VOL. 27, pg. 776 (1957).
7. Hauptmann, E.G.; "An Experimental Investigation of Forced Convection Heat Transfer to a Fluid in the Region of its Critical Point", Ph.D. Thesis, California Institute of Technology, Pasadena, California (1966).
8. Styrikovich, M.A., Shitsman, M.E., and Miroploski, Z.L.; "Certain Data on the Temperature Region of Vertical Boiler Pipes at Near Critical Pressures", Teploenergetika, VOL. 3, pg. 32 (1956).
9. Hsu, Y.Y.; "Discussion of an Investigation of Heat Transfer of Fluids Flowing in Pipes Under Super-critical Conditions", International Developments in Heat Transfer, ASME 188-189D (1961).
10. Griffith, J.D. and Sabersky, R.H.; "Convection in a Fluid at Super-critical Pressures", Journ. A.R.S., VOL. 30, pg. 289 (1960).
11. Hines, W.S. and Wolf, H.; "Heat Transfer Vibrations with Hydrocarbon Fluids at Supercritical Pressures and Temperatures", presented at A.R.S. Propellants, Combustion, and Liquid Rockets Conference (1961).
12. Goldmann, K.; "Heat Transfer to Supercritical Water at 5000 PSI Flowing at High Mass Flow Rates Through Round Tubes", International Developments in Heat Transfer, pg. 565, A.S.M.E. (1963).
13. Sabersky, R.H. and Hauptmann, E.G.; "Forced Convection Heat Transfer to Supercritical Pressure Carbon Dioxide", Int. J. Heat Mass Transf., VOL. 10, pg. 1499 (1967).

14. Green, R.; "Forced Convection Heat Transfer from a Cylinder in Supercritical Carbon Dioxide", M.A.Sc. Thesis, University of British Columbia, (1970).
15. Deissler, R.G.; "Heat Transfer and Fluid Friction for Fully-developed Turbulent Flow of Air and Supercritical Water with Variable Fluid Properties", Trans. A.S.M.E., VOL. 76, pg. 73 (1954).
16. Wood, R.D.; "Heat Transfer in the Critical Region: Experimental Investigation of Radial Temperature and Velocity Profiles", Ph.D. Thesis, Northwestern University, Evanston, Illinois (1963).
17. Simoneau, R.J.; "Velocity and Temperature Profiles in Near-critical Nitrogen Flowing Over a Heated Flat Plate", Ph.D. Thesis, North Carolina State University, Raleigh, North Carolina (1970).
18. Eckert, E.R.G.; "Discussion of Heat Transfer and Fluid Friction for Fully-developed Turbulent Flow of Air and Supercritical Water with Variable Fluid Properties", Trans. A.S.M.E., VOL. 76, p. 83 (1954).
19. Bringer, R.P. and Smith, J.M.; "Heat Transfer in the Critical Region", A.I.Ch.E. Journal, VOL. 3, pg. 49 (1957).
20. Hess, H.L. and Kunz, K.R.; "A Study of Forced Convection Heat Transfer to Supercritical Hydrogen", A.S.M.E. Paper Number 63-WA-205 (1963).
21. Krasnoshchekov, E.A. and Protopopov, V.S.; "Heat Exchange in the Supercritical During the Flow of Piped Carbonic Acid and Water", Teploenergetika, Vol. 6 (12), pg. 26 (1959).
22. Gunsen, W.E. and Kellog, H.B.; "Engineering Application Technique for Supercritical-Pressure Heat Transfer Correlations", A.S.M.E. Paper Number 66-WA/HT-11 (1966).
23. Swenson, H.S., Carver, J.R., and Kakarala, C.R.; "Heat Transfer to Supercritical Water in Smooth Base Tubes", J. Heat Transfer, VOL. 87, pg. 477 (1965).
24. Miropolski, Z.L. and Shitsman, M.E.; "Heat Transfer to Water and Steam with Varying Specific Heat in the Critical Region", Journal of Technical Physics, Vol. 27, pg. 2359 (1951).
25. Hendricks, R.C., Graham, R.W., Hsu, Y.Y., and Medeiros, A.A.; "Correlation of Hydrogen Heat Transfer in Boiling and Supercritical Pressure States", ARS Journ., VOL. 32, pg. 244 (1962).
26. Graham, R.W.; "Penetration Model Explanation for Turbulent Forced Convection Heat Transfer Observed in Near Critical Fluids", NASA TND 5522 (1969).
27. Deissler, R.G. and Presler, H.F.; "Computed Reference Temperatures for Turbulent Variable Property Heat Transfer in a Tube for Several Common Gases", International Development in Heat Transfer, A.S.M.E., pg. 579 (1963).

28. Goldmann, K.; "Heat Transfer to Supercritical Water and Other Fluids with Temperature Dependent Properties", Chem. Eng. Prog. Symp. Ser., VOL. 50, No. 11, pg. 105 (1954).
29. Tanaka, H., Nishiwaki, N., Hirata, M., and Tsuge, A.; "Forced Convection Heat Transfer to Fluid Near Critical Point Flowing in Circular Tube", Int. J. Heat Mass Transfer, VOL. 14, pg. 739 (1971).
30. Hsu, Y.Y. and Smith, J.M.; "The Effect of Density Variations on Heat Transfer in the Critical Region", J. Heat Transfer, VOL. 83, pg. 176 (1961).
31. Yoshida, S., Fujii, T., and Nisikawa, K.; "Analysis of Turbulent Forced Convection Heat Transfer to a Supercritical Fluid Flowing in a Tube", J.S.M.E., VOL. 35, pg. 3185 (1972).
32. Kato, H., Nishiwaki, N., and Hirata, M.; "Turbulent Heat Transfer in Smooth Pipes at High Prandtl Numbers", Proc. 11th Int. Cong. Appl. Mech., pg. 1101 (1964).
33. Shiralkar, B.S. and Griffith, P.; "Deterioration in Heat Transfer to Fluids at Supercritical Pressure and High Heat Fluxes", A.S.M.E. Paper Number 68-HT-39 (1968).
34. Sastry, V.S. and Schnurr, N.M.; "An Analytical Investigation of Forced Convection Heat Transfer to Fluids Near the Thermodynamic Critical Point", J. Heat Transfer, VOL. 97C, pg. 226 (1975).
35. Hall, W.B.; "The Effects of Buoyancy Forces on Forced Convection Heat Transfer in a Vertical Pipe", Simon Engineering Lab. Report NE1, University of Manchester (1968).
36. Tanaka, H., Tsuge, A., Hirata, M., and Nishiwaki, N.; "Effects of Buoyancy and Acceleration Owing to Thermal Expansion on Forced Turbulent Convection in Vertical Circular Tubes", Int. J. Heat Mass Transfer, VOL. 16, pg. 1267 (1973).
37. Malhotra, A. and Hauptmann, E.G.; "Heat Transfer to a Supercritical Fluid During Turbulent, Vertical Flow in a Circular Duct", International Seminar on Turbulent Buoyant Convection, I.C.H.M.T., Yugoslavia (1976).
38. Launder, B.E. and Spalding, D.B.; "Lectures in Mathematical Models of Turbulence", Academic Press, London and New York (1972).
39. Eckert, E.R.G. and Drake, Jr., Robert M.; ANALYSIS OF HEAT AND MASS TRANSFER, McGraw Hill Book Company (1972).
40. Nelson, M.N.; "An Explicit Finite Difference Analysis for Developing Internal Flows with Heat Transfer and Property Variations", M.Sc. Thesis, Iowa State University, Ames, Iowa (1972).
41. Pletcher, R.H. and Nelson, M.N.; "Heat Transfer to Laminar and Turbulent Flow in Tubes with Variable Fluid Properties", Proceedings of the Fifth International Heat Transfer Conference, Tokyo, VOL. II, pg. 146 (1974).

42. McEligot, D.M., Smith, S.B., and Bankston, C.A.; "Quasi-developed Turbulent Pipe Flow with Heat Transfer", A.S.M.E. Paper Number 70-HT-8 (1970).
43. Patankar, S.V. and Spalding, D.B.; HEAT AND MASS TRANSFER IN BOUNDARY LAYERS, 2nd Ed., Intertext Books (1970).
44. Spalding, D.B.; "A Single Formula for the Law of the Wall", Journal of Applied Mechanics, VOL. 28, Series E, pg. 455 (1961).
45. Sastry, V.S.; "An Analytical Investigation of Forced Convection Heat Transfer in a Circular Duct at Supercritical and Near-critical Pressures", Ph.D. Thesis, Vanderbilt University (1974).
46. Launder, B.E., Reece, G.J., and Rodi, W.; "Progress in Development of Reynolds Stress Closure", J. Fluid Mech., VOL. 68, pg. 537 (1975).
47. Hanjalic, K.; "Two-dimensional Asymmetric Turbulent Flow in Ducts", Ph.D. Thesis, University of London (1970).
48. Rotta, J.; "Statische Theorie Nichthomogener", Turbulenz Z. Phys., VOL. 129, pg. 547 (1951).
49. Naot, D., Shavit, A., and Wolfshtein, M.; "Two-point Correlation Model and the Redistribution of Reynolds Stresses", Phys. Fluids, VOL. 16 (1973).
50. Crow, S.C.; "The Viscoelastic Properties of Fine-grained Incompressible Turbulence", J. Fluid Mech., VOL. 33 (1968).
51. Irwin, H.P.A.H.; "Measurements in Blown Boundary Layers and Their Prediction by Reynolds Stress Modelling", Ph.D. Thesis, McGill University (1974).
52. Wolfshtein, M., Naot, D., and Lin, C.C.; "Models of Turbulence", Ben-Gurion University of the Negev, Department of Mechanical Engineering Report Number ME-746(N).
53. Daly, B.J. and Harlow, F.H.; "Transport Equations in Turbulence", Physics of Fluids, VOL. 13, pg. 2634 (1970).
54. Prandtl, L.; "Über ein neues Formelsystem für die ausgebildete Turbulenz", Nachrichten von der Akad. der Wissenschaft in Göttingen (1945).
55. Tennekes, H. and Lumley, J.L.; A FIRST COURSE IN TURBULENCE, M.I.T. Press, Cambridge, Massachusetts (1972).
56. Hanjalic K. and Launder, B.E.; "A Reynolds Stress Model of Turbulence and its Applications to Symmetric Shear Flows", J. Fluid Mech., VOL. 52, pg. 609 (1972)

57. Khalil, E.E. and Whitelaw, J.H.; "The Calculation of Local Flow Properties in Two-dimensional Furnaces", Imperial College, Mech. Engng. Department Report HTS/74/38 (1974).
58. Rodi, W.; "The Prediction of Free Turbulent Boundary Layers by Use of a 2-equation Model of Turbulence", Ph.D. Thesis, University of London (1972).
59. Launder, B.E. and Spalding, D.B.; "The Numerical Computation of Turbulent Flow", Comp. Meth. in Appl. Mech. and Eng., VOL. 3, pg. 269 (1974).
60. Stephenson, P.L.; "A Theoretical Study of Heat Transfer in Two-dimensional Turbulent Flow in a Circular Pipe and Between Parallel and Diverging Plates", Int. J. Heat Mass Transfer, VOL. 19, pg. 413 (1976).
61. Laufer, J.; "The Structure of Turbulence of Fully-developed Pipe Flow", N.A.C.A. Report 1174 (1954).
62. DuFort, E.C. and Frankel, S.P.; "Stability Conditions in the Numerical Treatment of Parabolic Differential Equations", Mathematical Tables Aid Computation, VOL. 7, pg. 135 (1953).
63. Pletcher, R.H.; "On a Finite Difference Solution for the Constant Property Turbulent Boundary Layer", AIAA Journal, VOL. 7, pg. 305 (1969).
64. Schlichting, H.; BOUNDARY LAYER THEORY, McGraw Hill Book Company (1960).
65. Kays, W.M.; CONVECTIVE HEAT AND MASS TRANSFER, McGraw Hill Book Company (1966).
66. Mills, A.F.; "Experimental Investigation of Turbulent Heat Transfer in the Entrance Region of Circular Conduits", J. Mech. Engr. Sci., VOL. 4, pg. 63 (1962).
67. Jackson, J.D. and Evans-Lutterodt, K.; "Impairment of Turbulent Forced Convection Heat Transfer to Supercritical Pressure CO₂ Caused by Buoyancy Forces", Res. Report N.E. 2, University of Manchester, England (1968).
68. Schnurr, N.M.; "Heat Transfer to Carbon-dioxide in the Immediate Vicinity of the Critical Point", A.S.M.E. Paper Number 68-HT-32 (1968).
69. Ikryannikov, N.P., Petukhov, B.S., and Protopopov, V.S.; "An Experimental Investigation of Heat Transfer in the Single-phase Near-critical Region with Combined Forced and Free Convection", Teplofizika Vysokikh Temperatur, VOL. 10, pg. 96 (1972).
70. Reynolds, A.J.; "The Prediction of Turbulent Prandtl and Schmidt Numbers", Int. J. Heat Mass Transfer, VOL. 18, pg. 1055 (1975).

71. Graber, H.; "Der Wärmeübergang in Glatten Rohren Zwischen Parallelen Platten in Ringspallen and Langs Rohrbündeln bei Exponentueller Wärmeflussverteilung in Erzwungener Laminarer oder Turbulenter Stromung", Int. J. Heat Mass Transfer, VOL. 13, pg. 1645 (1970).
72. Quaramby, A. and Quirk, R.; "Axisymmetric and Non-axisymmetric Turbulent Diffusion in a Plain Circular Tube at High Schmidt Number", Int. J. Heat Mass Transfer, VOL. 7, pg. 45 (1973).
73. Cebici, T.; "A Model of Eddy Conductivity and Turbulent Prandtl Number", A.S.M.E. Paper Number 72-WA/HT-13 (1971).
74. Na, T.Y. and Habib, I.S.; "Heat Transfer in Turbulent Pipe Flow Based on a New Mixing Length Model", Applied Scientific Res., VOL. 28, pg. 302 (1973).
75. Rotta, J.C.; "Temperaturverteilungen in der Turbulenten Grenzschicht an der Ebenen Platte", Int. J. Heat Mass Transfer, VOL. 7, pg. 215 (1964).
76. Gibson, M.M. and Launder, B.E.; "On a Calculation of Horizontal Turbulent Free Shear Flows Under Gravitational Influence", A.S.M.E. J. Heat Transfer, VOL. 98C (1976).
77. Bourke, P.J., Pulling, D.J., Gill, L.E., and Denton, W.H.; "Forced Convective Heat Transfer to Turbulent CO₂ in the Supercritical Region", Int. J. Heat Mass Transfer, VOL. 13, pg. 1339 (1970).
78. Hall, W.B. and Jackson, J.D.; "Laminarisation of Turbulent Pipe Flow by Buoyancy Forces", A.S.M.E. Paper Number 69-HT-55 (1969).
79. Bates, J.A., Schmall, R.A., Hasen, G.A., and McEligot, D.M.; "Effects of Buoyant Body Forces on Forced Convection in Heated Laminarizing Flows", Proceedings of the Fifth International Heat Transfer Conference, Tokyo, VOL. II, Pg. 141 (1974).
80. Polyakov, A.F.; "Mechanism and Limites on the Formation of Conditions for Impaired Heat Transfer at a Supercritical Coolant Pressure", Teplofizika Vysokikh Temperatur, VOL. 13, pg. 1210 (1975).
81. Petukhov, B.S.; "Turbulent Flow and Heat Transfer in Pipes Under Considerable Influence of Thermo-gravitational Forces", International Seminar on Turbulent Buoyant Convection, I.C.H.M.T., Yugoslavia (1976).
82. Launder, B.E.; "On the Effects of a Gravitational Field on the Turbulent Transport of Heat and Momentum", J. Fluid Mech., VOL. 68 (1975).
83. Hirschfelder, J.O., Curtiss, C.F., and Bird, R.B.; MOLECULAR THEORY OF GASES AND LIQUIDS, Wiley (1954).
84. Michels, A., Sengers, J.V., and Van der Gulik, P.S.; "The Thermal Conductivity of Carbon Dioxide in the Critical Region", Parts I and II, Physica, VOL. 28, pg. 1201 (1962).

85. Sastry, V.S.; "Private Communication", Department of Mechanical Engineering, Tennessee State University, Nashville, Tennessee (1975).
86. Michels, A. and Michels, C.; "Isotherms of CO₂ Between 0° and 150° and Pressures From 16 to 250 Atm (Amagat Densities 18-206)", Proceedings of the Royal Society of London, VOL. A153, pg. 201 (1935).
87. Michels, A, Blaisse, B., and Michels, C.; "The Isotherms of CO₂ in the Neighbourhood of the Critical Point and Round the Co-existence Line", Proc. Roy. Soc. of London (see 86 here), Vol. A160, pg. 358 (1937).
88. Koppel, L.B. and Smith, J.M.; "Thermal Properties of Carbon Dioxide in the Critical Region", Journal of Chemical and Engineering Data, VOL. 5, pg. 437 (1960).
89. Kestin, J., Whitelaw, J.H., and Zien, T.F.; "The Viscosity of Carbon Dioxide in the Neighbourhood of the Critical Points", Physica, VOL. 30, pg. 161 (1964).
90. Sengers, J.V. and Michels, A.; "The Thermal Conductivity of Carbon Dioxide in the Critical Region", Second Symposium on Thermophysical Properties, A.S.M.E., New York, Academic Press, pg. 434 (1961).

APPENDIX A

Properties of Supercritical Fluids

APPENDIX A. Properties of Supercritical Fluids

Hsu and Graham³ have reviewed the present state of knowledge concerning properties of near critical fluids. A useful treatment of the thermodynamics of the critical point can be found in Hirschfelder, Curtiss, and Bird⁸³.

Classical modelling of a fluid near the critical state has been based on Van der Waal's proposal. His model in which an allowance is made for the attractive and repulsive forces between molecules leads to an equation of state in the following form:

$$\left(p + \frac{a}{V^2}\right)(V - b) = R_t \quad . \quad (A.1)$$

The Van der Waal's equation predicts a value of infinity for C_p at the critical point. The Van der Waal's equation is a useful tool for understanding the thermodynamic behaviour near the critical state but it does not succeed in mapping the (P, ρ, T) surface with sufficient accuracy. Therefore, Virial type equations requiring several empirical coefficients are usually employed,

$$P = A(t)\rho + B(t)\rho^2 + C(t)\rho^3 + D(t)\rho^4 \quad . \quad (A.2)$$

A mathematically more analytic equation, based on the recently popular Ising model for ferromagnets has been proposed by Vicentini Missoni et al. For numerical work, however, it is probably not an efficient practice to use these equations directly in the computer program since these equations require an interactive solution. Therefore, use was made of tabulated

values of properties.

In most supercritical heat transfer systems, the pressure is maintained above the critical pressure. Therefore, singularities such as an infinite value for specific heat are avoided. However, the property variation is still severe in the vicinity of the critical point. For example, the peak in specific heat is still large even at pressures considerably removed from the critical pressure.

Like the specific heat, the thermal conductivity also exhibits a peak around the critical point but because of the difficulties in measuring this quantity near the critical state, there was considerable controversy regarding the behaviour of thermal conductivity near the critical state until very recent times. Some investigators believed that there is no spike in thermal conductivity. However, experiments due to Michels, Sengers, and Van der Gulik⁸⁴ have demonstrated that there is a large spike in thermal conductivity right around the critical point. Subsequently, similar spikes have been noticed in other fluids as well. Property values used in this investigation include this spike.

Compared to thermal conductivity, variations in viscosity around the critical point are less drastic. It is likely that there is a slight detectable spike in viscosity as well. However, because of uncertainty in the precise magnitude of this peak, it is normally neglected in engineering applications. The viscosity data obtained in this investigation contained slight irregularities but these were smoothed out prior to feeding the property tables in the computer program.

The property data for CO₂ used in this investigation are the same

as that used with two previous numerical studies due to Schnurr⁶⁸ and Sastry^{9,85}. The density data is from Michels and Michels^{8,86,87}. Enthalpy and specific heat data are from Koppel and Smith⁸⁸. Viscosity data are from Kestin, Whitelaw, and Zien⁸⁹ and thermal conductivity data are from Sengers and Michels⁹⁰. Table A.1 gives an example of how the property tables were set up at $p/p_c = 1.027$ prior to feeding in the computer program. A good agreement between the experimental and predicted heat transfer data in a number of test runs indicates that the property data used in this investigation are probably accurate enough for the work carried out in this investigation. The cases where such an agreement was not achieved appear largely to be a result of approximations in the theoretical model rather than inaccuracies in the property data. However, as theoretical prediction schemes improve and more accurate property data becomes available in future, it should be employed in numerical prediction schemes.

TABLE A.1* Properties of Carbon Dioxide (Pressure = 1100.00 PSIA).

N**	TEMPERATURE (RANKINE)	VISCOSITY (LBM/FT-SEC)	SP. HEAT (BTU/LBM-R)	CONDUCTIVITY (BTU/SEC-FT-R)	DENSITY (LBM/CU FT)
1	483.3	.7334E-04	.496	.1904E-04	61.505
2	492.6	.6939E-04	.537	.1835E-04	60.017
3	502.0	.6530E-04	.572	.1759E-04	58.321
4	510.3	.6169E-04	.611	.1674E-04	56.455
5	517.5	.5866E-04	.651	.1584E-04	54.431
6	525.0	.5512E-04	.735	.1490E-04	51.850
7	531.9	.5132E-04	.848	.1418E-04	49.544
8	537.3	.4559E-04	.937	.1338E-04	47.603
9	542.0	.3937E-04	1.200	.1261E-04	45.320
10	545.5	.3405E-04	1.635	.1139E-04	42.410
11	547.8	.3037E-04	2.218	.1057E-04	39.564
12	549.0	.2828E-04	2.878	.1529E-04	36.927
13	549.4	.2744E-04	3.294	.1595E-04	34.250
14	549.7	.2661E-04	3.709	.1662E-04	31.575
15	550.1	.2564E-04	3.861	.1726E-04	28.689
16	550.6	.2437E-04	3.397	.1785E-04	25.316
17	551.1	.2298E-04	2.930	.1804E-04	22.100
18	552.2	.2038E-04	2.427	.1433E-04	20.291
19	554.4	.1630E-04	1.892	.8252E-05	18.433
20	557.7	.1461E-04	1.408	.6588E-05	16.877
21	562.2	.1407E-04	1.068	.5256E-05	15.545
22	567.6	.1375E-04	.789	.4760E-05	14.446
23	574.9	.1352E-04	.618	.4543E-05	13.350
24	584.1	.1333E-04	.514	.4458E-05	12.246
25	595.7	.1337E-04	.446	.4404E-05	11.255
26	607.0	.1347E-04	.409	.4389E-05	10.527
27	618.4	.1359E-04	.384	.4389E-05	9.951
28	631.8	.1373E-04	.362	.4422E-05	9.428
29	645.6	.1386E-04	.344	.4460E-05	8.945
30	659.7	.1398E-04	.330	.4499E-05	8.509
31	677.8	.1416E-04	.321	.4574E-05	8.117
32	694.3	.1433E-04	.309	.4653E-05	7.798
33	710.6	.1450E-04	.297	.4732E-05	7.489
34	726.8	.1468E-04	.287	.4811E-05	7.199
35	743.1	.1486E-04	.278	.4890E-05	6.935

* The data here is described in British Units because this is the manner in which it was fed to the computer program. The relevant conversion factors to S.I. units are contained in the computer program and are from Eckert and Drake³⁹.

** ENTHALPY = 30.0 + 5(N - 1), (BTU/LBM).

APPENDIX B

Equations for the Turbulence Model

Reynolds Stress Equation

The starting point for deriving equations for turbulent quantities are the Navier-Stokes equations. These may be written as:

$$\frac{\partial \tilde{u}_i}{\partial t} + \tilde{u}_k \frac{\partial \tilde{u}_i}{\partial x_k} = - \frac{1}{\rho} \frac{\partial \tilde{p}}{\partial x_i} + \frac{1}{\rho} \frac{\partial}{\partial x_k} \left(\mu \frac{\partial \tilde{u}_i}{\partial x_k} \right) . \quad (\text{B.1})$$

The instantaneous motions can be broken into mean and fluctuating components. The resulting equation is:

$$\begin{aligned} \frac{\partial (\hat{u}_i + u_i)}{\partial t} + \hat{u}_k \frac{\partial \hat{u}_i}{\partial x_k} + \hat{u}_k \frac{\partial u_i}{\partial x_k} + u_k \frac{\partial \hat{u}_i}{\partial x_k} + u_k \frac{\partial u_i}{\partial x_k} = - \frac{1}{\rho} \frac{\partial}{\partial x_i} (p + p') \\ + \frac{1}{\rho} \frac{\partial}{\partial x_k} \left[\mu \frac{\partial}{\partial x_k} (\hat{u}_i + u_i) \right] . \end{aligned} \quad (\text{B.2})$$

The time averaged form of these equations are the Reynolds equations,

$$\frac{\partial \hat{u}_i}{\partial t} + \hat{u}_k \frac{\partial \hat{u}_i}{\partial x_k} = - \frac{1}{\rho} \frac{\partial \bar{p}'}{\partial x_i} + \frac{1}{\rho} \frac{\partial}{\partial x_k} \left(\mu \frac{\partial \hat{u}_i}{\partial x_k} \right) - \frac{1}{\rho} \frac{\partial}{\partial x_k} (\rho \overline{u_i u_k}) . \quad (\text{B.3})$$

Subtracting equation (B.3) from (B.2) results in the equation for the fluctuating component u_i (equation (3.1)). This is repeated here for convenience:

$$\frac{\partial u_i}{\partial t} + \hat{u}_k \frac{\partial u_i}{\partial x_k} = - \frac{1}{\rho} \frac{\partial p'}{\partial x_i} + \frac{1}{\rho} \frac{\partial}{\partial x_k} \left(\mu \frac{\partial u_i}{\partial x_k} \right) - u_k \frac{\partial \hat{u}_i}{\partial x_k} + \frac{1}{\rho} \frac{\partial}{\partial x_k} (\rho \overline{u_i u_k} - \rho u_i u_k) . \quad (\text{B.4})$$

Multiplying equation (B.4) by u_j and adding to it the corresponding equation for u_j multiplied by u_i , leads to:

$$\begin{aligned}
\frac{\partial U_i U_j}{\partial T} + \hat{U}_k \frac{\partial U_i U_j}{\partial X_k} = & - U_k U_j \frac{\partial \hat{U}_i}{\partial X_k} - U_k U_i \frac{\partial \hat{U}_j}{\partial X_k} - \frac{U_j}{\rho} \frac{\partial p'}{\partial X_i} - \frac{U_i}{\rho} \frac{\partial p'}{\partial X_j} \\
& + \frac{U_j}{\rho} \frac{\partial}{\partial X_k} \left(\mu \frac{\partial U_i}{\partial X_k} \right) + \frac{U_i}{\rho} \frac{\partial}{\partial X_k} \left(\mu \frac{\partial U_j}{\partial X_k} \right) \\
& - \frac{U_j}{\rho} \frac{\partial}{\partial X_k} \left(\rho U_i U_k - \rho \overline{U_i U_k} \right) \\
& - \frac{U_i}{\rho} \frac{\partial}{\partial X_k} \left(\rho U_j U_k - \rho \overline{U_j U_k} \right) .
\end{aligned} \tag{B.5}$$

During the simplifications, use is made of the continuity equations,

$$\frac{\partial \rho \hat{U}_i}{\partial X_i} = 0, \quad \frac{\partial \rho \hat{U}_j}{\partial X_j} = 0, \quad \text{and} \quad \frac{\partial \rho U_i}{\partial X_i} = 0 . \tag{B.6}$$

The continuity equation (B.6) allows transformations such as

$$\rho U_k \frac{\partial}{\partial X_k} (F) = \frac{\partial}{\partial X_k} (\rho U_k F) , \tag{B.7}$$

where F is any general flow property.

Further rearrangements of the left-hand side of equation (B.5)

lead to:

$$\begin{aligned}
\frac{\partial U_i U_j}{\partial T} + \hat{U}_k \frac{\partial U_i U_j}{\partial X_k} = & - U_k U_j \frac{\partial \hat{U}_i}{\partial X_k} - U_k U_i \frac{\partial \hat{U}_j}{\partial X_k} + \frac{p'}{\rho} \frac{\partial U_i}{\partial X_j} + \frac{p'}{\rho} \frac{\partial U_j}{\partial X_i} \\
& - \frac{1}{\rho} \frac{\partial p' U_i}{\partial X_i} - \frac{1}{\rho} \frac{\partial p' U_j}{\partial X_j} + \frac{1}{\rho} \frac{\partial}{\partial X_k} \left(\mu U_j \frac{\partial U_i}{\partial X_k} \right) \\
& + \frac{1}{\rho} \frac{\partial}{\partial X_k} \left(\mu U_i \frac{\partial U_j}{\partial X_k} \right) - 2 \frac{\mu}{\rho} \frac{\partial U_i}{\partial X_k} \frac{\partial U_j}{\partial X_k} - \frac{1}{\rho} \frac{\partial}{\partial X_k} \left(\rho U_i U_j U_k \right)
\end{aligned}$$

$$+ \frac{U_i}{\rho} \frac{\partial}{\partial X_k} (\rho \overline{U_i U_k}) + \frac{U_j}{\rho} \frac{\partial}{\partial X_k} (\rho \overline{U_j U_k}) , \quad (B.8)$$

or,

$$\begin{aligned} \frac{\partial U_i U_j}{\partial T} + \hat{U}_k \frac{\partial U_i U_j}{\partial X_k} = & - \left[U_j U_k \frac{\partial \hat{U}_i}{\partial X_k} + U_i U_k \frac{\partial \hat{U}_j}{\partial X_k} \right] - 2\nu \frac{\partial U_i}{\partial X_k} \frac{\partial U_j}{\partial X_k} + \frac{p'}{\rho} \left(\frac{\partial U_i}{\partial X_j} + \frac{\partial U_j}{\partial X_i} \right) \\ & - \frac{1}{\rho} \frac{\partial}{\partial X_k} \{ \rho U_i U_j U_k - \mu \frac{\partial U_i U_j}{\partial X_k} - p' (\delta_{jk} U_i + \delta_{ik} U_j) \} \\ & + \frac{U_i}{\rho} \frac{\partial}{\partial X_k} (\rho \overline{U_i U_k}) + \frac{U_j}{\rho} \frac{\partial}{\partial X_k} (\rho \overline{U_j U_k}) . \end{aligned} \quad (B.9)$$

Averaging equation (B.9) leads directly to the Reynolds stress equation which is equation (3.2).

Turbulence Dissipation Equation

An equation for the transport of the dissipative correlation was obtained in the following manner. Equation (B.4) is differentiated with the operator $\frac{\partial}{\partial X_\ell}$ leading to:

$$\begin{aligned} \frac{\partial}{\partial T} \left(\frac{\partial U_i}{\partial X_\ell} \right) + \hat{U}_k \frac{\partial}{\partial X_k} \left(\frac{\partial U_i}{\partial X_\ell} \right) + \frac{\partial \hat{U}_k}{\partial X_\ell} \frac{\partial U_i}{\partial X_k} = & - \frac{\partial}{\partial X_\ell} \left(\frac{1}{\rho} \frac{\partial p'}{\partial X_i} \right) - U_k \frac{\partial^2 \hat{U}_i}{\partial X_\ell \partial X_k} - \frac{\partial \hat{U}_i}{\partial X_k} \frac{\partial U_k}{\partial X_\ell} \\ & - \frac{\partial}{\partial X_\ell} \left(U_k \frac{\partial U_i}{\partial X_k} \right) + \frac{\partial}{\partial X_\ell} \left\{ \frac{1}{\rho} \frac{\partial}{\partial X_k} (\rho \overline{U_i U_k}) \right\} \\ & + \frac{\partial}{\partial X_\ell} \left\{ \frac{1}{\rho} \frac{\partial}{\partial X_k} (\mu \frac{\partial U_i}{\partial X_k}) \right\} . \end{aligned} \quad (B.10)$$

Multiplying equation (B.10) with $\frac{\partial U_i}{\partial X_\ell}$ results in

$$\begin{aligned}
\frac{1}{2} \frac{\partial}{\partial T} \left[\left(\frac{\partial U_i}{\partial X_\ell} \right)^2 \right] + \frac{\hat{U}_k}{2} \frac{\partial}{\partial X_k} \left[\left(\frac{\partial U_i}{\partial X_\ell} \right)^2 \right] = & - \frac{\partial U_i}{\partial X_\ell} \frac{\partial \hat{U}_k}{\partial X_\ell} \frac{\partial U_i}{\partial X_k} - \frac{\partial U_i}{\partial X_\ell} \frac{\partial}{\partial X_\ell} \left(\frac{1}{\rho} \frac{\partial p'}{\partial X_i} \right) \\
& - U_k \frac{\partial U_i}{\partial X_\ell} \frac{\partial^2 \hat{U}_i}{\partial X_\ell \partial X_k} - \frac{\partial \hat{U}_i}{\partial X_k} \frac{\partial U_k}{\partial X_\ell} \frac{\partial U_i}{\partial X_\ell} \\
& - \frac{\partial U_i}{\partial X_\ell} \frac{\partial U_i}{\partial X_k} \frac{\partial U_k}{\partial X_\ell} - U_k \frac{\partial U_i}{\partial X_\ell} \frac{\partial}{\partial X_k} \left(\frac{\partial U_i}{\partial X_\ell} \right) \\
& + \frac{\partial U_i}{\partial X_\ell} \frac{\partial}{\partial X_\ell} \left[\frac{1}{\rho} \frac{\partial}{\partial X_k} (\rho \overline{U_i U_k}) \right] \\
& + \frac{\partial U_i}{\partial X_\ell} \frac{\partial}{\partial X_\ell} \left[\frac{1}{\rho} \frac{\partial}{\partial X_k} (\mu \frac{\partial U_i}{\partial X_k}) \right]. \tag{B.11}
\end{aligned}$$

Rearranging the preceeding equation and multiplying throughout by 2ν ,

$$\begin{aligned}
\nu \frac{\partial}{\partial T} \left[\frac{\nu}{\nu} \left(\frac{\partial U_i}{\partial X_\ell} \right)^2 \right] + \nu U_k \frac{\partial}{\partial X_k} \left[\frac{\nu}{\nu} \left(\frac{\partial U_i}{\partial X_\ell} \right)^2 \right] = & - \frac{\nu}{\rho} \frac{\partial}{\partial X_k} \left[\frac{\rho}{\nu} \nu U_k \left(\frac{\partial U_i}{\partial X_\ell} \right)^2 \right. \\
& \left. - 2 \frac{\partial U_i}{\partial X_\ell} \frac{\partial}{\partial X_\ell} (\mu \frac{\partial U_i}{\partial X_k}) \right] - 2\nu \frac{\partial U_i}{\partial X_\ell} \frac{\partial}{\partial X_\ell} \left(\frac{1}{\rho} \frac{\partial p'}{\partial X_i} \right) \\
& - 2\nu \frac{\partial \hat{U}_i}{\partial X_k} \left(\frac{\partial U_i}{\partial X_\ell} \frac{\partial U_k}{\partial X_\ell} + \frac{\partial U_\ell}{\partial X_i} \frac{\partial U_k}{\partial X_k} \right) - 2\nu U_k \frac{\partial U_i}{\partial X_\ell} \frac{\partial^2 \hat{U}_i}{\partial X_\ell \partial X_k} \\
& - 2\nu \frac{\partial U_i}{\partial X_k} \frac{\partial U_i}{\partial X_\ell} \frac{\partial U_k}{\partial X_k} + 2\nu \frac{\partial U_i}{\partial X_\ell} \frac{\partial}{\partial X_\ell} \left[\frac{1}{\rho} \frac{\partial}{\partial X_k} (\mu \frac{\partial U_i}{\partial X_k}) \right] \\
& - 2 \frac{\nu}{\rho} \frac{\partial}{\partial X_k} \left[\frac{\partial U_i}{\partial X_\ell} \frac{\partial}{\partial X_\ell} (\mu \frac{\partial U_i}{\partial X_k}) \right] \\
& + 2\nu \frac{\partial U_i}{\partial X_\ell} \frac{\partial}{\partial X_\ell} \left[\frac{1}{\rho} \frac{\partial}{\partial X_k} (\rho \overline{U_i U_k}) \right]. \tag{B.12}
\end{aligned}$$

Replacing $v(\frac{\partial U_i}{\partial x_l})^2$ by ϵ' and averaging leads directly to the desired equation which is equation (3.14).

Algebraic Stress Modelling

Equation (3.22) was derived by Rodi using only one of the components of the pressure-strain correlation. A similar expression using the full pressure-strain correlation (equation (3.7)) is derived here. Using

$$\frac{D \overline{U_i U_j}}{Dt} - \Gamma(\overline{U_i U_j}) = \frac{\overline{U_i U_j}}{K} (P - \epsilon) , \quad (B.13)$$

the Reynolds stress equation can be written as:

$$\begin{aligned} \frac{\overline{U_i U_j}}{K} (P - \epsilon) = & \frac{2}{3} \epsilon \delta_{ij} - C_1 \frac{\epsilon}{K} (\overline{U_i U_j} - \frac{2}{3} \delta_{ij} K) + P_{ij} - L(P_{ij} - \frac{2}{3} \delta_{ij} P) \\ & - MK \left(\frac{\partial \hat{U}_i}{\partial x_j} + \frac{\partial \hat{U}_j}{\partial x_i} \right) - N \left(D_{ij} - \frac{2}{3} \delta_{ij} P \right) , \end{aligned} \quad (B.14)$$

where,

$$L = \frac{C_2 + 8}{11}, \quad M = \frac{30 C_2 - 2}{55}, \quad \text{and } N = \frac{8 C_2 - 2}{11} . \quad (B.15)$$

Equation (B.14) can be rearranged as:

$$\begin{aligned} \frac{\overline{U_i U_j} - \frac{2}{3} \delta_{ij} K}{K} = & \frac{\Lambda_1}{\epsilon} (P_{ij} - \frac{2}{3} \delta_{ij} P) + \frac{\Lambda_2}{\epsilon} (D_{ij} - \frac{2}{3} \delta_{ij} P) \\ & + \frac{\Lambda_3}{\epsilon} K \left(\frac{\partial \hat{U}_i}{\partial x_j} + \frac{\partial \hat{U}_j}{\partial x_i} \right) , \end{aligned} \quad (B.16)$$

where,

$$\Lambda_1 = \frac{1 - L}{(P/\epsilon - 1 + C_1)}, \Lambda_2 = \frac{-N}{(P/\epsilon - 1 + C_1)}, \text{ and } \Lambda_3 = \frac{-M}{(P/\epsilon - 1 + C_1)}. \quad (\text{B.17})$$

Equation (B.16) can then be expanded for thin shear flows to yield expressions for the stress components $\overline{U_1 U_2}$, $\overline{U_1^2}$, and $\overline{U_2^2}$. These are:

$$\frac{\overline{U_1 U_2}}{K} = \frac{\Lambda_1}{\epsilon} (-\overline{U_2^2} \frac{\partial \hat{U}_1}{\partial X_2}) + \frac{\Lambda_2}{\epsilon} (-\overline{U_1^2} \frac{\partial \hat{U}_1}{\partial X_2}) + K \frac{\Lambda_3}{\epsilon} (\frac{\partial \hat{U}_1}{\partial X_2}), \quad (\text{B.18})$$

$$\frac{\overline{U_2^2} - 2/3 K}{K} = -\frac{2}{3} \frac{\Lambda_1}{\epsilon} P + \frac{4P}{3} \frac{\Lambda_2}{\epsilon}, \quad (\text{B.19})$$

$$\frac{\overline{U_1^2} - 2/3 K}{K} = -\frac{2}{3} \frac{\Lambda_1}{\epsilon} P + \frac{4P}{3} \frac{\Lambda_2}{\epsilon}. \quad (\text{B.20})$$

Substituting equations (B.19) and (B.20) in equation (B.18) yields

$$\overline{U_1 U_2} = \frac{K^2}{\epsilon} \Lambda_3 \frac{\partial \hat{U}_1}{\partial X_2} - \frac{2}{3} \frac{K^2}{\epsilon} (\Lambda_1 + \Lambda_2) (1 - \Lambda_1 \frac{P}{\epsilon} + 2\Lambda_2 \frac{P}{\epsilon}) \frac{\partial \hat{U}_1}{\partial X_2}, \quad (\text{B.21})$$

or

$$\overline{U_1 U_2} = -\frac{2}{3} \frac{K^2}{\epsilon} \frac{[3/2 M(P/\epsilon - 1 + C_1) + \{(L - 2N)P/\epsilon + C_1 - 1\}(1 - L - N)]}{(P/\epsilon - 1 + C_1)^2} \frac{\partial \hat{U}_1}{\partial X_2}. \quad (\text{B.22})$$

Further substitution for L, M, and N leads to equation (3.24).

A Relation Connecting the Constants of the Dissipation Equation

In order to derive this relation, use will be made of equations

(3.32), (3.33), (3.34), (3.35), (3.36), and (3.37) of Chapter III.

Replacing $\frac{\partial u}{\partial y}$ in equation (3.33) through equation (3.34) and K through (3.36) gives

$$\epsilon = \left(\frac{\tau}{\rho}\right)^{3/2} \frac{1}{\kappa y} . \quad (\text{B.23})$$

Equation (3.30) for fully developed constant property pipe flow can be written as

$$\frac{1}{r} \frac{\partial}{\partial r} \left(r \frac{K^2}{\epsilon \sigma'_{\epsilon}} \frac{\partial \epsilon}{\partial r} \right) = (C_{\epsilon_2} - C_{\epsilon_1}) \frac{\epsilon^2}{K} . \quad (\text{B.24})$$

Using equation (3.37) and noting that $y = R - r$, equation (B.23) can be written as

$$\epsilon = \left(\frac{\tau \omega}{\rho R}\right)^{3/2} \frac{1}{\kappa} \frac{r^{3/2}}{R - r} . \quad (\text{B.25})$$

Further,

$$\frac{\partial \epsilon}{\partial r} = \left(\frac{\tau \omega}{\rho R}\right)^{3/2} \frac{1}{\kappa} \left[\frac{3}{2} \frac{r^{1/2}}{R - r} + \frac{r^{3/2}}{(R - r)^2} \right] . \quad (\text{B.26})$$

Using the results expressed in equations (B.26), (3.34), and (3.35),

$$r \frac{K^2}{\sigma'_{\epsilon} \epsilon} \frac{\partial \epsilon}{\partial r} = \left(\frac{\tau}{\rho}\right)^2 \frac{1}{\sigma'_{\epsilon} C_{\mu}} \left[\frac{3}{2} + \frac{r}{R - r} \right] , \quad (\text{B.27})$$

and further,

$$\frac{\partial}{\partial r} \left(r \frac{K^2}{\sigma'_{\epsilon} \epsilon} \frac{\partial \epsilon}{\partial r} \right) = \left(\frac{\tau \omega}{\rho R}\right)^2 \left[3r + \frac{3r^2}{R - r} + \frac{r^3}{(R - r)^2} \right] . \quad (\text{B.28})$$

Now putting $R - r = y$, and noting that $r \approx R$ and further substituting the value of K from equation (3.35), ϵ from (B.23) in equation (B.24) results in

$$\kappa \left[1 + \frac{3y}{R} + \frac{3y^2}{R^2} \right] = \sigma'_\epsilon (C_{\epsilon_1} - C_{\epsilon_2}) C_\mu^{3/2}. \quad (\text{B.29})$$

It should be pointed out that the entire treatment in this section is only valid for the fully turbulent near wall region.

APPENDIX C

Computer Program

The computer program was compiled and executed on an IBM system 370, Model 168 computer under control of the MTS operating system. The Watfiv fortran compiler was used since the nature of the task undertaken required frequent debugging. However, the coding used in the program consists of commonly used fortran IV statements (with the exception of PRINT) and therefore the program should be compatible with other fortran IV compilers as well. The execution time for a run typical to the present work is about 40 seconds.

The Main Segment

The overall structure of the program is illustrated in the adjoining flow chart (Figure 39). Control of operations is maintained through the main segment of the program. This section of the program contains all of the READ statements as well as most of the WRITE statements used in the program. Except for the subroutine VANDR, all other subroutines are brought into operation only through this section of the program.

For convenience of description and understanding, the main segment of the program has been divided into seven chapters. These divisions are marked on the computer listing contained in Appendix D. However, it was not possible to make strict demarcations of the main segment because of several small auxilliary calculations that are carried out in this section of the program. The approximate contents of the various chapters are described next.

Chapter I. Dimensioning of arrays as well as statements containing input data.

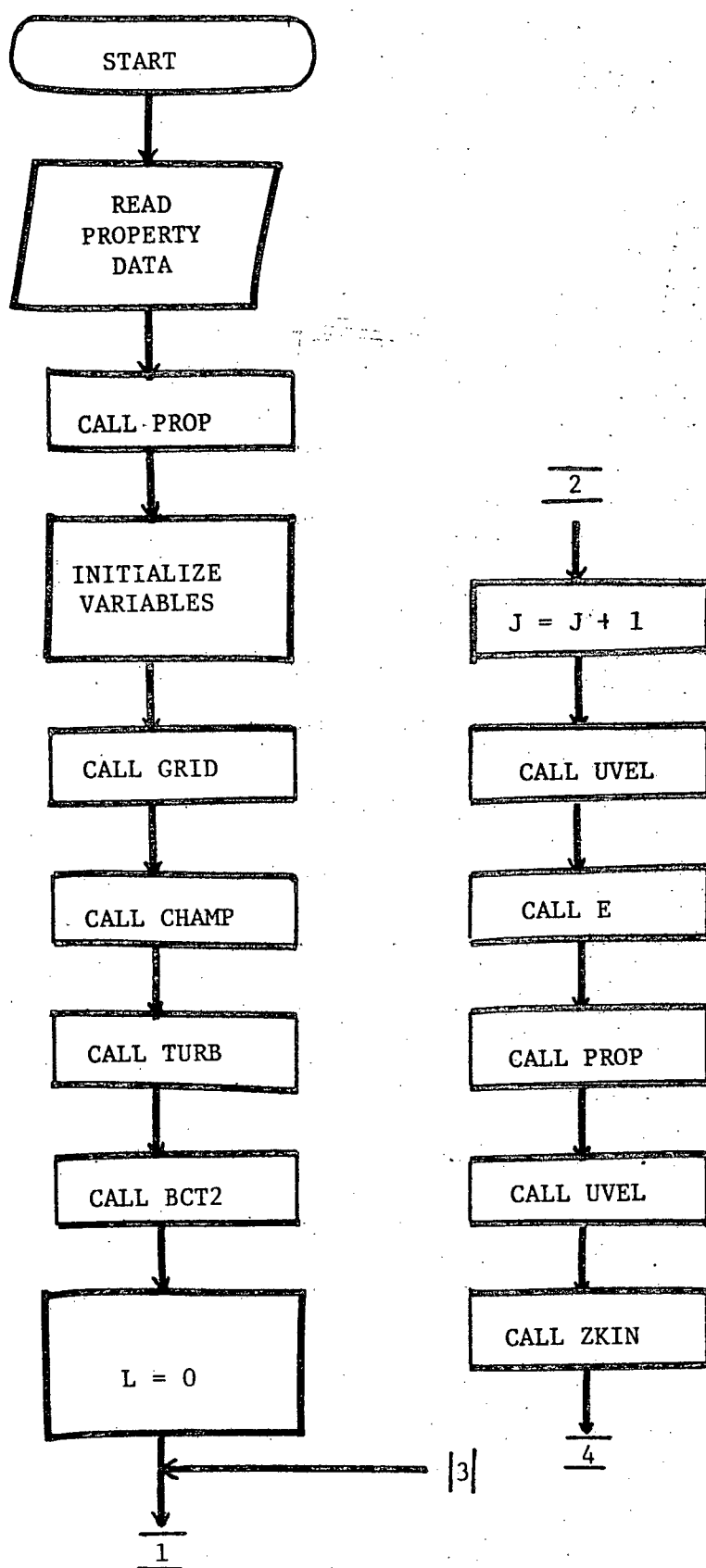
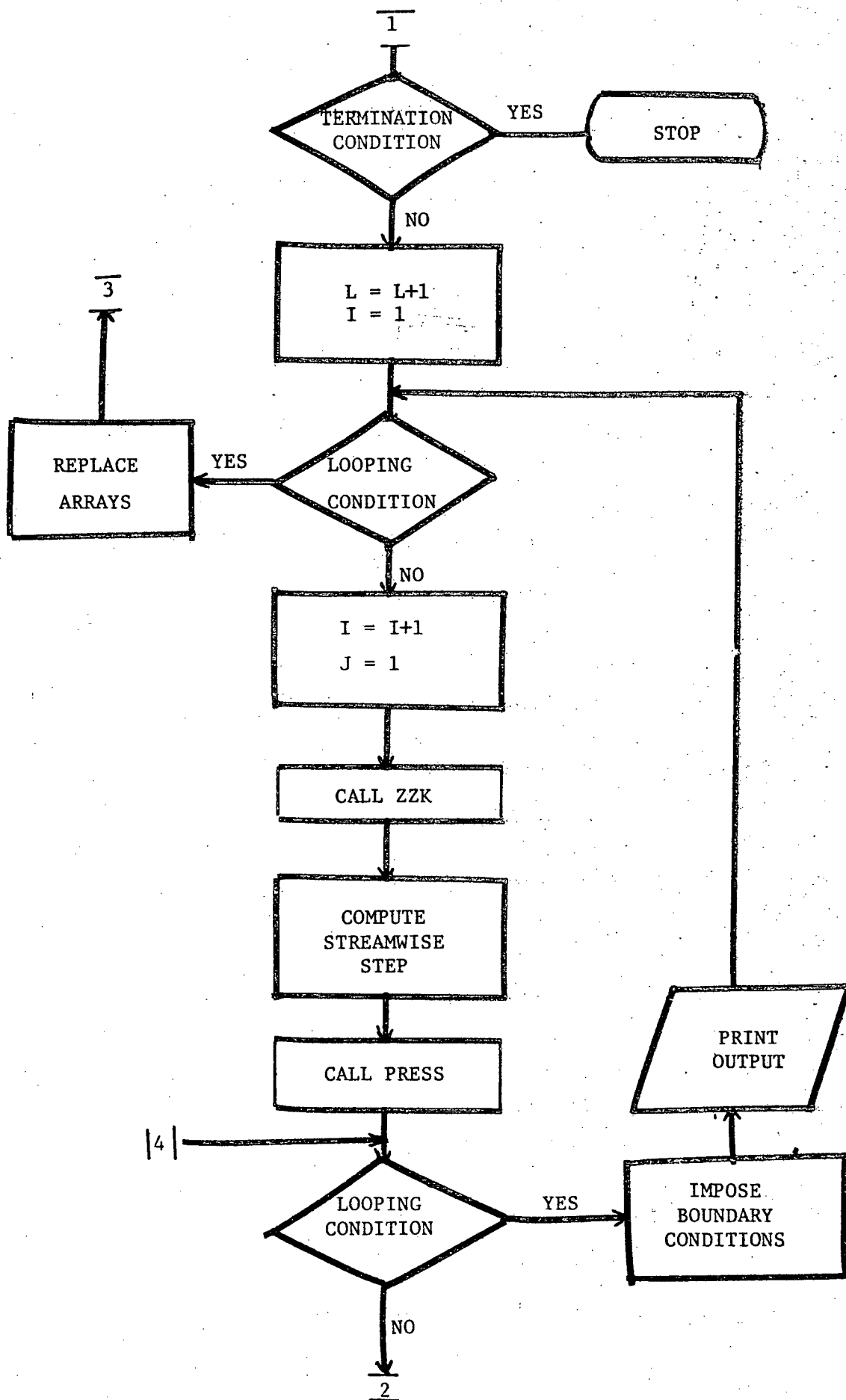


FIGURE 39. Flow Chart of Computer Program.



CHAPTER II. READ statements for property data and conversion to appropriate units.

CHAPTER III. Initialisation of variables.

CHAPTER IV. CALL statements for subroutines concerned with the starting profiles and Y-grid divisions.

CHAPTER V. Call statements for subroutines concerned with solution of the differential equations and the pressure equation. Subroutines used in assembling effective viscosities are also called in this section of the program.

CHAPTER VI. Contains statements for imposing boundary conditions and the WRITE statements for dependent variables.

CHAPTER VII. Contains statements for rearrangement of array so that the computed variables do not exceed the allocated storage.

Chapter V of the main segment utilizes a major portion of the total execution time (about 90%). Therefore, the programming approach for most of the other chapters gives preference to convenience rather than computational efficiency. For example, subroutine GRID is called in Chapter IV of the program. This subroutine is actually required only for the Blasius flat plate problem. For other problems, it is superfluous. It was left in because this subroutine was frequently used for testing the program.

All computations are performed in SI units. Therefore, all inputs with the exception of physical property data are given in SI units. The appropriate conversion factors for the property data are included in

the program.

A description of the important aspects of the computer program is provided next.

Storage Allocation

A description of the arrays is given in Table C.1. The five dependent variables, U, V, T, DE, and ZK, as well as the properties RHO , VISC, XK, and CP are stored in arrays of size 10 x 100 (10 columns and 100 rows). The program will also work without any change in the logic of computation with arrays of a size as small as 3 x N, where N is the number of grid divisions used in a particular problem. Rather than changing N for every problem, 100 rows in the arrays are provided in the DIMENSION statement since the Y-grid divisions rarely exceed this quantity. 100 rows imply 200 nodal points along each diameter of a pipe. A minimum of 3 columns are necessary in this program for each of these arrays because values of variables from two previous steps are stored in the first and second column and the new computed values are stored in the third column. After the three columns are used up, variables from the second and third columns can be transferred into the first and second columns respectively. However, repeated replacements utilize more computational time. Therefore, a larger array size of 10 x 100 was used in the program. In this way, computation proceeds up to the 10th streamwise step. Subsequently, the information from the 9th and 10th columns is reassigned to 1st and 2nd columns of the arrays. Larger array sizes were not used in order to keep the core usage within reasonable limits.

TABLE C.1. Description of Arrays Used in the Main Segment

ARRAY	DESCRIPTION
CP(I,J)	Specific heat C_p at node (I,J).
DE(I,J)	Dissipation ϵ at node (I,J).
R(J)	Radial distance from axis of symmetry r , to J^{th} grid line.
RHO(I,J)	Density ρ at node (I,J).
RP(I,J)	Production P at node (I,J).
T(I,J)	Enthalpy h (or temperature t) at node (I,J).
TURV(I,J)	Turbulent viscosity μ_t at node (I,J).
U(I,J)	Velocity U at node (I,J).
UPL(J)	Non-dimensional velocity U^+ (location varies on the J^{th} grid line).
V(I,J)	Velocity V at node (I,J).
VISC(I,J)	Viscosity μ or μ_{eff} (varies) at node (I,J).
X1(N)	Temperature t on the n^{th} line of the property table.
X2(N)	Viscosity μ on the n^{th} line of the property table.
X3(N)	Specific heat C_p on the n^{th} line of the property table.
X4(N)	Thermal conductivity k on the n^{th} line of the property tables.
X5(N)	Density ρ on the n^{th} line of the property table.
X7(N)*	Enthalpies corresponding to X1(N).
X(I)	Streamwise distance X to I^{th} grid.
XK(I,J)	Thermal conductivity k at node (I,J).
XKE(I,J)	$\rho k^2/\epsilon$ at node (I,J).

.... continued

* For arrays X1(N), X2(N), X3(N), X4(N), X5(N), and X7(N), the meaning given in this table should be regarded only as a preliminary meaning. During the course of computations, these will normally be changed.

TABLE C.1. Description of Arrays Used in the Main Segment (Continued)

ARRAY	DESCRIPTION
XX(I)	Auxilliary variable containing predecided streamwise step divisions.
Y(J)	Distance from wall y to J th grid line.
YPL(J)	Non-dimensional distance y^+ (location varies on J th grid line.
ZK(I,J)	Turbulence kinetic energy K at node (I,J).

The remaining arrays are mostly one-dimensional and constitute a relatively minor proportion of the storage.

Statements Defining Data and Operating Conditions

Table C.2 describes the major input variables for the program.

It will be noted in Table C.2 that some input variables apply specifically to plane flow problems and others such as RADS are specifically for pipe flow problems. If a pipe flow problem is being solved, then the plane flow variables are assigned arbitrary values and vice versa. It will be noted in the program listing that all of the variables of Table C.2 (in Chapter I) are defined by ARITHMETIC statements. The same purpose can also be served through READ statements and this change may easily be introduced if felt necessary by a future user.

TABLE C.2. Description of Input Variables

VARIABLE	DESCRIPTION
CF	If CF = 1, then computation scheme skips calculations for kinetic energy K and dissipation ϵ . If CF = 0, then these calculations are performed.
GQ	Mass flow rate.
JEU	Number of Y-grid divisions.
JPRINT	Number of streamwise steps that are skipped before output is printed.
LNTP	If LNTP = 1, calculations are performed for turbulent case. If LNTP = 0 and CF = 1, then laminar flow computations are performed.
NC	Number which determines the location Y(NC) where the multi-equation turbulence model takes over from the near wall algebraic formulations.
QW	Wall heat flux.
RADS	Radius of pipe.
SSTF	Constant F_x for calculating streamwise step increments.
TO	Initial temperature.
TW	Constant wall temperature used for isothermal boundary condition problems.
UO	Free stream velocity. Use in plane flow problems.
UD	Unheated distance on a flat plate for plane flow problems.

The first executable statement of subroutines UVEL and PRES both assign a value to variable GRAV. If the flow direction is vertically upward, then GRAV is assigned a value equal to $-g$. If buoyancy force is to be neglected, then GRAV is assigned a value equal to zero and if the flow direction is downward, then GRAV is assigned a value equal to $+g$.

The program as described solves for enthalpy as the dependent variable of the energy equation. If it is required that the temperature be the dependent variable, then the following statements contained in Chapter II of the program are removed.

```

      TO = SLOP
      DO 110 N = 1,35
      X7(N) = X1(N0
      X1(N) = (25.0 + 5.0*N)*C7
      X4(N) = X4(N)/X3(N)
      X3(N) = 1.0
110 CONTINUED.

```

Chapter IV of the computer program contains the following statement,

$$R(J) = RADS - Y(J) .$$

This is only applicable to axisymmetric flows. For plane flow problems, this is changed to read,

$$R(J) = 1.0.$$

Another important change that will be required for each problem is in the calculation of starting profiles. The program listings described in Appendix D makes use of subroutine CHAMP for obtaining the Y-grid division and starting velocities. This subroutine is applicable only for turbulent fully-developed flow starting conditions. For other problems, this subroutine is replaced by other problem-dependent subroutines. Another subroutine CHANGE included in the program listing applies to turbulent flat

plate problems.

The program as described in Appendix D is set up for pipe flow problems where starting conditions require uniform enthalpy profiles and fully developed velocity profiles. After understanding the working of the program, a prospective user should be able to make the necessary problem-dependent changes.

Description of Subroutines

A description of the subroutines is provided in Table C.3.

All variables are handled as non-subscripted variables in the subroutines U, V, E, and ZKIN. In order to simplify the notation used for different variables in these subroutines, the following nomenclature is used. A number which stands for the nodal location (as described in Chapter II) is attached to the variable name. For example, the velocity u will be named around and at a central node as described in Figure 40.

TABLE C.3. Description of Subroutines

SUBROUTINE	DESCRIPTION
BCT2	Generates starting profiles of turbulence energy K and dissipation ϵ .
CHAMP	Generates the Y-grid and fully-developed starting velocity profiles for pipe flow problems.
CHANGE	Generates the Y-grid and starting velocity profiles for turbulent flow over a flat plate.
E	Computes enthalpies or temperatures through the finite difference formulations for the energy equation.
GRID	Generates the Y-grid for laminar flow over a flat plate, starting at the leading edge.
INITIA	Initializes the arrays $U(I,J)$, $V(I,J)$, and $T(I,J)$.
PRES	Computes pressures through the mass flow constraint.
PROP	Computes properties by linear interpolation of values in the property tables.
TURB	Computes and assembles effective viscosities and effective conductivities through algebraic formulations.
UVEL	Computes velocities U through the finite difference formulation for momentum equation.
VANDR	Computes velocity gradients in one-dimensional flows through the use of Van Driest hypothesis.
VVEL	Computes velocities V through the finite difference formulations for the continuity equation.
ZKIN	Computes turbulence energy k and dissipation ϵ through the finite difference formulations of their respective equations.
ZZK	Computes and assembles effective viscosities and effective conductivities according to the $K - \epsilon$ turbulence model.

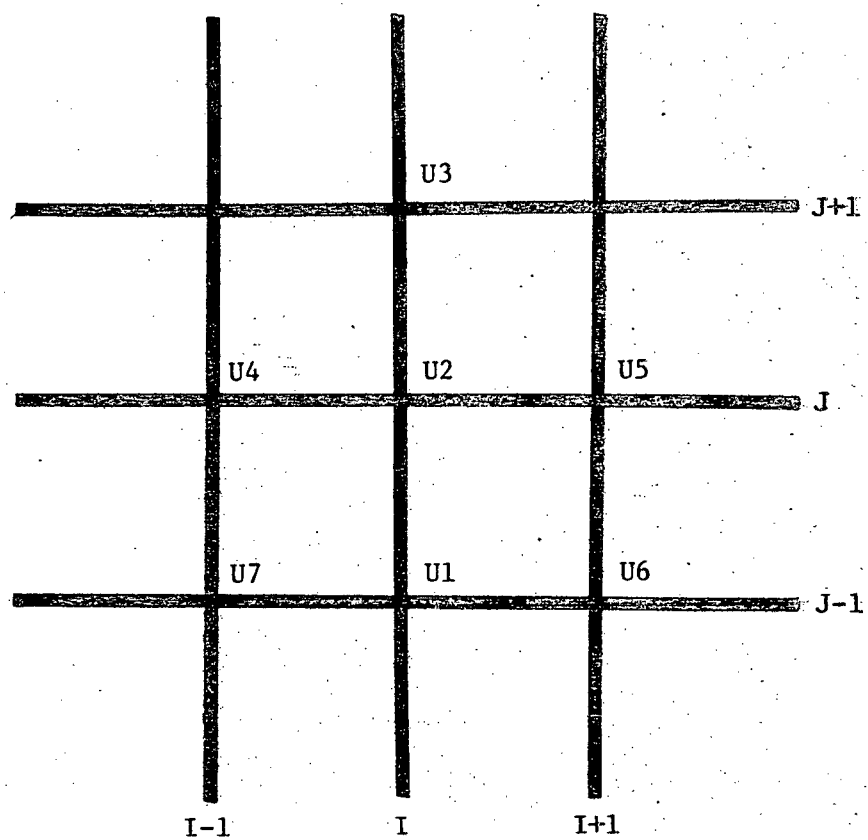


FIGURE 40. Nomenclature for Variables in Subroutines.

APPENDIX D

Listing of Computer Program

LISTING OF ASHN+...

```
COMMON INDEX
  DIMENSION XP(100),X(100),Y(100),U(10,100),V(10,100),
  IRHO(10,100),VISC(10,100),R(100)
  1,XX(300)
  1,XK(10,100),CP(10,100),T(10,100)
  1,TURV(10,100)
  DIMENSION X1(35),X2(35),X3(35),X4(35),X5(35),X7(35)
  DIMENSION YPL(100),UPL(100)
  DIMENSION XKE(10,100),ZK(10,100),RP(10,100),DE(10,100)
  JPRINT=10
  JPR=JPRINT
  TO=292.55
  PI=3.1416
  XXXP=7*10.0**6.0
  RADS=.01
  GQ=.2
  QW=5000
  TW=TO
  UD=.45
  UD=.1
  NC=35
  CF=0.0
  JEU=50
  DELF=1
  SSTF=0.5
  DELTA=RADS
  LNTP=1
```

CHAPTER 2-----

```
INDEX=2
XP(1)=XXXP
```

LISTING OF ASHN+...

```
XP(2)=XXXP
C1=5.0/9.0
C2=1.4882
C3=1000.0/0.23884
C4=3600.0/0.5778
C5=1.60184*10.0
C7=1.89/1356.0/6.0*10.0**7.0
PEAK=-3.0
PEAK=3.0
DO 102 N=1,35
READ(5,101) X1(N),X2(N),X3(N),X4(N),X5(N)
101 FORMAT(5G9.4)
X1(N)=C1*X1(N)
X2(N)=C2*X2(N)
X3(N)=C3*X3(N)
X4(N)=C4*X4(N)
X5(N)=C5*X5(N)
102 CONTINUE
IF(PEAK.GE.0.0) GO TO 104
DO 103 N=11,22
READ(5,101) X4(N)
X4(N)=C4*X4(N)
103 CONTINUE
104 CONTINUE
DO 109 N=1,35
X7(N)=(25.0+5.0*N)*C7
109 CONTINUE
CALL PROP(TO,XXXP,SRHO,SVISC,SXK,SCP,SLOP,X1,X2,X3,X4,X5,X7)
TO=SLOP
DO 110 N=1,35
```

LISTING OF ASHN+...

```

X7(N)=X1(N)
X1(N)=(25.0+5.0*N)*C7
X4(N)=X4(N)/X3(N)
X3(N)=1.0

```

110 CONTINUE

CHAPTER 3-----

```

PRT=SCP*SVISC/SXK
PRINT,PRT
CALL INITIA(U,V,T,UO,TO)
DO 12 I=1,10
DO 12 J=1,100
XKE(I,J)=0.0
ZK(I,J)=0.0
RP(I,J)=0.0
DE(I,J)=0.0
TURV(I,J)=0.0
RHO(I,J)=SRHO
VISC(I,J)=SVISC
CP(I,J)=SCP
XK(I,J)=SXK
XK(I,J)=SXK/SCP
CP(I,J)=1.0

```

12 CONTINUE

```

W=25.0*VISC(1,1)/UO/RHO(1,1)
XX(1)=0.0
FACTOR=0.37
XX(2)=FACTOR*W
DO 152 I=2,299
XX(I+1)=XX(I)+5.0*FACTOR/(UO*RHO(1,1)/VISC(1,1)/XX(I))**0.5

```

152 CONTINUE

LISTING OF ASHN+...

```

      DO 151 I=1,10
      X(I)=XX(I)
151  CONTINUE
      N=JEU

```

```

CHAPTER 4-----
      CALL GRID(W,N,Y)
      CALL CHAMP(RADS,N,Y,GQ,SRHO,SVISC,U,SHWA)
      I=1
      CALL TURB(U,VISC,RHO,Y,TURV,I,N,CP,XK,LNTP,DELTA,SHWA)
      CALL BCT2(U,Y,DE,ZK,NC,N,SHWA,SRHO)
      DO 1500 J=1,99
      XK(I,J)=XK(I,J)-TURV(I,J)*CP(I,J)
1500  VISC(I,J)=VISC(I,J)-TURV(I,J)
      X(1)=XX(1)
      X(2)=XX(2)
      STF=Y(2)/RADS
      DELTA=RADS
      DO 13 J=1,N
      R(J)=RADS-Y(J)
13  CONTINUE
      C2=1.9-.16/.3*(1.+3.*Y(NC)*Y(NC)/R(NC)/R(NC)
      1+3.*Y(NC)/R(NC))

```

```

CHAPTER 5-----
      DO 154 L=1,70
      DO 15 I=2,9
      IF(CF.GT.0.5) GO TO 777
      CALL      ZZK(XKE,ZK,DE,RP,U,VISC,RHO,Y,TURV
1, I,N,NC,RADS,CP,XK,SHWA,CF)
      GO TO 775
777  CALL TURB(U,VISC,RHO,Y,TURV,I,N,CP,XK,LNTP,DELTA,SHWA)

```

LISTING OF ASHN+...

```

775 PRINT,SHWA
  X(I+1)=STF*DELTA+X(I)
  CALL PRES(U,V,VISC,RHO,R,Y,GQ,N,I,X(I-1),X(I),X(I+1),
1XP(I-1),XP(I+1),SHWA)
  NN=N-1
  DO 14 J=2,NN
    CALL UVEL(U(I,J+1),U(I-1,J),U(I,J),U(I+1,J),U(I,J-1),
1RHO(I,J),VISC(I,J+1),VISC(I,J),VISC(I,J-1),V(I,J),
1R(J+1),R(J),R(J-1),Y(J+1),Y(J),Y(J-1)
1,XP(I-1),XP(I),XP(I+1),X(I-1),X(I),X(I+1))
    CALL E(U(I,J-1),U(I,J),U(I,J+1),T(I,J-1),T(I,J),T(I,J+1),
1T(I-1,J),T(I+1,J),XP(I),XP(I-1),XP(I+1),Y(J-1),Y(J),Y(J+1),R(J-1),
1R(J),R(J+1),RHO(I,J),CP(I,J),VISC(I,J),XK(I,J-1),XK(I,J),XK(I,J+1)
1,X(I),X(I-1),X(I+1),V(I,J))
    CALL PROP (T(I+1,J),XP(I+1),RHO(I+1,J),VISC(I+1,J),XK(I+1,J),
1CP (I+1,J),SLOP,X1,X2,X3,X4,X5,X7)
    CALL VVEL(U(I-1,J),U(I,J),U(I+1,J),U(I-1,J-1),U(I,J-1),U(I+1,J-1)
1,RHO(I-1,J),RHO(I,J),RHO(I+1,J),RHO(I-1,J-1),RHO(I,J-1),RHO(I+1,
1J-1),R(J+1),R(J),R(J-1),V(I+1,J),V(I+1,J-1),X(I-1),X(I),X(I+1),
1Y(J+1),Y(J),Y(J-1))
    IF(J.LE.NC) GO TO 105
    IF(CF.GE.0.5) GO TO 105
    CALL ZKIN (ZK(I,J-1),ZK(I,J),ZK(I,J+1),ZK(I-1,J),ZK(I+1,J),DE(
1I,J-1),DE(I,J),DE(I,J+1),DE(I-1,J),DE(I+1,J),XKE(I,J-1),XKE(I,J),
1XKE(I,J+1),Y(J-1),Y(J),Y(J+1),R(J-1),R(J),R(J+1),X(I-1),
1X(I),X(I+1),RHO(I,J),V(I,J),RP(I,J),U(I,J),C2)
105 CONTINUE
14 CONTINUE
CHAPTER 6-----
  IF(STF.LE.SSTF)STF=STF*1.2

```

LISTING OF ASHRAE...

```

1000 CONTINUE
    JC=3
    IP1=I+1
    DO 1000 J=1,99
        XK(I,J)=XK(I,J)-CP(I,J)*TURV(I,J)
1000    VISC(I,J)=VISC(I,J)-TURV(I,J)
        T(I+1,1)=T(I+1,2)+QW*Y(2)/XK(I,1)
        CALL PROP(T(I+1,1),XP(I+1),RHO(I+1,1),VISC(I+1,1),XK(I+1,1),CP
1(I+1,1),SLOP,X1,X2,X3,X4,X5,X7)
        DIAM=X(I+1)/RADS/2.0
        U(I+1,N)=U(I+1,NN)
        V(I+1,N)=0.0
        RHO(I+1,N)=RHO(I+1,NN)
        VISC(I+1,N)=VISC(I+1,NN)
        XK(I+1,N)=XK(I+1,NN)
        CP(I+1,N)=CP(I+1,NN)
        T(I+1,N)=T(I+1,NN)
        ENTH=0.0
        DO 2000 K=1,NN
            ENTH=ENTH+(T(I+1,K)*U(I+1,K)*RHO(I+1,K)+T(I+1,K+1)*U(I+1,K+1)*
1RHO(I+1,K+1))
            1*(R(K)+R(K+1))*(Y(K+1)-Y(K))*PI/2.0
2000 CONTINUE
        ENTH=ENTH/GQ
        WRITE(6,75) DIAM,SLOP,ENTH,SHWA
75    FORMAT(4X,'DIAMS=',F6.2,'WALL TEMP=',F7.3,'BULK ENTH.=',G11.4,
1'SHEAR ST.=',F6.2)
        INDEX=2
        JPR=JPR+1
        IF(JPR.LT.JPRINT) GO TO 779

```

LISTING OF ASHN+...

```

        WRITE(6,70) X(I)
        WRITE(6,71)
        WRITE(5,112)(U(I,K),K=1,N)
        WRITE(6,72)
        WRITE(5,112)(T(I,K),K=1,N)
        WRITE(6,73)
        WRITE(5,112) (ZK(I,K),K=NC,N)
        WRITE (6,74)
        WRITE(5,112) (DE(I,K),K=NC,N)
        WRITE(5,112)(TURV(I,K),K=1,N)
70  FORMAT(4X,'X=',F11.4)
71  FORMAT(4X,'VELOCITIES')
72  FORMAT(4X,'ENTHALPY')
73  FORMAT(4X,'KIN.ENER.')
74  FORMAT(4X,'DISP.')
        JPR=0
779  CONTINUE
15  CONTINUE
CHAPTER 7-----
        DO 18 I=1,2
        XP(I)=XP(I+8)
        DO 18 J=1,N
        ZK(I,J)=ZK(I+8,J)
        DE(I,J)=DE(I+8,J)
        XKE(I,J)=XKE(I+8,J)
        RP(I,J)=RP(I+8,J)
        U(I,J)=U(I+8,J)
        V(I,J)=V(I+8,J)
        RHO(I,J)=RHO(I+8,J)
        VISC(I,J)=VISC(I+8,J)

```

LISTING OF ASHN+...

```

      XK(I,J)=XK(I+8,J)
      X(I)=X(I+8)
      CP(I,J)=CP(I+8,J)
      T(I,J)=T(I+8,J)
10  CONTINUE
      PRINT,X(I+1)
112 FORMAT(1X,10G11.4)
15+ CONTINUE
770 CONTINUE
      STOP
      END
      SUBROUTINE ZKIN(ZK1,ZK2,ZK3,ZK4,ZK5,DE1,DE2,DE3,DE4,DE5,
1XKE1,XKE2,XKE3,Y1,Y2,Y3,R1,R2,R3,X4,X2,X5,RH02,V2,RP2,U2,
1C2)
      SIGK=1.0/J.09
      ZZ1=0.5/R2/(Y3-Y1)*(R3-R2)/(Y3-Y2)
      ZZ2=0.5/R2/(Y3-Y1)*(R1+R2)/(Y2-Y1)
      Z1=ZZ1*(XKE2+XKE3)/SIGK
      Z2=ZZ2*(XKE1+XKE2)/SIGK
      COEF=RH02*U2/(X5-X4)+0.5*(Z1+Z2)
      TERM=RP2-DE2*RH02+Z1*(ZK3-0.5*ZK4)-Z2*(0.5*ZK4-ZK1)
1-RH02*V2*(ZK3-ZK1)/(Y3-Y1)+RH02*U2*ZK4/(X5-X4)
      ZK5=TERM/COEF
C      ASSUMING Z,S AND COEF ARE SAME
      TERM1=RP2*C2*DE2/ZK2-1.9*RH02*DE2*DE2/ZK2
1-Z1*(DE3-0.5*DE4)-Z2*(0.5*DE4-DE1)-RH02*V2*(DE3-DE1)/(Y3-Y1)
1+RH02*U2*DE4/(X5-X4)
      DE5=TERM1/COEF
      RETURN
      END

```


LISTING OF ASHN+...

```

SUBROUTINE BCT2(U,Y,DE,ZK,NC,N,SHWA,SRHO)
DIMENSION U(10,100),Y(100),ZK(10,100),DE(10,100)
NC=NC-10
UST=SHWA/SRHO
DU=(U(1,NC+1)-U(1,NC-1))/(Y(NC+1)-Y(NC-1))
UK1=.16/.3*Y(NC)*Y(NC)*DU*DU
UK2=0.840*UST
U2=U(1,N)
U1=U(1,NC)
C1=(UK2**1.0-UK1**1.0)/(U2-U1)
C2=UK1**1.0-U1*C1
NN=N-1
DO 10 J=NC,NN
DU=(U(1,J+1)-U(1,J-1))/(Y(J+1)-Y(J-1))
ZK(1,J)=(C1*U(1,J)-C2)**1.0
ZK(2,J)=ZK(1,J)
DE(1,J)=0.3*ZK(1,J)*DU
DE(2,J)=DE(1,J)
10 CONTINUE
NC=NC+10
RETURN
END
SUBROUTINE ZZK(XKE,ZK,DE,RP,U,VISC,RHO,Y,TURV
1,I,N,NC,RADS,CP,XK,SHWA,XX)
DIMENSION XKE(10,100),ZK(10,100),DE(10,100),RP(10,100),
1U(10,100),VISC(10,100),RHO(10,100),TURV(10,100),CP(10,100),
1XK(10,100),Y(100),YPL(100),UPL(100)
DE(I,N)=DE(I,N-1)
ZK(I,N)=ZK(I,N-1)
SHWA=VISC(I,1)*U(I,2)/Y(2)

```

LISTING OF ASHN+...

```

      NCF=10
      UST=(SHWA/RHO(I,1))*0.5
      DO 1 J=1,NC
      YPL(J)=Y(J)*UST/VISC(I,1)*RHO(I,1)
      UPL(J)=U(I,J)/UST
1    CONTINUE
      DO 2 J=2,NC
      RPL =0.4*Y(J)
      IF(YPL(J).LE.125.0) RPL=RPL*(1.0-EXP(-YPL(J)/28.0))
      TURV(I,J)=RHO(I,J)*RPL**2.0*(U(I,J+1)-U(I,J-1))/(Y(J+1)-Y(J-1))
      IF(TURV(I,J).LE.0.0) TURV(I,J)=-TURV(I,J)
2    CONTINUE
      ZKWA=3.333*UST**2.0
      NCF=NCF+1
      IF(YPL(NCF).LE.75.0) GO TO 6
      DU=(U(I,NCF+1)-U(I,NCF-1))/(Y(NCF+1)-Y(NCF-1))
      ZK(I,NCF)=.16/.3*Y(NCF)*Y(NCF)*DU*DU
      DE(I,NCF)=.3*ZK(I,NCF)*DU
      DE(I+1,NC)=DE(I,NC)
      ZK(I+1,NC)=ZK(I,NC)
      NCC=NC+1
      DO 10 J=NCC,N
      XKE(I,J)=RHO(I,J)*ZK(I,J)*ZK(I,J)/DE(I,J)
10   CONTINUE
      XKE(I,NC)=RHO(I,NCF)*ZK(I,NCF)*ZK(I,NCF)/DE(I,NCF)
      FACT=(Y(NCC)-Y(NC))/(Y(NCC)-Y(NCF))
      ZK(I,NC)=ZK(I,NCC)-FACT*(ZK(I,NCC)-ZK(I,NCF))
      DE(I,NC)=DE(I,NCC)-FACT*(DE(I,NCC)-DE(I,NCF))
      NN=N-1
      DO 35 J=NCC,NN

```

LISTING OF ASHN+...

```

      RP(I,J)=XKE(I,J)*(U(I,J+1)-U(I,J-1))*(U(I,J+1)-U(I,J-1))
      1/(Y(J+1)-Y(J-1))/(Y(J+1)-Y(J-1))*0.09
      TURV(I,J)=0.09*XKE(I,J)
3>  CONTINUE
      TURV(I,N)=TURV(I,NN)
      NNN=N-2
      DO 3 J=2,NNN
3  TURV(I,J)=(TURV(I,J-1)+TURV(I,J)+TURV(I,J+1))/3.0
      PRT=0.9
      DO 4 J=1,N
      VISC(I,J)=VISC(I,J)+TURV(I,J)
      XK(I,J)=XK(I,J)-TURV(I,J)*CP(I,J)/PRT
4  CONTINUE
      RETURN
      END

```

LISTING OF ...ASH2+...

```

SUBROUTINE GRID(W,N,Y)
  DIMENSION Y(100)
  Y(1)=0.0
  NN=N
  FAC=0.25
  DO 1 I=2,NN
    Y(I)=FAC*I*W
  1 CONTINUE
  WRITE(5,111)(Y(K),K=1,N)
  111 FORMAT(1X,10G11.4)
  RETURN
END
SUBROUTINE UVEL(U3,U4,U2,U5,U1,RHO2,VISC3,VISC2,VISC1,V2,
  IR3,R2,R1,Y3,Y2,Y1,XP4,XP2,XP5,X4,X2,X5)
  COMMON INDEX
  GRAV=-9.8
  IF (INDEX.GT.1) GO TO 50
  TERM=(U2-U1)/(Y2-Y1)
  IF (V2.LT.0.0) TERM=(U3-U2)/(Y3-Y2)
  TERM2=(XP5-XP2)/(X5-X2)+.5/R2/(Y3-Y1)*((R2+R3)*(VISC2+VISC3)*((Y3-
  U2)/(Y3-Y2)-(R1+R2)*(VISC1+VISC2)*(U2-U1)/(Y2-Y1))-RHO2*V2*TEMP)
  U5=TERM2*(X5-X2)/U2/RHO2+U2
  GO TO 77
50 CONTINUE
  Z1=0.5/R2/(Y3-Y1)*((R3+R2)*(VISC2+VISC3)/(Y3-Y2)
  Z2=0.5/R2/(Y3-Y1)*((R1+R2)*(VISC1+VISC2)/(Y2-Y1)
  COEF=RHO2*U2/(X5-X4)+0.5*(Z1+Z2)
  TERM=-(XP5-XP4)/(X5-X4)-RHO2*V2*(U3-U1)/(Y3-Y1)
  I-Z1*(U3-0.5*U4)-Z2*(0.5*U4-U1)
  I+RHO2*U2*U4/(X5-X4)+RHO2*GRAV

```

LISTING OF ...+ASH2+...

```

      U5=TERM/CDEF
77  CONTINUE
      RETURN
      END
      SUBROUTINE VVEL(U4,U2,U5,U7,U1,U6,RH04,RH02,RH05,RH07,RH01,
1RH06,R3,R2,R1,V5,V6,X4,X2,X5,Y3,Y2,Y1)
      COMMON INDEX
      IF(INDEX.GT.1) GO TO 50
      TERM=-(R2+R1)* (RH05*U5-RH02*U2+RH06*U6-RH01*U1)/(X5-X2)
      TERM=TERM/4.0
      V5=(TERM*(Y2-Y1)+RH06*V6*R1)/RH05/R2
      GO TO 78
50  CONTINUE
      TERM=(R1+R2)/4.0/(X5-X4)* (RH05*U5-RH04*U4+RH06*U6-RH07*U7)
      TERM=-TERM
      V5=(TERM*(Y2-Y1)+RH06*V6*R1)/RH05/R2
78  CONTINUE
      RETURN
      END
      SUBROUTINE E(U1,U2,U3,T1,T2,T3,T4,T5,XP2,XP4,XP5,Y1,Y2,Y3,
1R1,R2,R3,RH02,CP2,VISC2,XK1,XK2,XK3,X2,X4,X5,V2)
      COMMON INDEX
      CJ=1.0
      IF(INDEX.GT.1) GO TO 50
      TERM=U2*(XP5-XP2)/(X5-X2)*CJ-0.5/R2/(Y3-Y1)* ((R2+R3)* (XK2+XK3)
1*(T3-T2)/(Y3-Y2)-(R1+R2)* (XK1+XK2)* (T2-T1)/(Y2-Y1))
1-VISC2*((U2-U1)/(Y2-Y1))*2.0-RH02*V2*CP2*(T2-T1)/(Y2-Y1)
      T5=TERM*(X5-X2)/RH02/U2/CP2+T2
      GO TO 79
50  CONTINUE

```

LISTING OF ...ASH2+...

```

      Z1=0.5/R2/(Y3-Y1)*(R3+R2)*(XK3+XK2)/(Y3-Y2)
      Z2=0.5/R2/(Y3-Y1)*(R2+R1)*(XK2+XK1)/(Y2-Y1)
      COEF=RH02*U2*CP2/(X5-X4)+0.5*(Z1+Z2)
      TERM=U2*(XP5-XP4)/(X5-X4)*CJ-RH02*V2*CP2*(I3-T1)/(Y3-Y1)+Z1*(T3
1-0.5*T4)-Z2*(0.5*T4-T1)+VISC2*(U3-U1)*(U3-U1)/(Y3-Y1)
1+RH02*U2*CP2*T4/(X5-X4)
      T5=TERM/COEF
79 CONTINUE
      RETURN
      END
      SUBROUTINE PROP(XQM, SXP, SRHO, SVISC, SXK, SCP, SLOP, X1, X2, X3, X4, X5, X7)
      DIMENSION X1(35), X2(35), X3(35), X4(35), X5(35), X7(35)
      I=2
3  IF(XQM.LE.X1(I)) GO TO 2
      I=I+1
      IF (I.EQ.35) GO TO 2
      GO TO 3
2  I=I-1
      FACT=(XQM-X1(I))/(X1(I+1)-X1(I))
      SRHO=FACT*(X5(I+1)-X5(I))
      SVISC=FACT*(X2(I+1)-X2(I))
      SCP=FACT*(X3(I+1)-X3(I))
      SXK=FACT*(X4(I+1)-X4(I))
      SLOP=FACT*(X7(I+1)-X7(I))
      RETURN
      END
      SUBROUTINE INITIA(U, V, T, UO, TO)
      DIMENSION U(10,100), V(10,100), T(10,100)
      TW=TC
      DO 12 I=1,10

```

LISTING OF ...+ASH2+...

```

      DO 12 J=1,100
      U(I,J)=U0
      V(I,J)=0.0
      T(I,J)=T0
12  CONTINUE
      DO 14 I=1,10
      T(I,1)=TW
      U(I,1)=0.0
14  CONTINUE
      RETURN
      END
      SUBROUTINE TURB(U,VISC,RHO,Y,TURV,I,N,CP,XK,LNTP,DELTA,SHWA)
      DIMENSION U(10,100),VISC(10,100),RHO(10,100),TURV(10,100),
      ICP(10,100),XK(10,100),Y(100),YPL(100),UPL(100)
      SHWA=VISC(I,1)*U(I,2)/Y(2)
      UST=(SHWA/RHO(I,1))**0.5
      DO 1 J=1,N
      YPL(J)=Y(J)*UST/VISC(I,1)*RHO(I,1)
      UPL(J)=U(I,J)/UST
1  CONTINUE
      NN=N-1
      DO 2 J= 2,NN
      RPL=0.4*Y(J)
      IF(YPL(J).LE.100.0)RPL=RPL*(1.0-EXP(-YPL(J)/28.0))
      IF(RPL.GE.(0.089*DELTA)) RPL=0.089*DELTA
      TURV(I,J)=RHO(I,J)*RPL**2.0*(U(I,J+1)-U(I,J-1))/(Y(J+1)-Y(J-1))
      IF(TURV(I,J).LE.0.0)TURV(I,J)=-TURV(I,J)
2  CONTINUE
3+  NNN=N-2
      DO 3 J=2,NNN

```

LISTING OF ...+ASH2+...

```

3  TURV(I,J)=(TURV(I,J-1)+TURV(I,J)+TURV(I,J+1))/3.0
   PRT=1.0
   DO 4 J=1,N
     VISC(I,J)=VISC(I,J)+TURV(I,J)
     XK(I,J)=XK(I,J)-TURV(I,J)*CP(I,J)/PRT
4  CONTINUE
33 CONTINUE
   RETURN
   END
   SUBROUTINE VANDR(SHWA,YC,SVISC,SRHO,DU)
     YP=YD*(SHWA/SRHO)**0.5/SVISC*SRHO
     IF(YP.GE.100.0)YP=100.0
     C=0.16*SRHO*YD**2.0*(1.0-EXP(-YP/28.0))**2.0
     DU=-SVISC*(SVISC**2.0-4.0*SHWA*C)**0.5
     DU=DU/2.0/C
   RETURN
   END
   SUBROUTINE CHAMP(RADS,N,Y,GQ,SRHO,SVISC,U,SHWA)
     REAL LAMDA,PI
     DIMENSION Y(100),U(10,100),UT(100)
     DIMENSION R(100)
     PI=3.1416
     Y(1)=0.0
     Y(N)=RADS
     SN=7.0
     UBAR=GQ/(SRHO*PI*RADS*RADS)
     UMAX=UBAR*(SN+1.0)**(2.0*SN+1.0)/2.0/SN/SN
     REYN=2.0*SRHO*UBAR*RADS/SVISC
     LAMDA=0.3164/REYN**0.25
     SHWA=1.0/8.0*LAMDA*SRHO*UBAR*UBAR

```


LISTING OF ...-ASH2-...

```

      Y(2)=SVISC/SRHO/(SHWA/SRHO)**0.5
      DYM=(0.99*RADS/Y(2))**(1.0/(N-3))
      PRINT,DYM
      UT(1)=0.0
      NN=N-1
      DO 1 J=3,NN
1     Y(J)=DYM*Y(J-1)
      DO 2 J=1,N
      U(1,J)=UMAX*(Y(J)/RADS)**(1.0/5N)
      U(2,J)=U(1,J)
2     CONTINUE
      DO 3 J=2,NN
      YD=(Y(J)+Y(J-1))/2.0
      SH=SHWA*(RADS-Y(J))/RADS
      CALL VANDR(SH,YD,SVISC,SRHO,DU)
      UT(J)=UT(J-1)-(Y(J)-Y(J-1))*DU
3     CONTINUE
      DO 4 J=2,NN
      IF(UT(J).LE.U(1,J)) U(1,J)=UT(J)
      U(2,J)=U(1,J)
4     CONTINUE
      PRINT,SHWA,REYN,UMAX,UBAR
      WRITE(5,112)(U(2,K),K=1,N)
      WRITE(5,112)(Y(K),K=1,N)
112  FORMAT(1X,10G11.4)
      DO 6 J=1,N
6     R(J)=RADS-Y(J)
      U(1,N)=U(1,NN)
      U(2,N)=U(2,NN)
      SUM=0.0

```

LISTING OF ...ASH2+...

```

DO 5 J=1,NN
  SUM=SUM+0.5*(U(2,J)-U(2,J+1))*(R(J)+R(J+1))*(Y(J+1)-Y(J))*SRHO
  GO=SUM*PI
  PRINT ,GO
  RETURN
END
SUBROUTINE PRES(U,V,VISC,RHO,R,Y,GQ,N,I,X44,X22,X55,XP4,XP5,SHW6)
  REAL PA(100),PB(100),PC(100),PI
  DIMENSION V(10,100),U(10,100),VISC(10,100),RHO(10,100),R(100),
  1Y(100),F1(100),F2(100)
  GRAV=-9.8
  PI=3.1416
  DEXM=X22-X44
  DEXP=X55-X22
  NN=N-1
  DO 1 J=2,NN
    DELP=Y(J+1)-Y(J)
    DELM=Y(J)-Y(J-1)
    PA(J)=4.0*RHO(I,J)*U(I,J)*R(J)*(DELP+DELM)*DELP*DELM
    1+(DEXP+DEXM)*DELM*(R(J+1)+R(J))*(VISC(I,J+1)+VISC(I,J))
    1+(DEXP+DEXM)*DELP*(R(J)+R(J-1))*(VISC(I,J)+VISC(I,J-1))
    PB(J)=-4.0*RHO(I,J)*RHO(I,J)*R(J)*DELP*DELM*(DEXP+DEXM)
    1*V(I,J)*(U(I,J+1)-U(I,J-1))-2.0*RHO(I,J)*(DEXP+DEXM)*DELM*
    1(VISC(I,J+1)+VISC(I,J))*(U(I,J+1)-0.5*U(I-1,J))*(R(J+1)+R(J))
    1+2.0*RHO(I,J)*(DEXP+DEXM)*DELP*(VISC(I,J)+VISC(I,J-1))
    1*(U(I,J-1)-0.5*U(I-1,J))*(R(J)+R(J-1))
    PB(J)=PB(J)+4.0*RHO(I,J)*RHO(I,J)*U(I-1,J)*R(J)*(DELP+DELM
    1)*DELP*DELM
    PB(J)=PB(J)+4.0*RHO(I,J)*RHO(I,J)*R(J)*(DEXP+DEXM)*(DELP+DELM)
    1*DELP*DELM*GRAV

```

LISTING OF ...+ASH2+...

```

      PC(J)=-4.0*RHO(I,J)*R(J)*(DELP+DELM)*DELP*DELM
1  CONTINUE
      PA(1)=0.0
      PB(1)=0.0
      PC(1)=0.0
      PA(N)=PA(NN)
      PB(N)=PB(NN)
      PC(N)=PC(NN)
      F1(1)=0.0
      F2(1)=0.0
      DO 2 J=2,N
      F1(J)=PB(J)/PA(J)
      F2(J)=PC(J)/PA(J)
2  CONTINUE
      SUM1=0.0
      SUM2=0.0
      DO 3 J=1,NN
      SUM1=SUM1+(F1(J)+F1(J+1))*(R(J)+R(J+1))*(Y(J+1)-Y(J))*PI/2.0
      SUM2=SUM2+(F2(J)+F2(J+1))*(R(J)+R(J+1))*(Y(J+1)-Y(J))*PI/2.0
3  CONTINUE
      DELPR=(GQ-SUM1)/SUM2
      XP5=DELPR+XP4
      RETURN
      END

```

LISTING OF ...-SOURCE-

```

SUBROUTINE CHANGE(SRHO,SVISC,UD,UD,Y,XX,U,V,N,SHWA,DELTA)
DIMENSION XX(300),Y(100),U(10,100),V(10,100),YPLC(10),YPLC1(10)
DIMENSION UT(2,100)
RX=SRHO*UD*UD/SVISC
SHWA=SRHO*UD**2.0*0.185/(ALOG10(RX))**2.58
DELTA=5.0*UD*RK**(-0.5)
DELTA=0.37*UD*RK**(-0.2)
FACL=DELTA/DELTA
DELTA=DELTA/FACL
Y(1)=0.0
Y(2)=7.0/(SHWA/SRHO)**0.5*SVISC/SRHO
Y(2)=Y(2)/FACL
FACTOR=0.65
XX(2)=UD
XX(3)=XX(2)+0.37*FACTOR*XX(2)*[UD*XX(2)*SRHO/SVISC]**(-0.2)
XX(1)=UD-XX(3)+XX(2)
RX1=SRHO*UD*XX(1)/SVISC
DELTA1=0.37*XX(1)*RX1**(-0.2)
DELTA1=DELTA1/FACL
SHWA1=SRHO*UD**2.0*0.185/(ALOG10(RX1))**2.58
DO 100 J=3,N
100 Y(J)=1.1*Y(J-1)
YPLM=(SHWA/SRHO)**0.5/SVISC*SRHO
DO 102 J=2,N
IF(Y(J).LE.DELTA) U(2,J)=UD*(Y(J)/DELTA)**(1.0/7.0)
IF(Y(J).LE.DELTA1) U(1,J)=UD*(Y(J)/DELTA1)**(1.0/7.0)
102 CONTINUE
UT(1,1)=0.0
UT(2,1)=0.0
DO 104 J=2,30

```

LISTING OF ...*SOURCE*

```

      YD=(Y(J)+Y(J-1))/2.0
      CALL VANDR(SHWA,YD,SVISC,SRHO,DU)
      UT(2,J)=UT(2,J-1)+{Y(J)-Y(J-1)}*DU
      CALL VANDR(SHWA1,YD,SVISC,SRHO,DU)
      UT(1,J)=UT(1,J-1)+(Y(J)-Y(J-1))*DU
104  CONTINUE
      DO 105 J=2,N
      TERM=-0.5*(U(2,J)-U(1,J)-U(2,J-1)-U(1,J-1))/(XX(2)-XX(1))
105  V(2,J)=TERM*(Y(J)-Y(J-1))+V(2,J-1)
      PRINT,SHWA,RX,DELTA
      WRITE(5,112)(U(2,K),K=1,N)
      WRITE(5,112)(V(2,K),K=1,N)
      WRITE(5,112)(Y(K),K=1,N)
114  FORMAT(1X,10G11.4)
      RETURN
      END
$SIGNOFF
EXECUTION TERMINATED

```